PNL - 3462

Investigation of Basalt-Radionuclide Distribution Coefficients: Fiscal Year 1980 Annual Report

L.L. Ames
J.E. McGarrah

Pacific Northwest Laboratory

Rockwell International

Rockwell International

Rockwell Hanford Operations
Energy Systems Group
Richland, WA 99352

DISCLAIMER

INVESTIGATION OF BASALT-RADIONUCLIDE
DISTRIBUTION COEFFICIENTS:
FISCAL YEAR 1980 ANNUAL REPORT

L. L. Ames
J. E. McGarrah

Pacific Northwest Laboratory

December 1980

Rockwell International

SUMMARY

The Basalt Waste Isolation Project (Rockwell Hanford Operations) is conducting a safety assessment of nuclear waste storage in a repository on the Hanford Site. Pacific Northwest Laboratory, in support of the assessment effort, is generating radionuclide distribution coefficient data between simulated groundwaters and basalts and their secondary mineral products under the range of physicochemical conditions expected in a repository in basalt.

Experimental radionuclide distribution coefficients were determined for crushed Pomona, Flow E, and Umtanum basalts at 23°, 60°, 150°, and 300^oC at both normal oxygen partial pressure (~0.2 atm) and lower oxygen partial pressure ($\sim10^{-7}$ atm), using a static technique. Little or no changes in distribution coefficients were noted for selenium, uranium, technetium, neptunium, or plutonium over the oxygen partial pressure range noted above. Sodium dithionite and hydrazine are now under study as system additives to lower Eh to -0.3 to -0.5 V, the conditions expected to prevail in the closed repository in basalt. Radium, strontium, cesium, and americium are not expected to change oxidation states under repository conditions, while iodine remains an anion in either oxidation state. Lowering the system Eh to the -0.3 to -0.5 V expected in a repository in basalt should result in an oxidation state change and enhanced removal from solution for selenium, uranium, technetium, neptunium, and plutonium. Sorption of iodine was not affected by the Eh changes.

Temperature change effects on most radionuclide distribution coefficient (Kd) values over the 23° to 300^oC range were major with the exception of iodine and technetium, neither of which were appreciably sorbed at normal to $\sim10^{-7}$ atm oxygen partial pressure. Uranium Kd values increased with an increase in temperature. In addition, uranium Kd values at 23^oC decrease by an order of magnitude in response to added CO_3^{2-} in the solution. Cesium basalt Kd values decreased from 23° to 150^oC and increased from 150° to 300^oC. Americium and plutonium Kd values increased from 100 to 200 mL/g at 23^oC to several thousand mL/g at 150^oC. Strontium Kd values reacted to temperature increases in an individualistic response that apparently depended upon the basalt contacted. Flow E basalt showed little strontium Kd change

between 23° and 150^OC, while an order of magnitude strontium Kd increase was noted for Umtanum basalt over the same temperature range. Selenium Kd values increased from ~5 mL/g at 23^OC to 100 mL/g at 150^OC.

The effect of radionuclide concentration on the Kd value was shown graphically for cesium and strontium over a range of from 1×10^{-10} or 10^{-12} to $1 \times 10^{-4}\underline{M}$. Molarity was plotted versus Kd on log scales. The Kd values remained linear with increasing cesium or strontium concentration until ~12 $\times 10^{-7}\underline{M}$ concentration were attained. Above $1 \times 10^{-7}\underline{M}$, the Kd values decreased.

When the natural log of equilibrium solution concentration (moles/liter) was plotted versus the natural log of equilibrium solids loading (moles/gram) the strontium sorption data were linearized in a Freundlich plot. The cesium sorption data, on the other hand, were linearized by the Dubinin-Radushkevich relationship.

The use of ^{99}Tc to study technetium concentration effects on sorption was unsuccessful. Technetium-95m will be utilized for this purpose in the future.

Initial work was begun on Kd values obtained under controlled Eh and pH conditions to simulate specific oxygen partial pressure and pH conditions expected to occur in the repository environment. Eh values from +0.60 to -0.55 V and pH values of ~6 to 10 are expected over a period of time in the repository. Hydrazine and sodium dithionite are under investigation for use in Eh control at the lower end of the Eh range and quinhydrone for inter-mediate Eh range. The upper end of the pH range also can be duplicated with hydrazine and the lower end with sodium dithionite.

CONTENTS

TABLES:

INTRODUCTION

The primary purpose of the sorption work described in this report is to assist the Basalt Waste Isolation Project in completing a safety assessment of potential radioactive waste storage in a repository in basalt on the Hanford Site. Specifically, the objective of the sorption work being conducted by Pacific Northwest Laboratory is to determine the distribution of radionuclides between geologic materials and synthetic groundwater solutions characteristic of a repository in Hanford basalt and its physicochemical environment.

The probable radionuclide transport pathway from the repository to the biosphere involves dissolution and movement in the groundwater. Migration of the radionuclides in solution may be retarded by sorption on basalts, secondary minerals, volcanic ash, or sediments contacted during groundwater movements in the Hanford environment. One of the measures of the ability of geologic materials to impede radionuclide migration velocity in relation to groundwater velocity is the radionuclide distribution coefficient (Kd). A Kd is defined as the ratio of the equilibrium radionuclide concentration on the solid phase (basalt, secondary minerals, volcanic ash, sediments) to the equilibrium concentration of the radionuclide dissolved in solution, and has the dimensions of solution volume per solid weight. The Kd values obtained under conditions relevant to measured repository physicochemical conditions will be used in both radionuclide transport modeling and in determining needs and priorities for development of engineered barriers for specific radioisotopes.

The radionuclides studied initially were those found in irradiated uranium fuel with long half-lives, or those continually generated in the radioactive decay chains. The Kd data will be used to assess the ranking of these radionuclides as to their relative migration rates in Hanford groundwaters as affected by possible changes in solution composition, pH, Eh, temperature, pressure, radionuclide concentration, and solids composition. The experimental conditions strongly affect Kd values. These experimental conditions, therefore, will simulate repository conditions as closely as possible.

The Kd used in the sorption work was considered to be a function of the solution-geologic material contact time duration. The primary reason for expressing the distribution coefficient as a function of time was the slow approach of the rock-solution system and, consequently, the radionuclide-rock-solution system to equilibrium at temperatures below $100^{\circ}C$. The most water-soluble portion of the basalts at all temperatures was the glassy groundmass. The glass is 70 to 80 wt% SiO_2, according to electron microprobe results and can, therefore, be considered essentially an amorphous silica. The addition of several salts to the solution to simulate analyzed natural Hanford basalt groundwaters depressed glass solubilities at $23^{\circ}C$ and, hence, may have facilitated the approach to rock-solution equilibrium. Equilibrium was approached in the Kd results, but very likely not attained.

CONCLUSIONS

Improvements in Kd experimental techniques have resulted in reproducible Kd data for americium and plutonium. The improvements included a new method for determining and accounting in the Kd calculations for sorption of the americium or plutonium on container walls rather than on the basalt. Three basalt flow samples from the Columbia River basalt sequence and a secondary smectite from the Pomona flow were utilized in the Kd determinations. Americium and plutonium sorption are not always legitimately described by the Kd concept, because radionuclide concentrations that exceed their solubility are often used in experimental systems.

The effects of cesium and strontium concentration on sorption of their radioisotopes at 23° and $60^{\circ}C$ from two synthetic groundwater compositions showed that cesium and strontium Kd values on three basalt flow samples and a secondary smectite remained stable until the concentration exceeded $\sim 1.00 \times 10^{-7}\underline{M}$. Above $\sim 1.00 \times 10^{-7}\underline{M}$ strontium or cesium, the Kd values began to decline. Cesium sorption was best described by the Dubinin-Radushkevich (DR) equation, while strontium sorption was described by the Freundlich equation. Mean cesium sorption energies derived from the DR equation indicated ion exchange was the sorption mechanism. Technetium sorption, on the other hand, was not a function of concentration over the range studied because, in its anionic form (TcO_4^-), it is not sorbed.

The Eh in a closed repository in basalt eventually would be poised between -150 mV at pH 7 to -350 mV at pH 10 by a magnetite-pyrite reaction. These natural basalt component reactions point to the need for Kd values obtained in relatively low-Eh conditions expected to prevail in a closed repository in basalt. Initial radionuclide sorption experiments at Eh +0.656 V ($PO_2 = \sim 8 \times 10^{-7}$ atm) yielded the same Kd values for technetium, neptunium, plutonium, selenium, and uranium as those obtained under normal atmospheric oxygen partial pressure. This was because lower Eh values are required to obtain the lower oxidation states of these elements that facilitate their removal from solution. Quinhydrone was found to be useful for Eh control from an Eh of +0.300 V at pH 8 to +0.100 V at pH 10. Sodium dithionite and hydrazine are under investigation for system Eh stabilization at Eh values of -0.150 to -0.350 V.

3

A cycle of heating due to radioactive decay is expected to occur in a closed repository in basalt environment. Hence, the effects of temperature on radionuclide basalt and secondary mineral sorption are under investigation. The glassy component of basalt was found to be the least stable in the presence of heat and water, with secondary minerals such as quartz and potassium feldspar formed from it. As these secondary products formed and the ionic strength of the solution increased with temperature, those radionuclides, such as strontium, that were able to enter the secondary product crystal structures greatly increased their Kd values on Umtanum basalt with increasing temperature. If the radionuclide could not enter secondary mineral structures, the Kd value decreased with temperature due to increasing solution ionic strength with increasing temperature. Cesium sorption to 150°C is a good example of a radionuclide whose Kd value decreases with increasing temperature.

STANDARD SORPTION STUDY MATERIALS

Several natural materials from the vicinity of a proposed repository in basalt were used in the radionuclide sorption studies.

ROCKS AND MINERALS

The characterization of the secondary mineralization (smectite) and Umtanum, Flow E, and Pomona basalts was completed. Essentially, the basalt samples are composed of augite, titaniferous magnetite, labradorite plagioclase, a minor amount of clay minerals (mainly smectites), and a glassy phase containing plagioclase microlites. The glassy phase is the least thermodynamically stable, furnishing silica and other elements, such as fluorine and potassium, that did not fit well into the main-stage basalt mineral phases to the solution.

The secondary mineralization is a dioctahedral smectite with about equal amounts of magnesium and iron in the octahedral position. It has a high-cation-exchange capacity and surface area, and is an expanding clay mineral. A summary of the rock and mineral characteristics is given in Table 1.

SYNTHETIC GROUNDWATER COMPOSITIONS

The synthetic groundwater formulations used in the sorption work are given in Table 2. Both compositions represent groundwaters sampled and analyzed in the vicinity of the proposed nuclear waste repository in basalt (Deju et al., 1978). The silica was added as silicic acid, usually requiring 24 hr to be dissolved into the solution. It is probable that neither of the two formulations achieve equilibrium with the basalt, because equilibrium between solution and basalt is approached very slowly at temperatures below 100°C.

TABLE 1. Rocks and Minerals Used in the Sorption Work and Their Characterization.

Sample	Mineralogy, vol%		Ethylene Glycol Surface Area, m^2/g	Size Range	Cation Strontium Exchange Capacity, meq/100
Umtanum Basalt	Groundmass	- 38%	17.7 ± 3.8	0.85 - 0.50 mm	1.7 ± 0.1
	Plagioclase	- 26%			
	Pyroxenes	- 21%			
	Secondary Minerals	- 8%			
	Metallics	- 7%			
Pomona Basalt	Groundmass	- 23%	31.2 ± 1.4	0.85 - 0.50 mm	2 - 3
	Plagioclase	- 34%			
	Pyroxenes	- 31%			
	Secondary Minerals	- 6%			
	Metallics	- 6%			
Flow E Basalt	Groundmass	- 14%	10.3 ± 1.0	0.85 - 0.50 mm	4.7 ± 0.2
	Plagioclase	- 46%			
	Pyroxenes	- 32%			
	Secondary Minerals	- 5%			
	Metallics	- 3%			
Secondary Mineralization	Smectite	- 98%	646 ± 19	2 m	60 - 70
	Secondary Minerals (calcite, iron oxides)	- 2%			

	wt% Oxides						
				Secondary Mineralization			
Oxide	Umtanum Basalt	Pomona Basalt	Flow E Basalt	1	2	3	4
SiO_2	55.64	51.87	54.47	43.2	45.5	44.5	44.3
Al_2O_3	13.62	15.02	14.37	6.5	6.6	6.6	6.5
Fe_2O_3	2.00	2.00	2.00	9.8	9.6	9.7	9.4
FeO	10.68	8.89	11.16	-	-	-	-
MnO	0.20	0.19	0.22	-	-	-	-
CaO	7.17	10.58	7.36	1.2	1.0	1.1	1.0
MgO	3.33	7.08	3.56	12.4	12.8	12.6	12.7
Na_2O	3.30	2.23	2.79	-	-	-	-
K_2O	1.62	0.39	1.58	0.7	0.7	0.7	0.7
TiO_2	2.05	1.55	2.11	-	-	-	-
P_2O_5	0.39	0.19	0.36	0.2	0.2	0.2	0.2
Total	100.00	100.00	100.00	(remainder was water)			

TABLE 2. Synthetic Groundwater Formulations.

| Constituents | Concentration, mg/L | |
	GR-1	GR-2
Na^+	30.7	225
K^+	9.0	2.5
Ca^{2+}	6.5	1.06
Mg^{2+}	1.0	0.07
Cl^-	14.4	131
CO_3^{2-}	0	59
HCO_3^-	81.5	75
F^-	0	29
SO_4^{2-}	11.1	72
SiO_2	25	108
	pH = 8.0	pH = 10.0

BASALT SAMPLE HOMOGENEITY

An experiment designed to test the homogeneity of the Umtanum basalt was completed (results listed in Table 3). For this experiment, three basalt samples were weighed after each of four mixings of the stock Umtanum basalt. Cesium-spiked GR-1 groundwater was added and the samples were allowed to equilibrate for a period of 56 d. The results indicate that the Umtanum basalt stock is indeed homogeneous. The average Kd value listed in Table 2 was derived from taking a mean of the four mixes. This average coincides with the Kd value (705 ± 18 mL/g) obtained by earlier Umtanum experiments performed under identical conditions, giving additional substantiation that the Umtanum basalt stock is homogeneous.

TABLE 3. Cesium Kd Values for Separate Samplings of Umtanum Basalt After 56 Days Contact at 23°C.

| | | Kd, mL/g | | |
Mix 1	Mix 2	Mix 3	Mix 4	Avg. Kd
722 ± 104	701 ± 176	703 ± 151	662 ± 127	697 ± 140

SECONDARY MINERALIZATION MOISTURE CONTENT

This experiment was designed to determine the moisture content of the stock secondary mineralization. With the clay's capacity to sorb moisture as well as radionuclides, a small variation in moisture content could make a considerable difference in weight and, hence, in Kd values. At present, the stock secondary mineralization is stored in a desiccator containing an adsorbent (P_2O_5), and removed only for weighing.

Three 1-g samples were weighed in metal cans, placed in an oven at $110^\circ C$ for 4 d, and reweighed. The moisture content was then determined. The results indicate that the method used for media storage is satisfactory, as there was only a 1.67 $\pm$ 0.14% water loss. This loss is within the acceptable weighing error of ± 1 to 2%.

Kd AND RELATED MEASUREMENTS

A batch contact or static method was used in this study to determine a Kd (Relyea et al., 1980). Briefly, the batch contact method consists of contacting a known volume and composition of solution containing a radionuclide with a characterized solid of known weight for a specific length of time. An aliquot of the solid-free contacting solution then is compared to an aliquot of blank solution that did not contact a solid. The concentration of radionclide per gram of solid divided by the concentration of radionuclide remaining in a milliliter of contacting solution is the distribution coefficient at the contact time.

The contact time necessary to produce an equilibrium distribution coefficient may be very long in basalt systems, so that solution-solid-radionuclide equilibrium cannot be assumed to prevail. The pH and chemical composition of the solution produced by the final solution-solid contact period should be determined. Three or more replicates of the distribution coefficient are required to improve the precision of the measurement.

All of the following Kd values are reported in milliliters per gram. However, surface areas per unit weight are also given for the rocks and minerals used in the sorption work, so that a Kd with the dimensions of milliliter per square meter may be easily computed. In many cases, the very high surface area materials with large Kd values based on weight may yield lower Kd values based on surface area than the lower surface area geologic materials with lower weight-based Kd values.

NORMAL OXYGEN ENVIRONMENT

Kd values obtained for several basalts and secondary mineralization are given in Table 4. The first value is a mean of triplicated experiments and is followed by an estimation of the standard deviation. Moles per liter of radionuclide contained in the starting solution, GR-1 groundwater in this case, also are given. The concentration values were obtained by comparing the solution counts with those of known standards. The uranium Kd results with [233]U are given in Table 5.

TABLE 4. Corrected Kd Values Obtained after 50 Days of Solid/GR-1
Synthetic GroundWater Contact.

	Initial Mol/L	Umtanum Basalt	Flow E Basalt	Pomona Basalt	Secondary Mineralization
			$23^{\circ}C$ Kd, mL/g		
^{75}Se	2.63×10^{-13}	5.4 ± 1.3	1.2 ± 0.3	2.4 ± 0.7	7.6 ± 0.3
^{85}Sr	5.54×10^{-12}	105 ± 4	91 ± 5	121 ± 9	274 ± 16
^{99}Tc	6.55×10^{-8}	26.8 ± 21.9	0	0	0
^{125}I	4.24×10^{-14}	6.8 ± 1.3	1.0 ± 0.4	2.0 ± 1.0	14.0 ± 1.8
^{137}Cs	8.76×10^{-10}	705 ± 18	278 ± 6	$1,685 \pm 245$	$10,000$
^{237}Np	6.47×10^{-8}	30.0 ± 13.0	4.1 ± 0.9	9.8 ± 0.5	36.9 ± 7.5
^{241}Am	2.09×10^{-10}	277 ± 103	622 ± 180	696 ± 93	$1,355 \pm 152$
^{241}Pu	1.62×10^{-11}	102 ± 97	165 ± 16	267 ± 18	$2,572 \pm 341$

	Initial Mol/L	Umtanum Basalt	Flow E Basalt	Pomona Basalt	Secondary Mineralization
			$60^{\circ}C$ Kd, mL/g		
^{75}Se	2.63×10^{-13}	0	1.0 ± 0.1	0	0
^{85}Sr	5.54×10^{-12}	122 ± 3	104 ± 1	130 ± 4	339 ± 5
^{99}Tc	6.55×10^{-8}	25.5 ± 5.2	0	0	0
^{125}I	4.24×10^{-14}	0	0	0	0
^{137}Cs	8.76×10^{-10}	463 ± 5	187 ± 6	747 ± 37	$1,432 \pm 695$
^{237}Np	6.47×10^{-8}	31.2 ± 4.7	8.3 ± 0.5	12.1 ± 3.2	53.5 ± 18.8
^{241}Am	2.09×10^{-10}	236 ± 98	400 ± 245	717 ± 3	$1,489 \pm 350$
^{241}Pu	1.62×10^{-11}	353 ± 224	300 ± 26	700 ± 108	$3,328 \pm 609$

TABLE 5. Uranium-233 60-Day Kd Values for GR-1 and GR-2 Groundwater
Experiments at $23^{\circ}C$ Temperature.

^{233}U Initial, mol/L	Ground-water	Umtanum Basalt	Flow E Basalt	Pomona Basalt	Secondary Mineralization
8.16×10^{-9}	GR-1	56 ± 11	13 ± 1	16 ± 2	147 ± 70
8.16×10^{-9}	GR-2	2.8 ± 0.9	1.0 ± 0.2	0.9 ± 0.2	72 ± 2

Several conclusions may be drawn from these data:

- The higher ionic-strength GR-2 groundwater does affect uranium Kd values, probably because GR-2 contains greater amounts of carbonate and is higher in pH than GR-1, leading to higher anionic uranyl carbonate complexing levels.

- The higher surface area secondary mineralization usually removed more of the radionuclide from solution than did the low-surface-area basalts.

- Temperature effects on Kd between 23° and $60^\circ C$ are relatively minor.

- Radionuclides that normally occur in anionic form, such as iodine and technetium, are relatively poorly removed from solution under oxic conditions.

One of the problems associated with Kd determinations is the differential adsorption of radionuclides on container walls in the absence and presence of solids. The magnitude of tube sorption by strontium, americium, and plutonium in the case of no solids present in the tube is shown in Table 6.

TABLE 6. Percentages of Strontium, Americium, and Plutonium Removed Onto the Containing Tube Walls at $23^\circ C$ from Solutions Containing No Solids. GR-1 groundwater at pH 8.0 was used as a common solution.

Blank Solutions

Radionuclide	Radionuclide Level, counts/min/mL	Radionuclide Molarity	Volume, mL	% Removal on Tube
^{85}Sr	4,638	2.04×10^{-12}	10	0.5
	8,888	3.92×10^{-12}	80	0.5
^{241}Am	37,900	2.30×10^{-8}	10	91
	65,900	3.99×10^{-8}	80	84
^{241}Pu	13,000	2.57×10^{-10}	10	86
	20,400	4.02×10^{-10}	80	66

11

While tube sorption was minimal for strontium, which is a noncomplexed, divalent cation, americium and plutonium were largely removed onto container walls. Attempting to use such blank solutions in the Kd computations can lead to a grossly distorted Kd value because container wall adsorption is much lower with solid present in the system (Table 7). The average container wall adsorption values in Table 7 were used to correct the Kd values. While the two radionuclides present in the highest concentrations were technetium and neptunium, only neptunium was appreciably adsorbed on container walls in the presence of solids. Adsorption was least on container walls in the presence of the highest surface-area solid (secondary mineralization). Strontium, technetium, iodine, and cesium did not appreciably adsorb on container walls in the presence of solids in GR-1 groundwater.

TABLE 7. Container Wall Sorption for the Various Radionuclides in the Presence of Solids at Two Temperatures for a 50-Day Contact Time with GR-1 Synthetic Groundwater.

| Radio-nuclide | $^\circ$C | Molarity | % Container Sorption with Solids Present | | | |
			Umtanum Basalt	Flow E Basalt	Pomona Basalt	Secondary Mineralization
^{75}Se	23	2.63×10^{-13}	17.30	16.38	18.35	11.52
	60		9.26	18.03	11.87	6.50
^{85}Sr	23	5.54×10^{-12}	<1	<1	<1	<1
	60		<1	<1	<1	<1
^{99}Tc	23	6.55×10^{-8}	<1	<1	<1	<1
	60		<1	<1	<1	<1
^{125}I	23	4.24×10^{-14}	6.22	<1	<1	<1
	60		<1	<1	0	<1
^{137}Cs	23	8.76×10^{-10}	<1	<1	<1	<1
	60		<1	<1	<1	<1
^{237}Np	23	6.67×10^{-8}	9.90	14.86	6.93	2.26
	60		4.42	3.74	3.71	1.06
^{241}Am	23	2.09×10^{-10}	49.79	21.26	3.85	<1
	60		9.69	15.32	23.80	2.17
^{241}Pu	23	1.62×10^{-11}	11.50	4.64	6.41	<1
	60		14.18	27.72	34.00	1.96

Dissolved Oxygen

The equilibrations at normal oxygen pressures ($\sim$0.2 atm) resulted in solutions that contained dissolved oxygen. The solution-dissolved oxygen content was measured with a calibrated Orion oxygen probe. Typical results are shown in Table 8. While there was some oxygen depletion evident in the secondary mineralization solutions, the basalt solutions remained largely unchanged. The differences in oxygen content between the 23° and 60°C solutions are due to temperature effects on gas solubility in aqueous solutions and not on oxygen depletion due to reactions with the solid. Secondary mineralization is an exception and probably contains small amounts of hydrated ferrous oxides, which changed in color from light blue to dark green upon exposure to air. However, even the secondary mineralization solutions contained appreciable oxygen at all times.

TABLE 8. Dissolved Oxygen in the Solution Contacting 20- to 50-Mesh Basalt Samples at 23° and 60°C. The 60°C solutions were left sealed and cooled to 23°C before oxygen measurements were made. The 8.3 mg/L O_2 corresponds to 4×10^{-2} atm O_2, or $\sim$one-fifth of the normal $\sim$0.2 atm.

Solid Weight/ Solution Volume, g/mL	23°C, Dissolved Oxygen, mg/L Secondary				
	Blank	Umtanum	Flow E	Pomona	Secondary Mineralization
	16 Days Contact Time				
1/10	8.25	8.00	8.30	8.20	
1/80	8.25	8.25	8.25	8.30	
	31 Days Contact Time				
1/10	8.25	8.15	8.30	8.30	
1/80	8.25	8.35	8.20	8.20	
	88 Days Contact Time				
1/10	8.25	-	-	-	5.70
1/80	8.25	-	-	-	7.10
	60°C, Dissolved Oxygen, mg/L				
1/10	5.10	5.30	5.50	5.50	3.90
1/80	5.10	5.00	5.05	5.10	4.95

Final Solution pH

Measurements of pH were completed on all experiments at the 23° and 60°C temperatures. Overall, the changes in solution pH by the presence of the geologic materials were relatively minor. Most of the measurements showed little change between the original and final solution pH values, as might be expected. The solution used in these studies (GR-1) was buffered by its content of bicarbonate ions. The pH of this solution would tend to remain constant in the presence of Hanford geologic materials.

The first group of pH data was taken on triplicate secondary mineralization samples and blanks (Table 9) to show that choosing and measuring a single representative from each group is a justified, time-saving, measurement procedure. The error associated with each measurement is ±0.2 of a pH unit. The remaining pH measurements for the various solid weight to solution volume ratios at 23° and 60°C are given in Tables 10 and 11. The pH values of the americium solutions changed significantly from blank to sample in both the 23° and 60°C solutions, declining in all solutions except those in contact with secondary mineralization. These were the samples in which americium precipitation was indicated by the Kd values. The pH effects with the secondary clay (secondary mineralization) may have been due to the hydrogen ions in solution produced by $Am(OH)_3$ precipitation (Am^{3+} + $3H_2O \rightleftharpoons Am(OH)_3 + 3H^+$).

LOW-OXYGEN ENVIRONMENT

Several experiments were also conducted at a low-oxygen environment, simulating transient repository conditions following repository closure.

14

TABLE 9. pH Values for Triplicate Samples of Secondary
Mineralization in GR-1 Groundwater.

Secondary Mineralization, 1 g/10 mL, 23°C, 67 Days Contact

Radionuclide	Solid-Solution			Initial Solution and Radionuclide		
^{75}Se	8.50,	8.48,	8.50	8.58,	8.52,	8.52
^{85}Sr	8.55,	8.57,	8.55	8.50,	8.52,	8.52
^{99}Tc	8.30,	8.30,	8.23	8.40,	8.32,	8.34
^{125}I	8.38,	8.50,	8.50	8.38,	8.48,	8.50
^{137}Cs	8.52,	8.55,	8.50	8.30,	8.50,	8.55
^{237}Np	8.28,	8.30,	8.28	8.30,	8.32,	8.30
^{238}U	8.30,	8.30,	8.25	8.25,	8.30,	8.30
^{241}Am	8.20,	8.20,	8.40	8.82,	8.80,	8.88
^{241}Pu	8.50,	8.55,	8.55	8.52,	8.48,	8.52

TABLE 10. Average pH Values for Samples at 1 g/80 mL and
23°C, GR-1 Groundwater.

Radio-nuclide	89 Days Contact				93 Days Contact	
	Blank Solution	Umtanum Basalt	Flow E Basalt	Pomona Basalt	Secondary Mineralization	Initial Solution and Radionuclide
^{75}Se	8.35	8.40	8.35	8.40	8.95	8.90
^{85}Sr	8.20	8.20	8.20	8.45	8.90	8.85
^{99}Tc	7.85	7.90	7.90	7.95	8.80	8.75
^{125}I	8.15	8.20	8.25	8.25	8.92	8.90
^{137}Cs	8.05	8.25	8.20	8.30	8.90	8.72
^{226}Ra	7.15	7.05	7.10	7.05	8.50	8.48
^{237}Np	7.55	7.50	7.60	7.55	8.70	8.50
^{238}U	8.65	8.65	8.60	8.65	8.78	8.70
^{241}Am	8.80	8.55	8.45	8.40	8.70	8.65
^{241}Pu	8.40	8.15	8.10	8.20	8.50	8.50

TABLE 11. Average pH Values for the 60°C Experiments, GR-1 Groundwater.

1 g/10 mL

| Radionuclide | 89 Days Contact | | | | 93 Days Contact | |
	Blank Solution	Umtanum Basalt	Flow E Basalt	Pomona Basalt	Secondary Mineralization	Blank Solution
^{75}Se	8.35	8.45	8.40	8.40	8.75	9.05
^{85}Sr	9.00	8.95	9.00	8.95	8.8D	8.95
^{99}Tc	8.10	8.35	8.35	8.45	8.50	8.68
^{125}I	8.80	8.80	8.8D	9.50	8.60	9.10
^{137}Cs	8.85	8.90	8.95	8.95	8.50	8.60
^{226}Ra	8.50	8.45	8.50	8.55	8.35	8.65
^{237}Np	8.85	8.80	8.90	8.85	8.60	8.65
^{238}U	8.85	8.90	8.90	8.95	8.60	8.72
^{241}Am	9.10	8.75	8.80	8.90	8.55	8.70
^{241}Pu	8.10	8.15	8.00	8.10	8.10	8.40

1 g/80 mL

Radionuclide	Blank Solution	Umtanum Basalt	Flow E Basalt	Pomona Basalt	Secondary Mineralization	Blank Solution
^{75}Se	8.25	8.75	7.70	7.80	8.85	8.90
^{85}Sr	8.90	8.60	8.35	8.40	8.40	8.40
^{99}Tc	8.10	8.35	8.40	8.40	8.1D	7.60
^{125}I	8.65	8.75	8.65	8.55	8.70	8.65
^{137}Cs	8.40	8.55	8.70	8.95	7.90	7.70
^{226}Ra	7.20	7.20	7.15	7.20	8.20	8.15
^{237}Np	8.10	7.85	7.90	7.95	8.40	8.25
^{238}U	8.30	8.30	8.35	8.30	8.65	8.60
^{241}Am	8.90	8.20	8.15	8.20	8.40	8.45
^{241}Pu	8.10	8.15	8.15	8.15	8.15	8.45

23°C Experiments

The fugacity capacity for oxygen in water at 23°C is 1.5 gmol/m^3, and in air is 40 gmol/m^3, a ratio of 26.67. In other words, oxygen in air at 8 gmol/m^3, for example, exerts the same fugacity of 0.2 atm as oxygen in water at 0.3 gmol/m^3 (10 p/m), and there is no net movement of oxygen between air and water (Mackay, 1979). Furthermore, fugacity is linearly proportional to concentration at the low-oxygen level (this study). Thus, the 26.67 ratio of oxygen fugacity capacities in air and in water can be used to estimate the oxygen partial pressure in solutions, when the oxygen partial pressure in the anoxic chamber atmosphere is ∿2.1 p/m, or 2.1 x 10^{-5} atm. The oxygen partial pressure in the solutions is ∿7.87 x 10^{-7} atm, far above the eventual repository condition of pyrite-magnetite oxygen equilibrium partial pressure of ∿10^{-60} atm. The anoxic chamber is still a mildly oxidizing environment at an atmospheric oxygen content of 2.1 p/m. Using Garrels and Christ's (1965) relationship between Eh, pH, and PO_2, Eh equals 1.23 + (0.059/4) log PO_2 - 0.059 pH. Assuming a pH of 8.0, the Eh is +0.668 V, or in a transitional environment between atmospheric contact and atmospheric isolation. This probably will be a reasonably representative repository environment immediately after repository closure.

The effects of low-oxygen partial pressure (∿7.87 x 10^{-7} atm O_2) on the Kd values for several radionuclides are given in Tables 12 and 13. The strontium was included for comparative purposes, with no effect expected as a result of low-oxygen partial pressure. Little or no enhanced selenium, technetium, neptunium, or plutonium sorption was apparent in the low-oxygen partial pressure environment utilized in these sorption experiments. There would almost certainly be observable effects on these radionuclide Kd values if the oxygen partial pressure approached the 10^{-60} atm predicted for the closed repository.

Included in the Kd values given in Tables 12 and 13 are corrections for container wall sorption. Strontium and technetium container wall sorption in the presence of secondary mineralization and basalts is minimal. The largest corrections were for plutonium at 14 to 21% sorption onto walls when Pomona basalt was present.

TABLE 12. Low-Oxygen Partial Pressure Sorption-Corrected Kd Values at 23°C and 53 Days of Contact at 1 g of Solid/10 mL of GR-1 Synthetic Groundwater.

Radio-nuclide	Initial Radionuclide Concentration, mol/L	Basalt Weight/ Solution Volume	Kd, mL/g			
			Flow E Basalt	Pomona Basalt	Umtanum Basalt	Secondary Mineralization
^{75}Se	2.63×10^{-13}	1 g/10 mL	1.0 ± 0.6	0	16.8 ± 4.0	3.3 ± 0.3
		1 g/2D mL	0.8 ± 0.7	0	-	5.5 ± 1.2
^{85}Sr	5.54×10^{-12}	1 g/10 mL	118 ± 5	157 ± 4	381 ± 136	-
		1 g/20 mL	139 ± 1	$2D1 \pm 4$	-	-
^{99}Tc	6.55×10^{-8}	1 g/1D mL	2.5 ± 1.7	0	$4,489 \pm 3165$	0
		1 g/20 mL	0	0	-	0
^{237}Np	6.47×10^{-8}	1 g/10 mL	11.2 ± 10.9	11.9 ± 2.5	148 ± 27	79 ± 10
		1 g/20 mL	0	0	-	87 ± 29
^{241}Pu	1.62×10^{-11}	1 g/10 mL	51.6 ± 14.4	70.8 ± 51.1	$5,190 \pm 3290$	415 ± 178
		1 g/20 mL	48.8 ± 35.3	62.9 ± 0.9	-	$1,814 \pm 439$

18

TABLE 13. Low-Oxygen Partial Pressure Sorption Corrected Kd Values
at $23^{\circ}C$ and 61 Days of Contact at 1 g of Solid/10 mL of
GR-2 Groundwater.

Radio-nuclide	Initial Radio-nuclide Concentration, mol/L	Kd, mL/g			
		Umtanum Basalt	Flow E Basalt	Pomona Basalt	Secondary Mineralization
^{85}Sr	2.63×10^{-13}	249 ± 49	206 ± 27	298 ± 93	278 ± 74
^{75}Se	5.54×10^{-12}	0.6 ± 0.3	0.4 ± 0.7	1.7 ± 1.6	2.2 ± 0.8
^{99}Tc	6.55×10^{-8}	35 ± 8	7.4 ± 3.9	3.4 ± 0.4	3.9 ± 0.2
^{237}Np	6.47×10^{-8}	58 ± 17	12.2 ± 1.9	5.9 ± 1.7	127 ± 30
^{241}Pu	1.62×10^{-11}	5.6 ± 0.3	3.1 ± 1.1	5.7 ± 0.6	$8,264 \pm 12,166*$
^{233}U	8.16×10^{-9}	9.3 ± 1.0	1.6 ± 0.7	2.0 ± 0.9	108 ± 23

*Nearly complete adsorption.

150° and $300^{\circ}C$ Experiments

The higher temperature Kd methodology was reviewed in Ames and McGarrah
(1980). Briefly, the method consists of using 300 to 500 mL, unstirred,
pressure vessels to contain the synthetic groundwaters and basalt or secondary
mineralization at 150° or $300^{\circ}C$. The vessels are fabricated of Inconel
600 alloy and lined with Teflon or Zircaloy to minimize wall reactions.
Physical stirring of the vessel contents was avoided to prevent a generation
of fines and an increase in surface area. Samples were taken at intervals at
temperature and pressure for up to 60 d from the beginning of the experiment.
A sketch of a typical pressure vessel is shown in Figure 1. Sorption
corrections on vessel walls was not possible in an above-atmospheric-pressure
system. The distribution coefficients derived from the counting of samples
taken at intervals were reproducible and little affected by increases in
pressure from 6.9 to 27.6 MPa.

Depending on the physical conditions prevailing in a repository,
lithostatic pressure represents an upper pressure limit. At a depth of 1 km
of basalt, the lithostatic pressure is ~27 MPa (3,916 lb/in.^{2}). Radio-
nuclide distribution coefficients are not directly affected by pressures of
that magnitude, but could be indirectly affected by ongoing mineral phase and
gross solution composition changes due to lithostatic (maximum) system
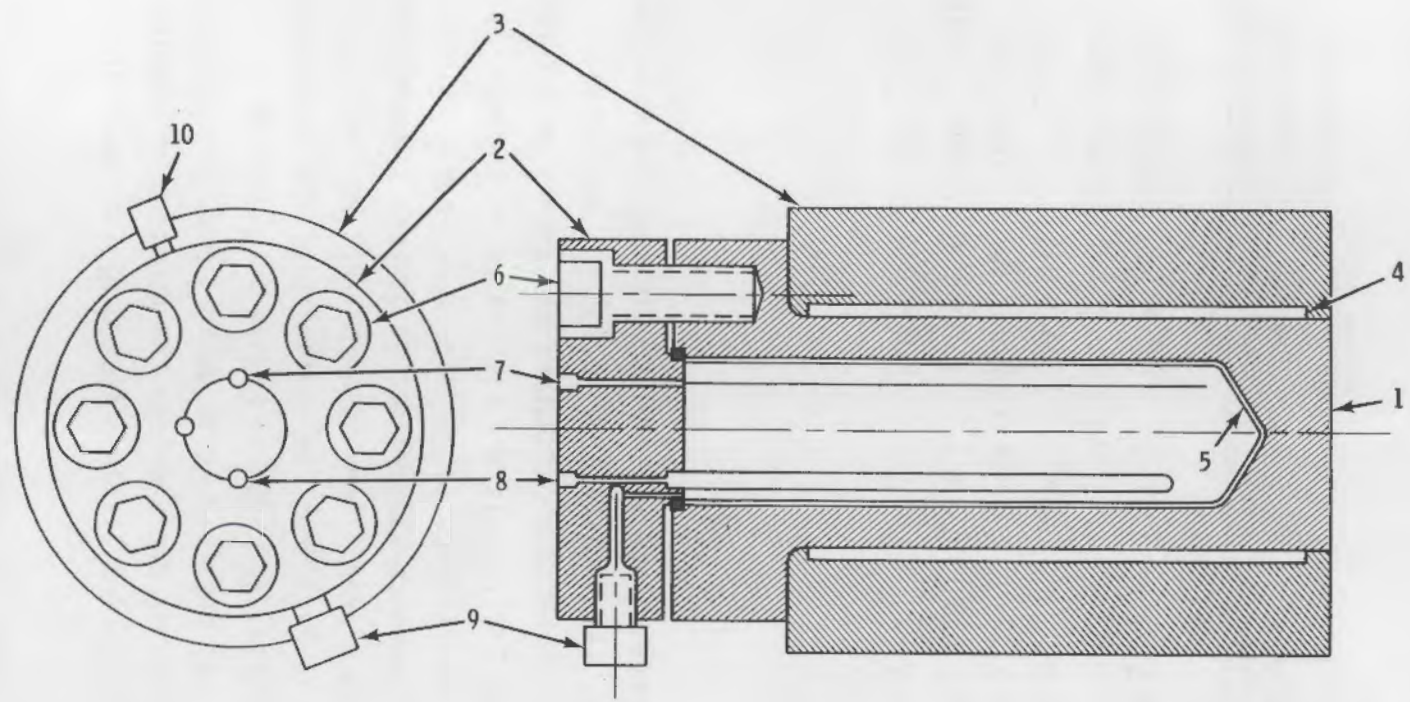
1. VESSEL BODY, INCONEL 600
2. VESSEL COVER, INCONEL 600
3. VESSEL HEATER INSULATION
4. BLADE HEATER, 750 W 240 V
5. TEFLON LINER

6. HEX SOCKET HEAD CAP SCREWS
7. SAMPLE APERTURE
8. THERMOCOUPLE APERTURE
9. RUPTURE DISC ASSEMBLY, INCONEL 600
10. GAS APERTURE

RCP8107-4

FIGURE 1. Sketch of the Basic 300-mL Inconel 600 Pressure Vessel.

pressures. The effect of pressure on reactions that result in phase and solution composition changes is given by LeChatelier's rule (Berner, 1971; Krauskopf 1979):

$$\frac{d\Delta G}{dP} = \Delta V \tag{1}$$

or the rate at which the reaction-free energy (d) change varies with pressure (P) is equal to the overall volume (V) change involved in the reaction. Thus, pressure would have a significant effect on the reaction only if the secondary phases produced are minerals of very high or low density compared to the original mineral phase. The above expression cannot be directly used to determine pressure effects, but the densities of smectites, zeolites, and opal, the usual basalt secondary reaction products, are similar to the density of the original basalt glassy phase, as seen in Table 14. Although measured density differences between the most reactive basalt constituent, the glassy phase, and its known reaction products cover a range, these differences are small and were not expected to appreciably affect the above reaction products. Hence, pressure effects on both reactions and their dependent Kd were expected to be minimal.

TABLE 14. Density Differences Between Original Basaltic
Glass and Reaction Products (Clark, 1966).

Density, g/cm^3		
Original Glass	Known Reaction Products	
2.5 to 2.7	Smectites	2.2 to 2.6
	Heulandite	2.1 to 2.2
	Potassium Feldspar	2.5 to 2.6
	Opal, Quartz	2.2 to 2.6

On the other hand, temperature effects were not expected to be minimal. Physical and chemical evidence from $300^\circ C$ nonradioactive experiments showed that both silica and potassium increased in concentration in the solution initially, while magnesium and calcium in solution decreased. At $300^\circ C$, phase changes for basalt involved dissolution of the glassy phase and precipitation of a potassium feldspar, an unidentified layer silicate, and quartz. The original glass was high in silica and potassium content. Solution

silica content increased to 1,200 mg $(H_4SiO_4)^O/1$ at 300°C. The solubility of amorphous silica in water at high temperatures is well documented (Fournier and Rowe, 1977; Potter et al., 1978) with solubility at the vapor pressure of the solution from 0° to 25°C given by: $\log C = -731/T + 4.52$, where C is the silica concentration in mg/kg of solution and T is the absolute temperature.

The solution volume to solids weight ratio used in the 150° and 300°C experiments was 250 mL per 25 g or 10:1. Other ratios will be investigated in future work. The relatively low volume to weight ratio was used initially to ensure that enough of the glassy portion of the basalt contacted the solution to attain solution-glass near-equilibrium as rapidly as possible at that temperature. The radionuclide concentrations used in the solutions are given in Table 15. The ^{238}U was determined chemically rather than by counting techniques. Uranium-233 is presently used as a uranium tracer.

TABLE 15. Radionuclide Concentrations Used in the 150° and 300°C Sorption Experiments.

Radionuclide	Disintegrations/ min/mL	Molarity
^{75}Se	4,200	1.74×10^{-12}
^{85}Sr	5,700	1.26×10^{-12}
^{99}Tc	1,570	4.16×10^{-7}
^{125}I	3,500	7.24×10^{-13}
^{137}Cs	4,800	1.83×10^{-10}
^{237}Np	600	1.62×10^{-6}
^{238}U	*	1.01×10^{-6}
^{241}Am	4,000	2.31×10^{-9}
^{241}Pu	9,000	1.51×10^{-10}

*Determined by argon plasma emission spectrometer.

To reduce potential sorption of radionuclides on Inconel 600 vessel walls, a Teflon liner was machined to fit the vessel interior. This liner worked well in most cases, reducing radionuclide vessel wall sorption to zero, but failed to reduce the sorption of plutonium and americium.

Inconel 600 does not resist oxidative corrosion in contact with the atmosphere at the relatively high temperatures and pressures used in these pressure vessels. Chromium, nickel, and cobalt could be added to the solutions if partial pressures of oxygen attained those values associated with using compressed air as a pressurization medium. Therefore, every effort was made to remove oxygen from the solution and the ~50 mL of air space above it were sparged with argon before bringing the vessel to running temperature and pressure. Argon of 99.99% minimum purity was used for pressurization. There was no practical way of measuring the oxygen content of the solution in the vessel, but analyses of solutions in contact with the Inconel 600 alloy were made. These analyses showed that nickel, cobalt, and chromium were below argon plasma emission spectrometer detection limits (<0.01 mg/L for each of the above), indicating negligible oxidative corrosion of the pressure vessels.

Initial experiments included sampling every 3 or 4 d over a time interval of ~50 d to determine the length of time required to attain near-equilibrium between solution, mineral, and radionuclide. The distribution results for cesium with 20- to 50-mesh Umtanum basalt at 250°C and 6.9 MPa (1,000 lb/in.^{2}g) are shown as an example of the sampling results in Figure 2: note that the distribution coefficient slowly increases to 98 mL/g and remains there. The pressure vessel was Teflon lined and was maintained at 6.9 MPa with argon. Near-equilibrium was attained after ~25 d of basalt-solution contact time. Cesium is predominantly a univalent and uncomplexed cation in aqueous solutions (Izrael and Rovinskii, 1970), and, hence, is presumably confined to ion exchange reactions.

The effect on cesium distribution coefficients of using the pressure vessel without a liner is shown in Figure 3. More time was required to reach near-equilibrium, and vessel wall sorption was added to sorption on the basalt sample. Hence, the unlined vessel cesium distribution coefficient at 150°C was 119.6 ± 4.5 mL/g compared to the lined vessel cesium distribution at 150°C of 98.0 ± 3.9 mL/g. Not all of the cationic radionuclides reacted in the same manner as cesium. Strontium, for example, was removed quantitatively from the solution at 300°C despite its ionic nature (Izrael and Rovinskii, 1970). The strontium was probably incorporated into the structure of a growing potassium feldspar reaction product. Radium also has been shown to concentrate in secondary reaction products (Ames and Rai, 1978).
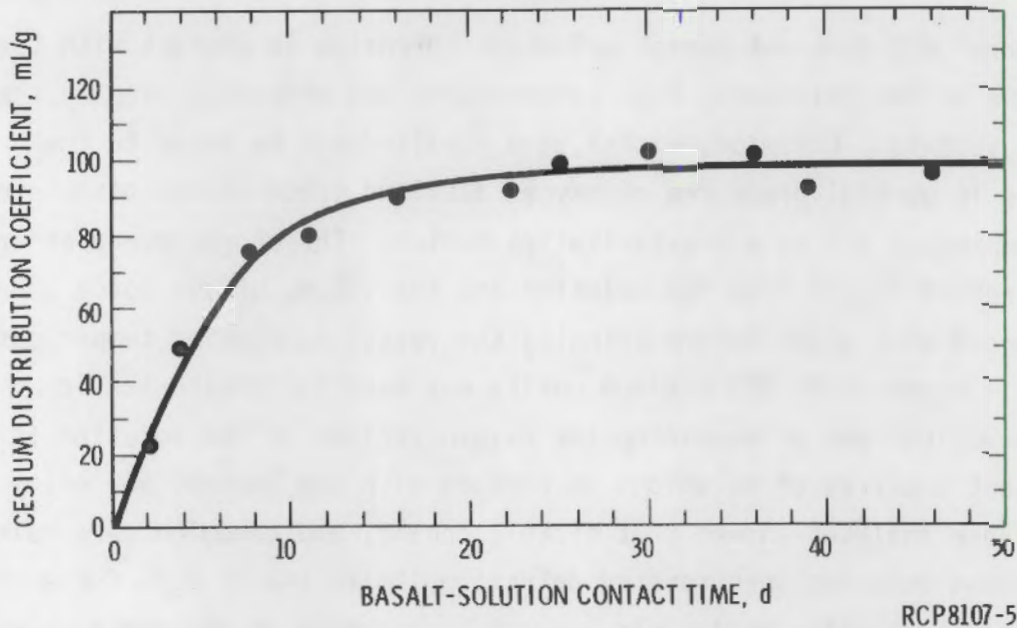
FIGURE 2. Cesium Distribution Coefficients for 20- and 50-Mesh Umtanum Basalt
and Synthetic Groundwater at 150°C and 6.9 MPa. The pressure ves-
sel was Teflon lined. The distribution mean for the last five values
was 98.0 mL/g, with an estimated standard deviation of 3.9 mL/g.
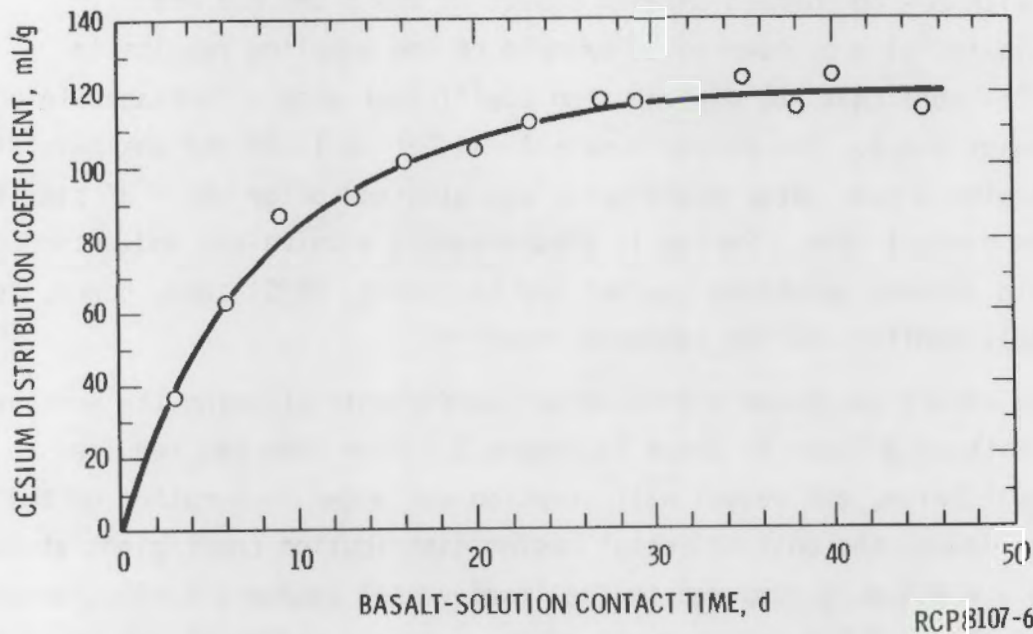
FIGURE 3. Cesium Distribution Coefficients for 20- and 50-Mesh Umtanum
Basalt and Synthetic Groundwater at 150°C and 6.9 MPa. The
Inconel 600 pressure vessel was unlined. The distribution
mean for the last five values was 119.6 mL/g, with an estimated
standard deviation of 4.5 mL/g.

A repeat of the experiment shown in Figure 2, with an increase in system pressure from 6.9 to 27.6 MPa (1,000 to 4,000 lb/in.^{2}g), is shown in Figure 4. Note that, while there is a somewhat greater range in data points, and the reaction kinetics appear to be more rapid, the cesium distribution coefficient is essentially the same at both pressures as expected.

RCP8107-7
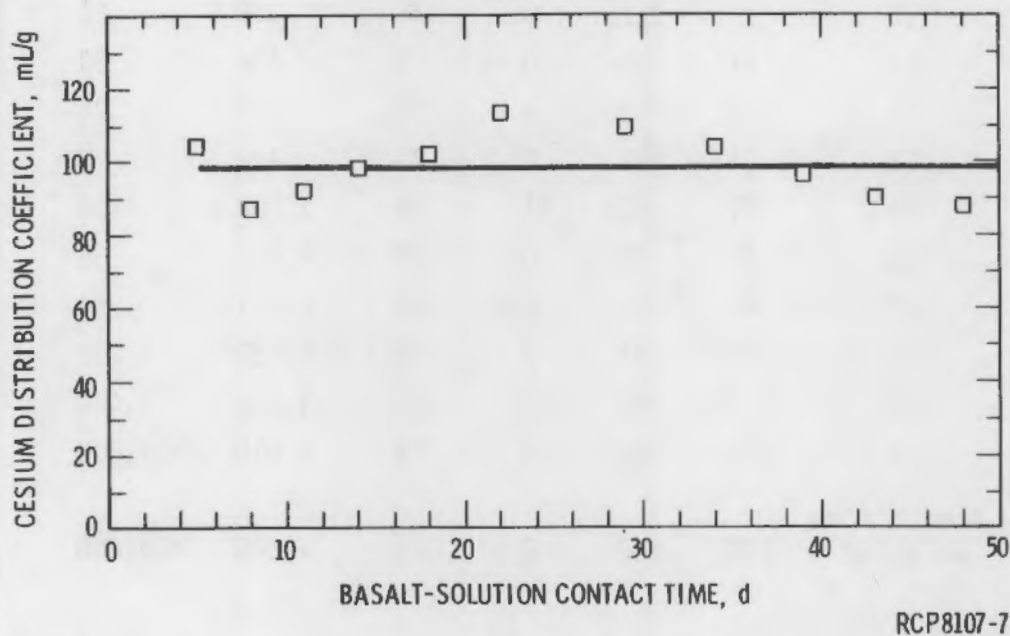
FIGURE 4. Cesium Distribution Coefficients for 20- to 50-Mesh Umtanum Basalt and Synthetic Groundwater at 150°C and 27.6 MPa. The Inconel 600 pressure vessel was Teflon lined. The distribution mean for 11 values was 98.4 mL/g, with an estimated standard deviation of 8.8 mL/g.

The 150° and 300°C Kd results are given in Tables 16 through 19. Various aspects of Kd response to temperature change can be discerned in these data. For example, iodine showed little tendency to adsorb on solids or become involved in secondary mineral formation. Strontium Kd tended to increase with temperature, while cesium Kd decreased to 150°C and then increased to 300°C as shown in Figures 5 and 6 for the Umtanum and Flow E basalts.

TABLE 16. Uncorrected Kd Values for Basalts in
Teflon-Lined Pressure Vessels at
150°C and 6.9 MPa Argon.

Contact Time, d	Flow E Kd, mL/g					Umtanum
	^{75}Se	^{85}Sr	^{125}I	^{137}Cs	^{241}Pu	^{241}Am
3	13	133	0	99	687	14
7	18	108	0	74	377	15
11	19	112	0	78	339	21
14	23	99	0	73	408	20
17	23	85	0	73	579	28
22	24	89	0	71	769	26
29	19	91	11	74	1,040	26
32	37	79	0	66	4,822	36
37	44	83	0.1	68	4,017	54
42	16	75	0	59	4,822	1,210
45	113	86	9	77	4,822	2,430
48	122	89	8	75	3,010	>10,000
Approximate Kd Value	100	100	0	73	4,000	>10,000

Contact Time, d	Umtanum Kd, mL/g				
	^{75}Se	^{85}Sr	^{125}I	^{137}Cs	^{238}U
2	19	212	9	23	>34
4	33	4,423	16	49	>34
8	100	>10,000	16	75	>34
11	311	251	21	80	>34
16	95	1,468	20	91	>34
22	126	232	16	92	>34
25	75	340	12	98	>34
30	82	536	0	102	>34
36	85	946	0	101	>34
46	105	>10,000	0	97	>34
Approximate Kd Value	100	1,000	0	100	>34

TABLE 17. Kd Values for Secondary Mineralization and Pomona Basalt at 150°C
and 6.9 MPa Argon, Uncorrected for Vessel Wall Sorption.

	Kd, mL/g				
	Secondary Mineralization				Pomona Basalt
Contact Time, d	^{137}Cs	^{125}I	^{75}Se	^{241}Pu	^{241}Am
2	205	2.1	8	2,139	81
6	120	0	41	1,141	53
9	351	0	81	3,571	64
13	590	0	156	2,676	102
16	556	0	134	3,571	77
20	560	0	119	4,019	81
23	604	0.6	208	2,676	96
27	463	0.5	358	2,004	109
30	525	0	88	2,200	106
34	624	0	134	2,350	136
Approximate Kd Value	600	0	200	2,500	100

TABLE 18. Cesium-137 Kd Values for Umtanum and Flow E Basalts at 300°C
and 9.2 MPa Argon, Uncorrected for Vessel Wall Sorption.

	Kd, mL/g	
Contact Time, d	Umtanum Basalt	Flow E Basalt
4	318	127
7	434	175
11	434	228
17	388	216
20	383	226
24	382	214
28	356	228
31	244	273
34	199	262
38	156	200
42	242	192
Approximate Kd Value	321	213

TABLE 19. Uranium-238 Kd Values for Umtanum and Flow E
Basalts at 300°C and 10.4 MPa Argon,
Uncorrected for Vessel Wall Sorption.

| | Kd, mL/g | |
Contact Time, d	Umtanum Basalt	Flow E Basalt
3	100	100
7	100	30.0
10	100	40.0
14	100	23.3
18	100	15.0
23	100	18.6
28	100	18.6
29	100	40.0
32	100	90.0
35	100	100
39	100	100
42	100	100
43	100	100
Approximate Kd Value	100	60
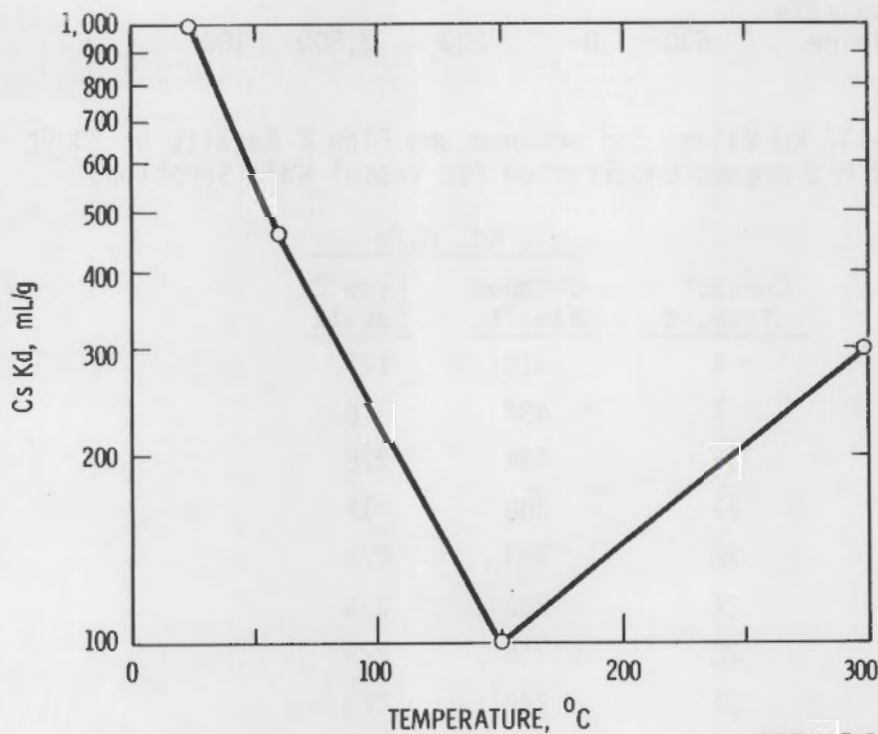
FIGURE 5. Cesium Kd Values for Umtanum Basalt at Several Temperatures.
GR-1 synthetic groundwater was used as the original solution.
Pressures vary from 0.1 at 23° and 60°C to 6.9 MPa argon at
150°C and 10.4 MPa argon at 300°C.

RCP3107-8

28
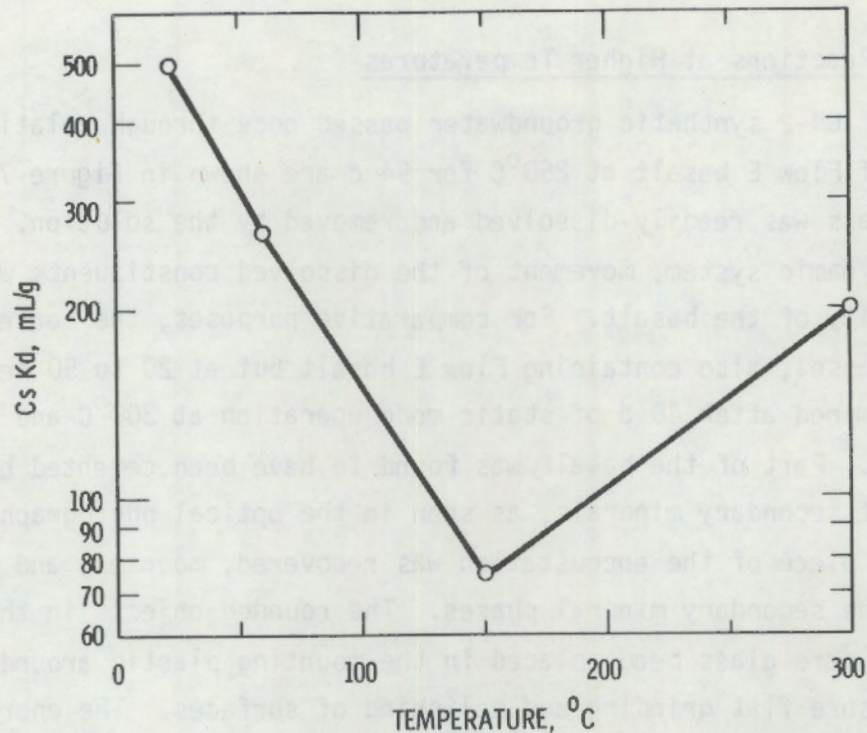
FIGURE 6. Cesium Kd Values for Flow E Basalt at Several Temperatures. GR-1
synthetic groundwater was used as the original solution. Pres-
sures vary from 0.1 at 23° and 60°C to 6.9 MPa at 150°C and
10.4 MPa argon at 300°C, respectively.

RCP8107-9

Distribution coefficient values for plutonium and americium were so large
that they became essentially meaningless, especially at high temperatures;
i.e., there was essentially complete adsorption on vessel walls, resulting in
a fraction with zero as the denominator. Complete sorption on the Teflon
liner occurred with no basalt present as well. Both radionuclides were
probably present at the pH 8.0 of the synthetic groundwater as charged
colloidal polymers (Cleveland, 1979) that tended to further polymerize and
sorb on surfaces as a result of increasing temperature and solution ionic
strength (Andelman and Rozzell, 1970; Lloyd and Haire, 1973). This process
cannot be properly described by ion exchange concepts such as the distribution
coefficient. However, plutonium and americium are removed from solution to
levels below their counting detection limits (<1 disintegration/min/mL) and,
hence, will not migrate under the experimental conditions.

Macrochemical Reactions at Higher Temperatures

Results of GR-2 synthetic groundwater passed once through relatively large chunks of Flow E basalt at $250^{\circ}C$ for 94 d are shown in Figure 7. The glassy groundmass was readily dissolved and removed by the solution. In the case of this dynamic system, movement of the dissolved constituents was away from the vicinity of the basalt. For comparative purposes, the contents of the pressure vessel, also containing Flow E basalt but at 20 to 50 mesh in size, were examined after 40 d of static mode operation at $300^{\circ}C$ and 10.4 MPa argon. Part of the basalt was found to have been cemented by an encrustation of secondary minerals, as seen in the optical photographs (Figure 8). A piece of the encrustation was recovered, mounted, and polished to determine the secondary mineral phases. The rounded objects in the 6.3X view (Figure 8) are glass beads placed in the mounting plastic around the specimen to ensure flat grinding and polishing of surfaces. The encrusting material is a darker gray than the surrounding plastic mounting medium. Note that the darker gray cementing minerals apparently occupy spaces within the Flow E basalt fragments; i.e., the original glassy groundmass was dissolved at least in part and the present material deposited therein. When the deposition occurred is not known because of the quenching method (air cooling) used to cool the pressure vessel between experiments. All of the secondary mineral deposition could have occurred during cooling of the vessel.

The same area shown in the lower optical photographs also is shown in the electron scattering area. The lighter colored, bottom area of the view is of the mounting plastic, while the upper area, including chemical analysis sites 1 and 2, are the secondary minerals. Analysis site 3 is not as easily distinguished, but is in a replaced groundmass area in the upper middle portion of the central Flow E basalt fragment. The primary crystals (plagioclase, pyroxenes, metallic oxides) in the basalt were essentially unchanged by their 40-d exposure to the $300^{\circ}C$ hydrothermal environment. The X-ray emission photographs (Figure 9) show the extent of the secondary mineralization, especially the potassium X-ray emission photograph. The chemical analyses of sites 1, 2 and 3 are given in Table 20 along with chemical analyses of the original Flow E glassy groundmass. Essentially only silica, alumina and potassium were contained in the original groundmass. The

50X

100X

250X

250X

250X

500X

6.3X

500X
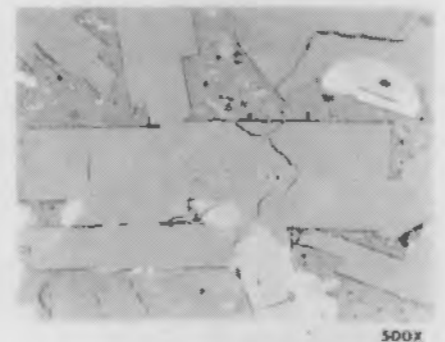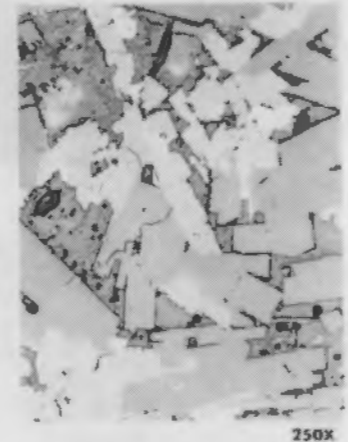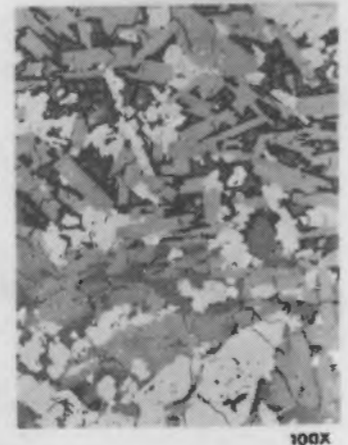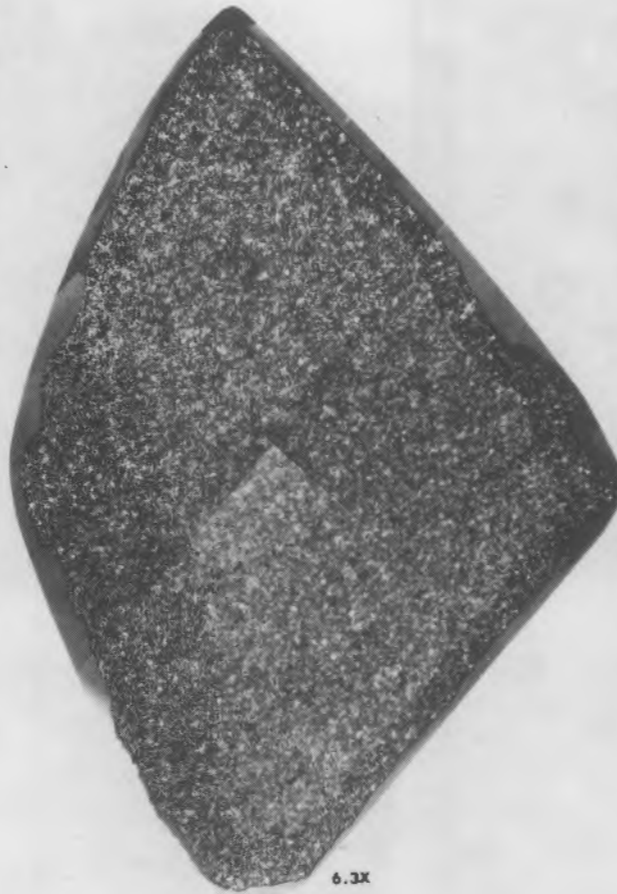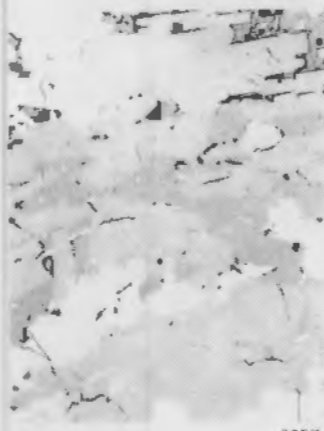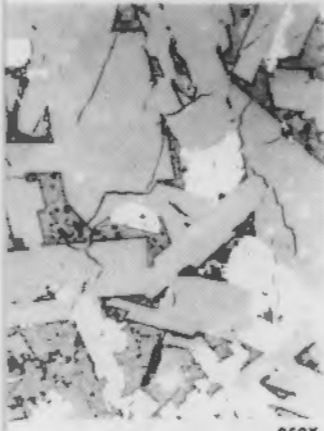
RCP8107-143

FIGURE 7. Flow E Basalt.
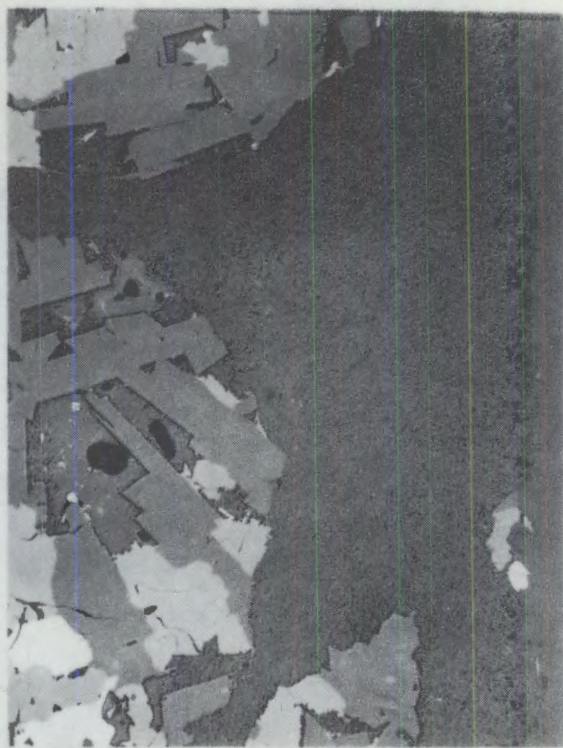
FIGURE 8.   Flow E Basalt Encrustation Optical Photographs.
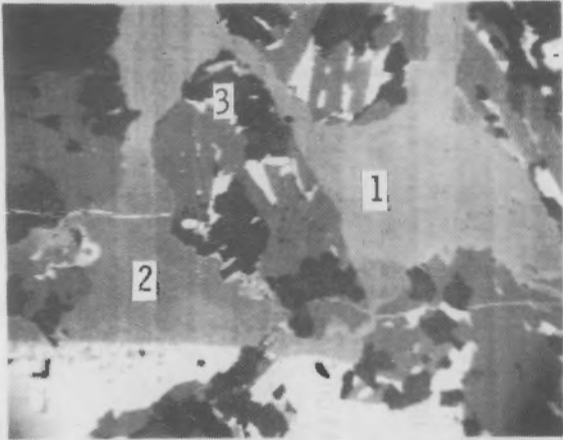
Electron Scattering, 100X
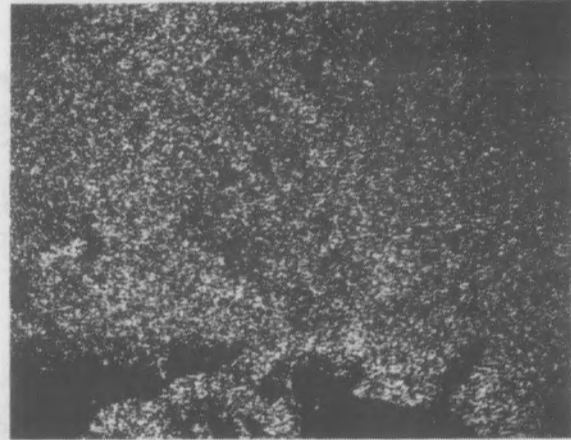
Si , 100X

K
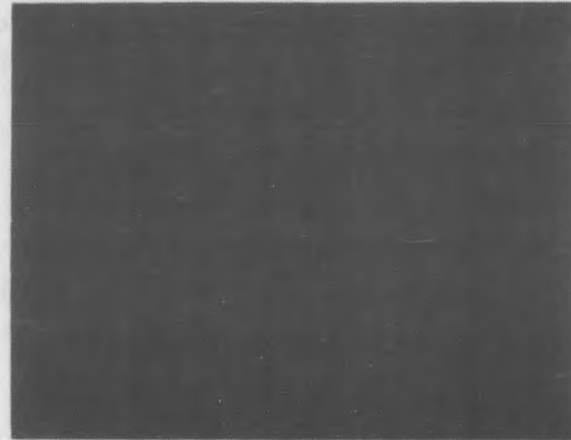
Na

RCP8107-145

FIGURE 9. Flow E Basalt Encrustation Element Dot Maps.

TABLE 20. Flow E Basalt Alteration Products After 40 Days at 300°C
and 10.34 MPa Argon. The orthoclase feldspars[a,b,c]
are located as shown in the electron scattering photographs.

	wt%				
Constituent	Orthoclase Feldspar[a]	Orthoclase Feldspar[b]	Orthoclase Feldspar[c]	As-Received Groundmass	
SiO_2	67.5	68.3	65.5	80.1	79.5
TiO_2	0.1	-	-	0.8	0.5
Al_2O_3	15.5	15.0	16.7	12.7	12.3
FeO	0.8	0.1	1.6	1.2	1.1
BaO	D.1	0.1	-	-	-
CaO	0.1	-	1.9	0.3	0.3
MgO	0.1	0.1	0.3	-	-
K_2O	14.4	14.8	13/8	4.9	5.8
Na_2O	0.7	0.3	0.8	0.5	0.8
Total	99.0	98.9	100.6	100.5	100.3

-----

[a]$(K_{3.72}, Na_{0.28})(Al_{3.69}, Si_{12.23})O_{32}, \sim 92\%; SiO_2, \sim 8\%.$
[b]$(K_{3.86}, Na_{0.12})(Al_{3.61}, Si_{12.33})O_{32}, \sim 92\%; SiO_2, \sim 8\%.$
[c]$(K_{3.26}, Na_{0.29}, Ca_{0.38})(Al_{3.66}, Si_{12.18})O_{32}, \sim 100\%.$

analysis at site 3 exhibited more than the usual amount of calcium found in a
potassium feldspar and may contain a small amount of plagioclase. The other
analyses were chiefly of potassium feldspar (orthoclase, microcline, or
adularia) with ~ 8 wt% quartz. Potassium feldspars normally contain
<1 wt% strontium oxide, but this would be more than adequate to explain the
disappearance of strontium radionuclides from solution with increasing
temperature. It is obvious that the potassium, silica, and alumina from the
basalt glassy groundmass are responsible for the quartz and potassium feldspar
secondary mineralization at 300°C.

Composition Changes in the Synthetic Groundwater
Due to Contact with Solids at Lower Temperatures

Chemical analyses of 31-d contacting solutions at 23° and 60°C are
given in Table 21. Potassium has not been included in these inductively
coupled plasma (ICP) spectrophotometer analyses because the apparatus was not

TABLE 21. Inductively Coupled Plasma Spectrophotometer Analyses of
Basalt-Contacting Synthetic Groundwater Solutions. Values
are given in milligrams per liter (parts per million). The 1/10
and 1/80 refer to grams of basalt per milliliter of solution.

| Original Constituent | 23°C, 31 Days | | | | | | 150°C, 30 Days | |
| | Umtanum Basalt | | Flow E Basalt | | Pomona Basalt | | Umtanum Basalt | Initial Solution |
	1/10	1/80	1/10	1/80	1/10	1/80	1/10	
Al	<0.1	<0.1	<0.1	<0.1	<0.1	<0.1	4.2	<0.1
As	<0.01	<0.01	<0.01	<0.01	<0.01	<0.01	0.05	<0.01
Ca	7.1	7.5	6.1	6.8	9.1	7.0	0.3	7.4
Cu	<0.01	<0.01	<0.01	<0.01	<0.01	<0.01	0.02	0.02
Fe	<0.1	<0.1	<0.1	<0.1	0.3	0.2	0.4	<0.1
Li	<0.05	<0.05	<0.05	<0.05	<0.05	<0.05	0.06	<0.05
Mn	0.08	<0.01	<0.01	0.01	0.01	0.01	0.01	<0.01
Mg	2.3	1.4	3.1	1.8	4.4	2.6	<0.05	1.1
Na	37	35	34	36	35	36	57	36
P	2.8	0.1	0.1	0.1	0.3	<0.1	0.3	0.1
Si	7.4	2.2	9.6	2.6	18.4	5.5	138.1	0.2
Sr	0.02	0.02	0.01	0.01	0.06	0.03	<0.01	0.01

| | 60°C, 31 Days | | | | | | | |
| | Umtanum Basalt | | Flow E Basalt | | Pomona Basalt | | Secondary Mineralization | |
	1/10	1/80	1/10	1/80	1/10	1/80	1/10	1/80
Al	0.14	0.31	0.12	0.20	<0.1	<0.1	<0.1	<0.1
As	<0.01	0.03	<0.01	<0.01	<0.01	<0.01	<0.01	<0.01
B	0.01	0.01	<0.01	<0.01	<0.01	<0.01	0.10	0.02
Ba	<0.01	<0.01	<0.01	<0.01	<0.01	<0.01	0.04	0.02
Ca	5.2	7.5	4.2	7.2	7.3	6.9	22.0	11.3
Fe	0.15	<0.10	<0.10	<0.10	<0.10	<0.10	0.56	0.98
Mn	<0.01	0.01	<0.01	<0.01	<0.01	<0.01	<0.01	<0.01
Mg	1.2	1.3	1.7	1.7	3.0	2.0	10.6	6.0
Na	38.6	39.7	37.9	40.0	38.6	38.3	26.9	31.7
P	<0.1	0.11	<0.1	0.1	0.11	<0.10	0.11	0.66
Si	20.4	10.3	25.2	10.1	33.8	14.7	18.6	14.0
Sr	0.01	0.01	0.01	0.01	0.04	0.03	0.18	0.09

set up for low-level potassium analyses. This capability will be included in future work with solution compositions. As can be seen in Table 20, two of the basalt samples leached a small amount of aluminum in solution at $60^{\circ}C$, whereas none was present at $23^{\circ}C$, except for one at the limit for aluminum. The $60^{\circ}C$ solutions also contained boron and barium. The high calcium and magnesium in the secondary mineralization solutions may represent calcite impurity or exchangeable cations on the secondary mineralization at $60^{\circ}C$. Also, 1 g of basalt/10 mL-solution samples contained much more silicon than the 1 g/80 mL solution samples. Apparently, the 1 g/80 mL ratio samples require more time to reach solid-solution equilibrium than the 1 g/10 mL ratio.

Sorption of anionic radionuclides, such as those of iodine, selenium, uranium, and technetium, is relatively low to zero. The results of ion chromatography (F^-, Cl^-, SO_4^{2-}) and ICP analyses of synthetic groundwater contacted with Umtanum basalt are shown in Table 22. The solution volume to basalt weight ratio was 1 g/5 mL. The basalt-contacted, groundwater anionic species content rose in all cases except for chlorine, which stayed essentially the same. In addition to the fact that most basalts exhibit a limited anion exchange capacity, they often contribute competing anionic species to the system. Hence, the low to zero sorption shown by anionic radionuclide forms might be expected. In this study, the final solution composition was usually not the initial solution composition. The higher the temperature of solid-solution equilibration, the greater the disparity between GR-1 and GR-2 original and final compositions.

TABLE 22. Determination of Anionic Species Present in a
Synthetic Groundwater Contacted 108 Days
with 20- to 50-Mesh Umtanum Basalt at $23^{\circ}C$.

	mg/L	
Constituent	Original Synthetic Groundwater	Umtanum Basalt + Synthetic Groundwater, 108 d
F^-	0.06	0.30
Cl^-	18	17
SO_4^{2-}	10	23
As	<0.01	0.02
B	<0.01	0.02
P	0.05	0.10

RADIONUCLIDE CONCENTRATION EFFECTS ON Kd

The concentration levels of radionuclides can be expected to vary over a range due to changes in the thermal and physicochemical status of the repository with time. The radionuclide Kd value is sensitive to concentration level changes above the trace range. Several experiments are under way to determine Kd values over a radionuclide concentration range and to establish the extent of the valid Kd range.

CESIUM AND STRONTIUM

The cesium and strontium isotherm experiments with GR-1 and GR-2 synthetic groundwaters were used to show the effects of concentration on Kd values. These experiments were performed at the 1 g solid:10 mL groundwater ratio at both the 23° and 60^oC temperatures for a solution-solid contact time of 54 d.

The Kd values for the strontium and cesium experiment are listed in Tables 23 and 24. For the cesium Kd values on all solids and strontium values for the basalts, there was a steady increase in Kd when going from higher to lower concentrations. The Kd values tended to eventually level off, with little effect caused by changes in concentration. The strontium Kd values for secondary mineralization for both 23° and 60^oC showed no change as a result of concentration increases. The Kd results of Tables 23 and 24 are graphically presented on log-log plots for strontium and cesium in Figures 10 through 25. The vertical lines are representative of the magnitude of the standard deviation for each Kd mean.

The cesium Kd values tended to be higher in the 23^oC isotherms and to level off at the $10^{-9}\underline{M}$ concentration for both temperatures. The strontium Kd values tended to remain constant for both temperatures and leveled off at the $10^{-7}\underline{M}$ concentration. The Kd results of GR-1 and GR-2 experiments suggest that those two groundwater compositions have little effect on the adsorption of strontium and cesium.

TABLE 23. Corrected ^{137}Cs and ^{85}Sr Kd Values in GR-1 Groundwater for 54 Days.

		^{137}Cs Kd, mL/g			
Temperature	Initial Molarity	Umtanum Basalt	Flow E Basalt	Pomona Basalt	Secondary Mineralization
23°C	10^{-3}	27 + 0	18 + 0	48 + 1	212 + 4
	10^{-5}	330 + 20	207 + 40	464 + 59	1,080 + 50
	10^{-7}	965 + 47	421 + 42	1,203 + 221	10,000 + 2,050
	10^{-9}	1,112 + 183	460 + 74	1,643 + 420	12,000
	10^{-10}	1,059 + 140	490 + 41	1,324 + 99	12,000
60°C	10^{-3}	18 + 1	12 + 0	39 + 2	167 + 3
	10^{-5}	195 + 11	140 + 23	328 + 9	960 + 144
	10^{-7}	449 + 19	225 + 26	699 + 29	12,400 + 4,400
	10^{-9}	473 + 33	269 + 8	752 + 31	11,600 + 2,500
	10^{-10}	475 + 27	284 + 8	903 + 68	11,800 + 2,900

		^{85}Sr Kd, mL/g			
23°C	10^{-4}	112 + 8	114 + 7	102 + 2	266 + 60
	10^{-6}	154 + 20	161 + 18	138 + 7	357 + 82
	10^{-8}	148 + 14	144 + 15	141 + 15	305 + 34
	10^{-10}	161 + 35	216 + 59	152 + 14	451 + 103
	10^{-12}	158 + 26	178 + 27	164 + 21	372 + 116
60°C	10^{-4}	112 + 8	76 + 3	101 + 4	470 + 181
	10^{-6}	132 + 19	133 + 3	157 + 19	599 + 110
	10^{-8}	154 + 48	147 + 17	190 + 35	942 + 620
	10^{-10}	173 + 24	142 + 11	176 + 21	380 + 62
	10^{-12}	151 + 18	144 + 28	225 + 58	1,078 + 129

TABLE 24. Corrected ^{137}Cs and ^{85}Sr Kd Values in GR-2 Groundwater for 54 Days.

		^{137}Cs Kd mL/g			
Temperature	Initial Molarity	Umtanum	Flow E	Pomona	Secondary Mineralization
25°C	10^{-3}	28 ± 1	20 ± 1	57 ± 1	228 ± 3
	10^{-5}	291 ± 15	213 ± 4	724 ± 58	2,125 ± 229
	10^{-7}	957 ± 109	494 ± 46	1,776 ± 393	5,968 ± 512
	10^{-9}	1,032 ± 151	558 ± 88	2,063 ± 173	9,795 ± 3,976
	10^{-10}	1,039 ± 248	610 ± 57	2,107 ± 280	10,000
60°C	10^{-3}	20 ± 1	15 ± 4	44 ± 1	153 ± 5
	10^{-5}	147 ± 3	107 ± 2	377 ± 22	1,162 ± 117
	10^{-7}	368 ± 27	219 ± 13	839 ± 26	10,000
	10^{-9}	416 ± 21	230 ± 9	959 ± 134	10,000
	10^{-10}	432 ± 7	253 ± 6	907 ± 46	4,885 ± 1,899

		^{85}Sr Kd, mL/g			
23°C	10^{-4}	84 ± 6	88 ± 11	125 ± 9	223 ± 50
	10^{-6}	155 ± 12	138 ± 14	163 ± 17	215 ± 58
	10^{-8}	141 ± 15	156 ± 25	163 ± 10	214 ± 41
	10^{-10}	138 ± 13	143 ± 20	188 ± 41	249 ± 49
	10^{-12}	133 ± 16	174 ± 16	185 ± 23	343 ± 82
60°C	10^{-4}	101 ± 13	115 ± 15	147 ± 17	304 ± 83
	10^{-6}	147 ± 19	144 ± 7	172 ± 12	275 ± 22
	10^{-8}	150 ± 8	135 ± 12	165 ± 19	273 ± 50
	10^{-10}	170 ± 22	137 ± 15	157 ± 21	226 ± 24
	10^{-12}	133 ± 15	154 ± 38	126 ± 6	239 ± 32

RCP8107-11
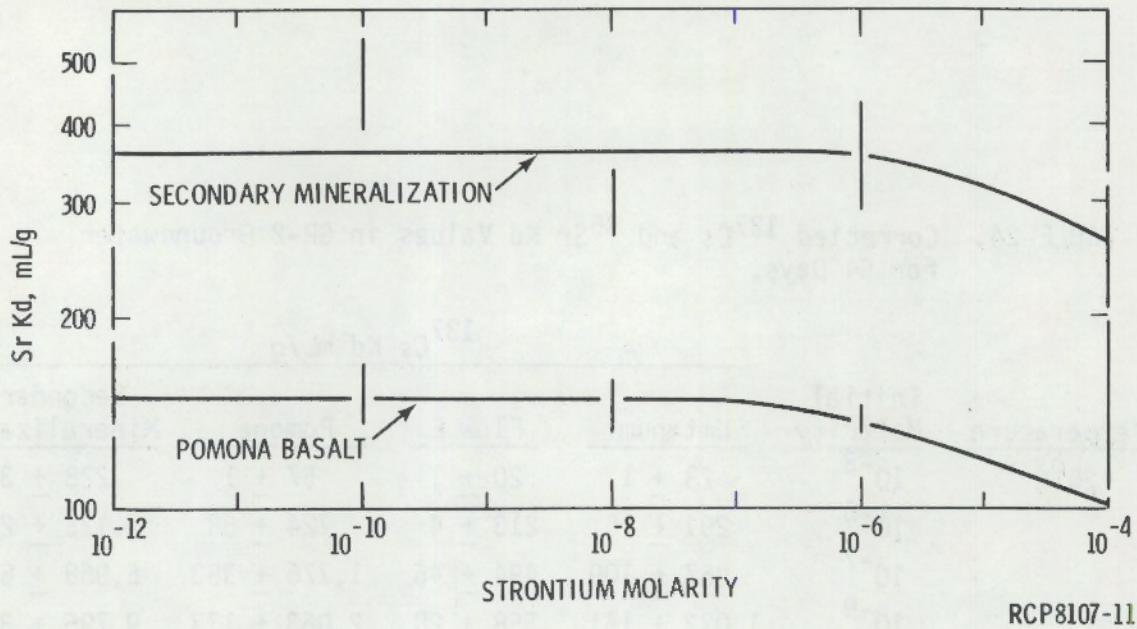
FIGURE 10. Graph of the Effects of Strontium Concentration on the
Kd Value at 23°C in GR-1 Groundwater.

RCP8107-10
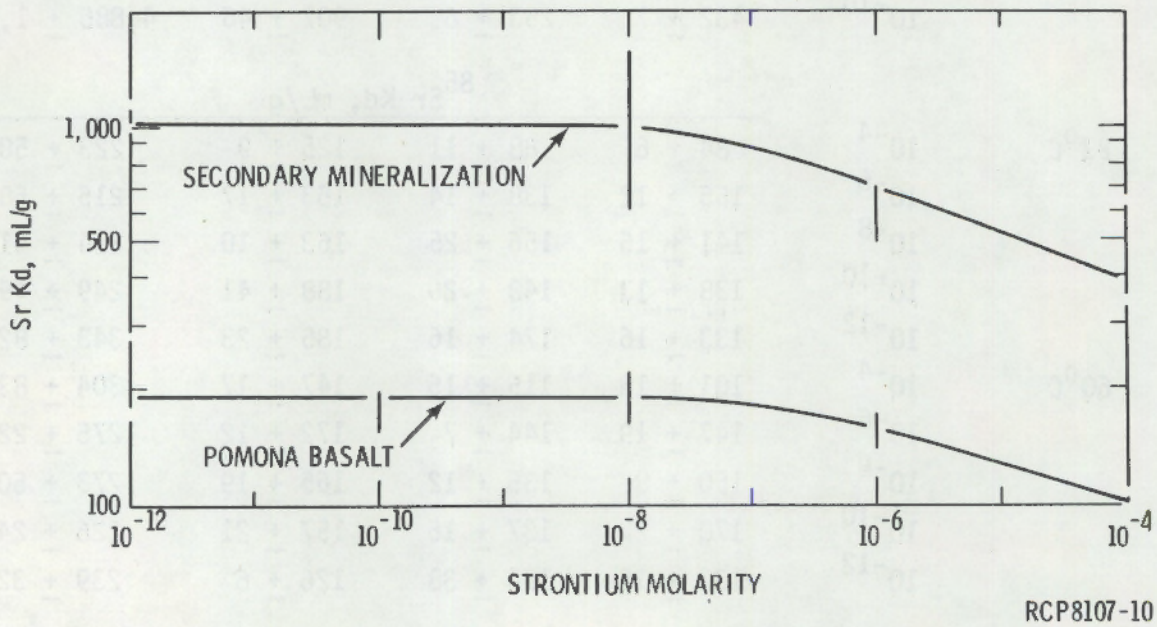
FIGURE 11. Graph of the Effects of Strontium Concentration on the
Kd Value at 60°C in GR-1 Groundwater.

40
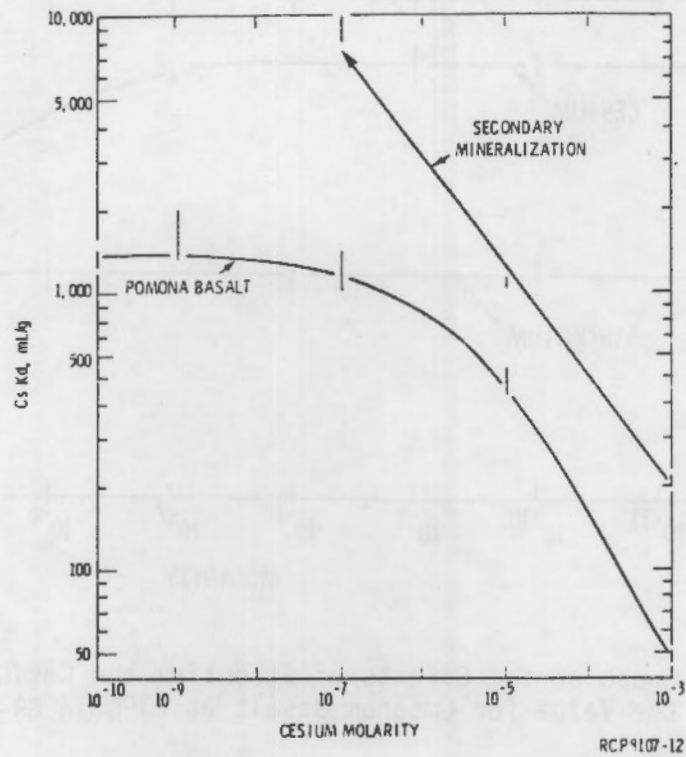
FIGURE 12. Graph of the Effects of Cesium Concentration on the Kd Value at 23°C in GR-1 Groundwater.
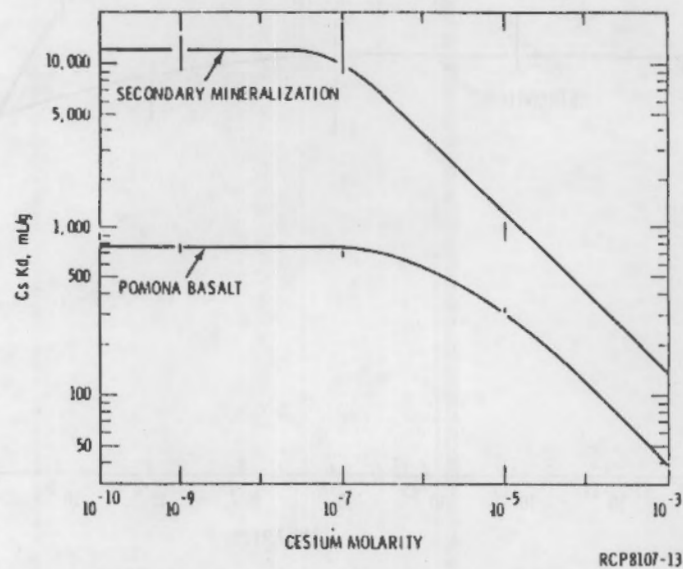
FIGURE 13. Graph of the Effects of Cesium Concentration on the Kd Value at 60°C in GR-1 Groundwater.
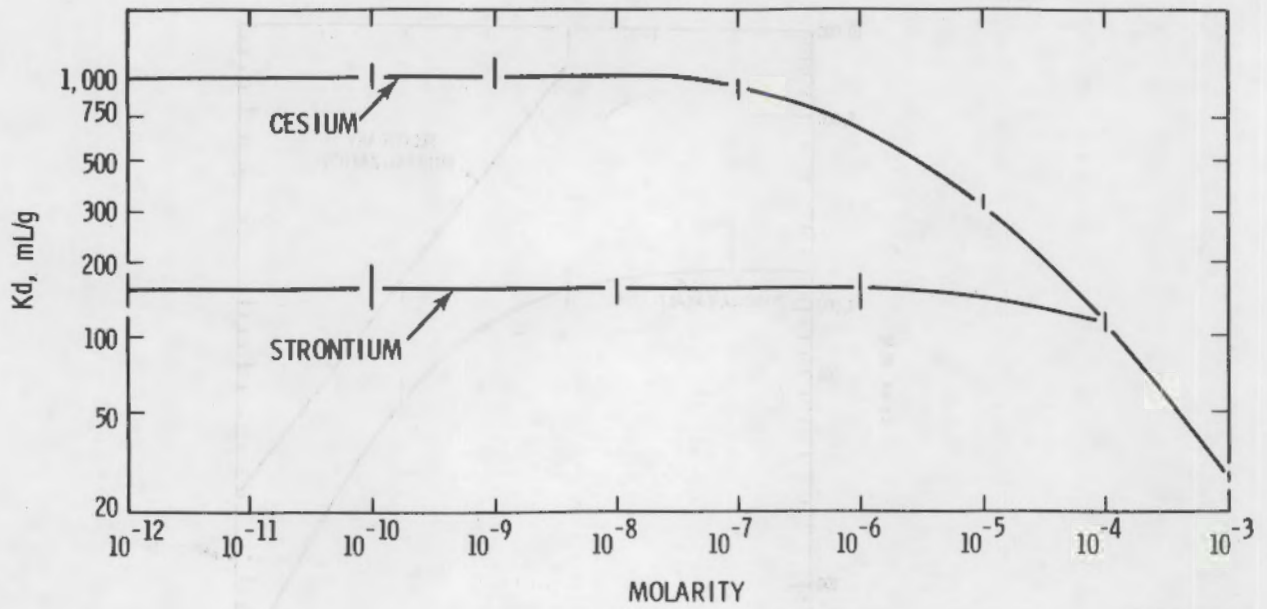
RCP8107-14

FIGURE 14. Graph of the Effects of Strontium and Cesium Concentration on
the Value for Umtanum Basalt at 23°C in GR-1 Groundwater.
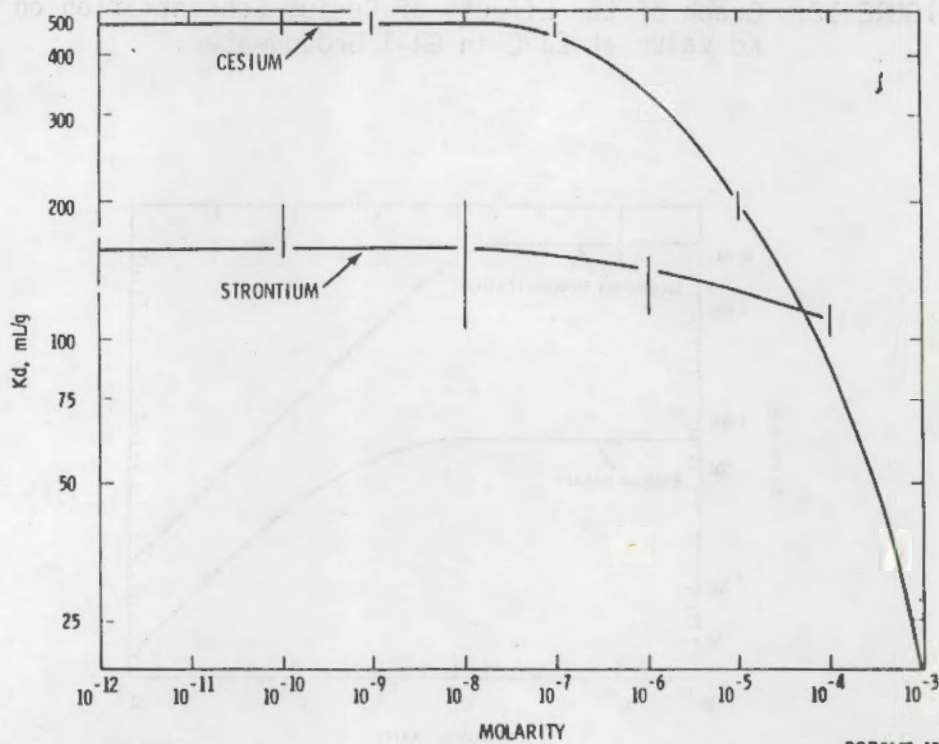
RCP8107-15

FIGURE 15. Graph of the Effects of Strontium and Cesium Concentration on
the Value for Umtanum Basalt at 60°C in GR-1 Groundwater.
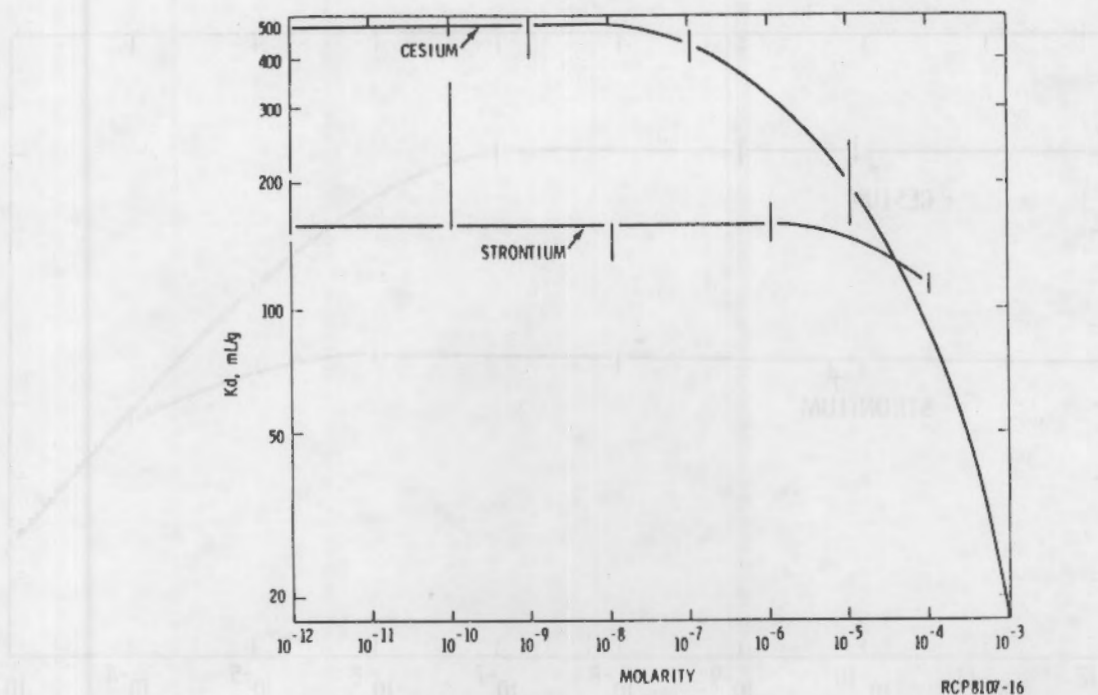
FIGURE 16. Graph of the Effects of Strontium and Cesium Concentration on
the Kd Value for Flow E Basalt at 23°C in GR-1 Groundwater.
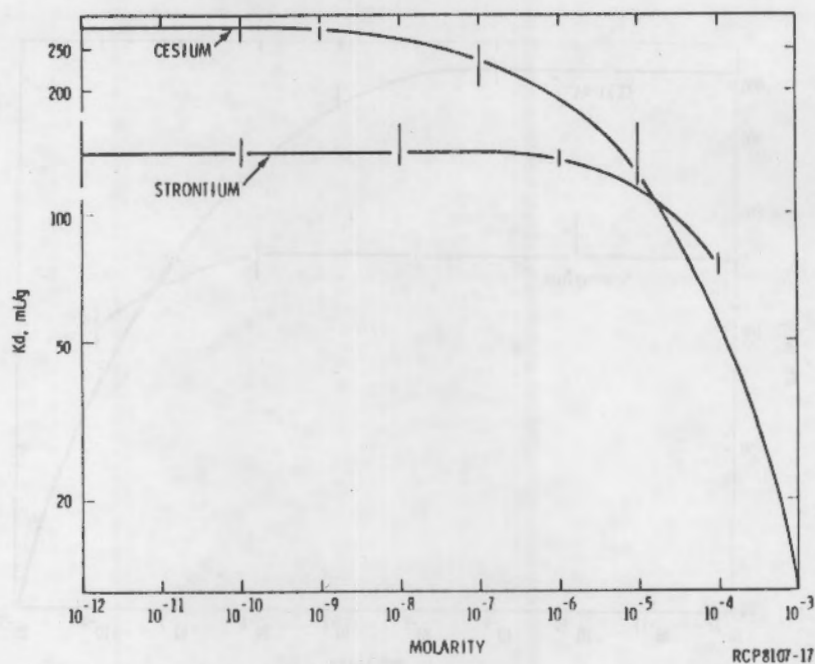
FIGURE 17. Graph of the Effects of Strontium and Cesium Concentration on
the Kd Value for Flow E Basalt at 60°C in GR-1 Groundwater.
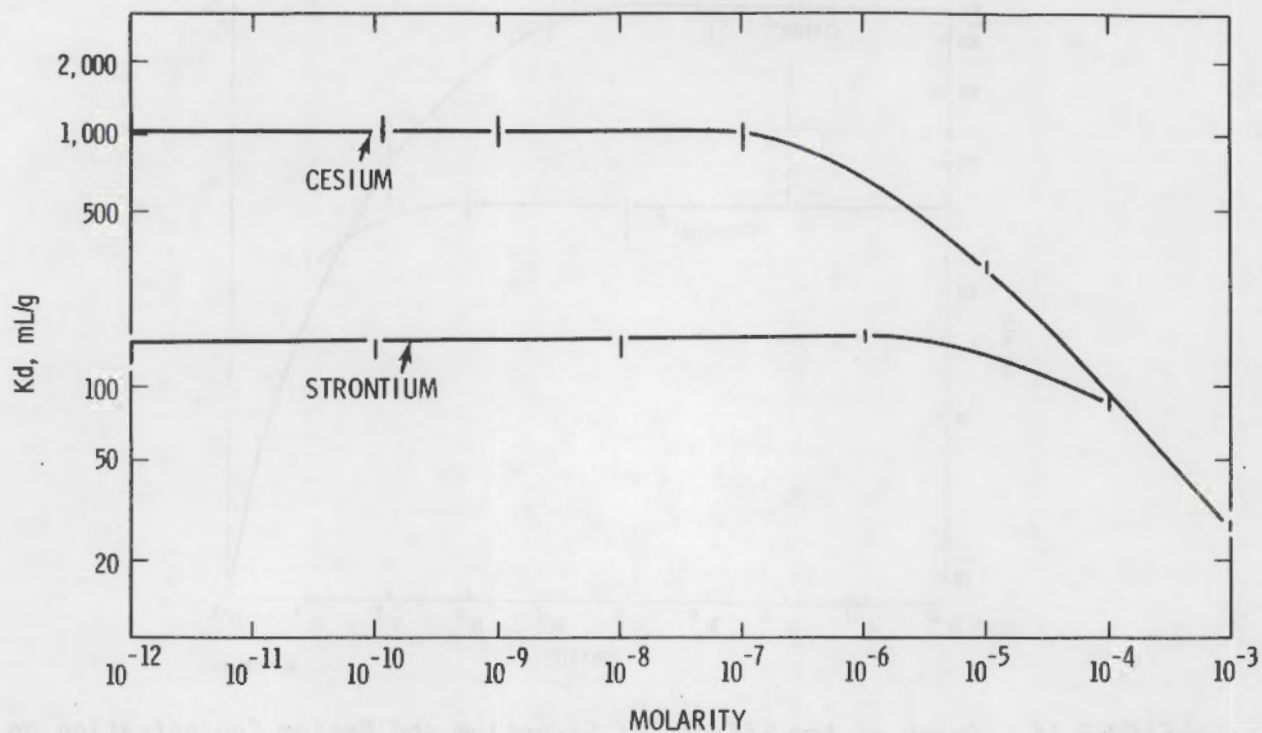
RCP8107-18

FIGURE 18.   Graph of the Effects of Strontium and Cesium Concentration on the Kd Value for Umtanum Basalt at 23°C with GR-2 Groundwater.
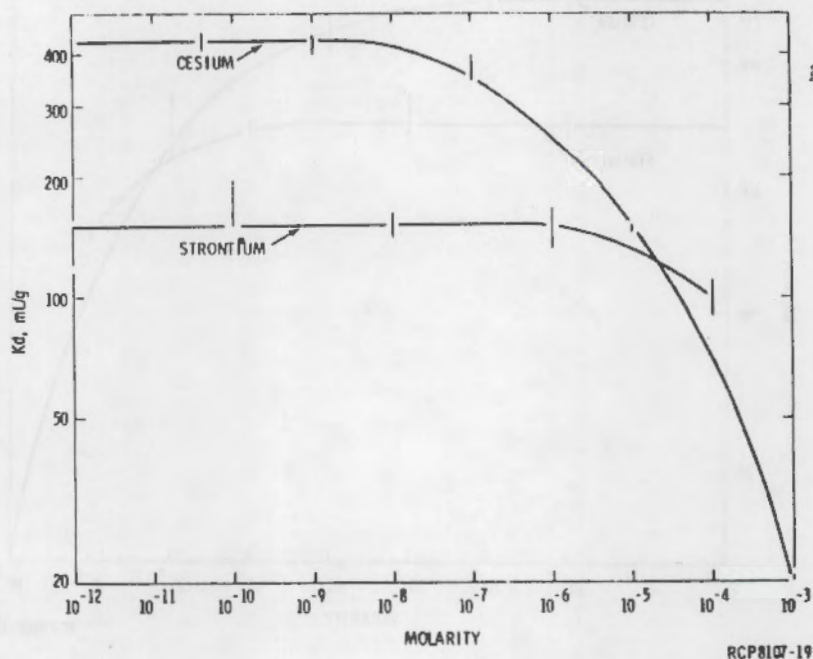
RCP8107-19

FIGURE 19.   Graph of the Effects of Strontium and Cesium Concentration on the Kd Value for Umtanum Basalt at 60°C with GR-2 Groundwater.

44
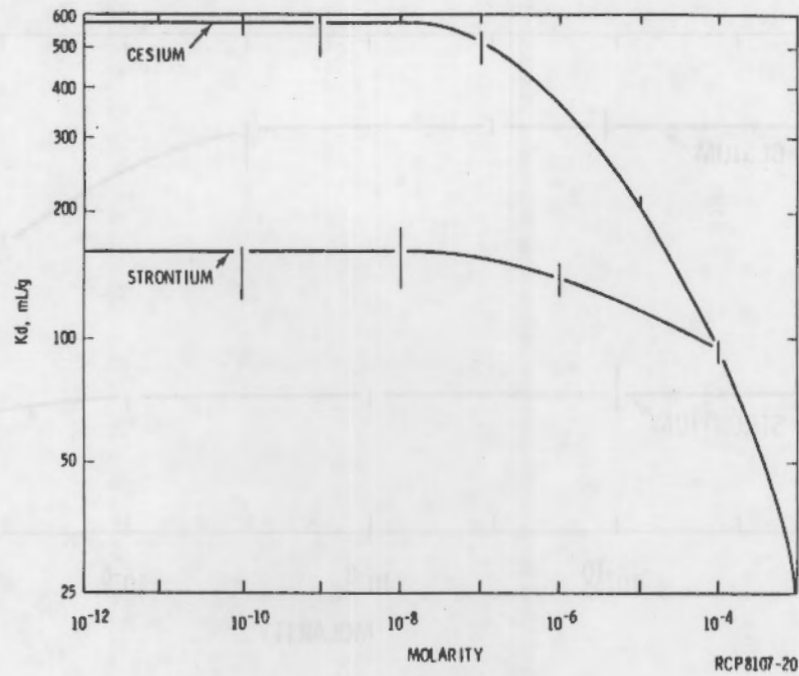
FIGURE 20. Graph of the Effects of Strontium and Cesium Concentration on the Kd Value for Flow E Basalt at 23°C with GR-2 Groundwater.
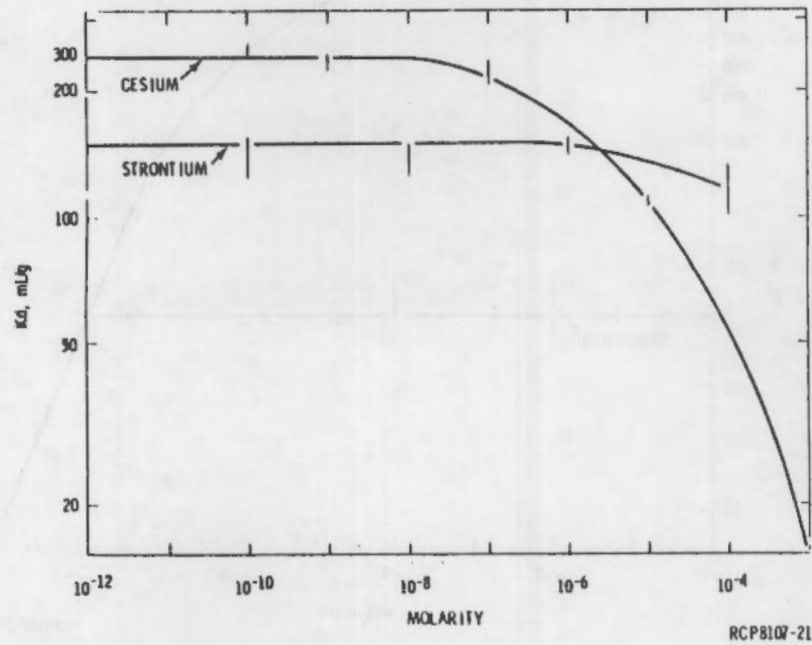
FIGURE 21. Graph of the Effects of Strontium and Cesium Concentration on the Kd Value for Flow E Basalt at 60°C with GR-2 Groundwater.
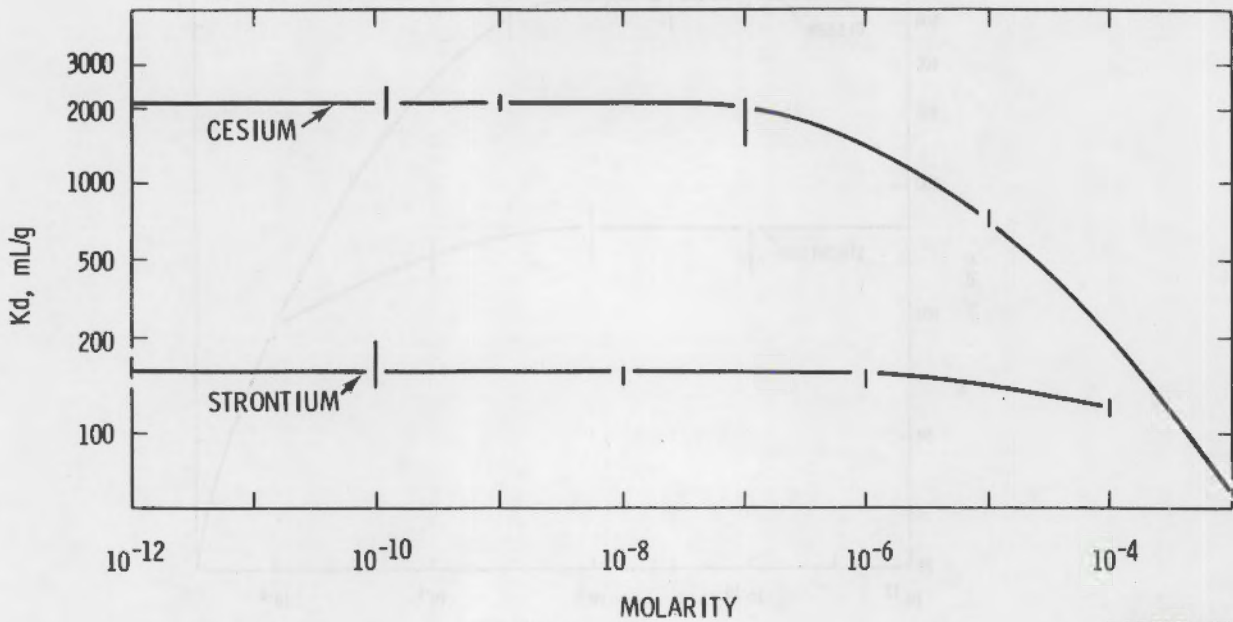
FIGURE 22. Graph of the Effects of Strontium and Cesium Concentration on the Kd Value for Pomona Basalt at 23°C with GR-2 Groundwater.
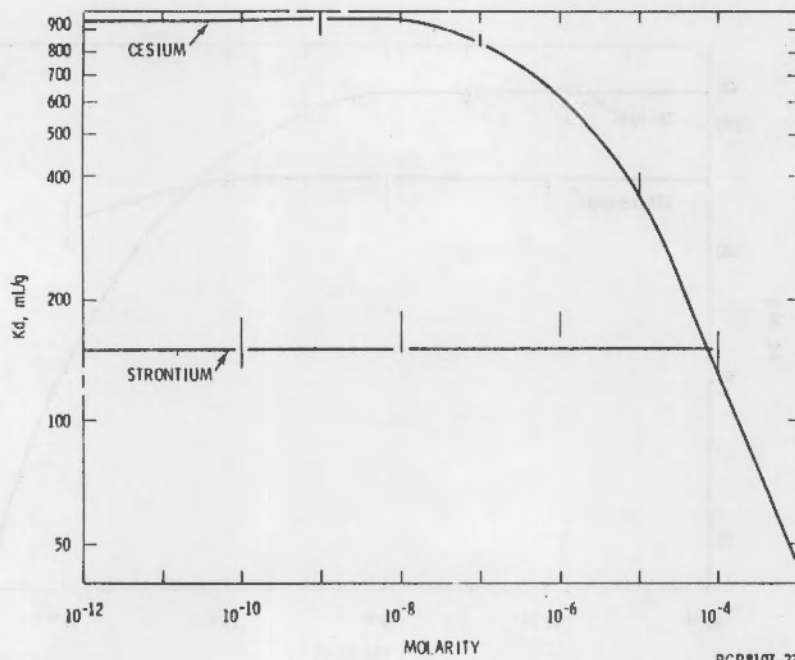
FIGURE 23. Graph of the Effects of Strontium and Cesium Concentration on the Kd Value for Pomona Basalt at 60°C with GR-2 Groundwater.

46
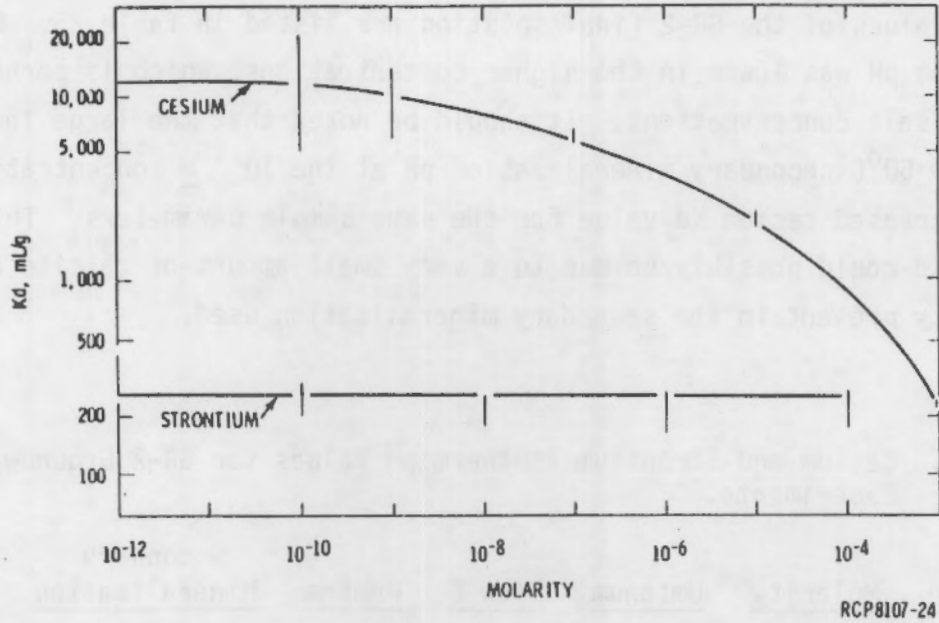
FIGURE 24. Graph of the Effects of Strontium and Cesium Concentration on the Kd Values for Secondary Mineralization at 23°C with GR-2 Groundwater.
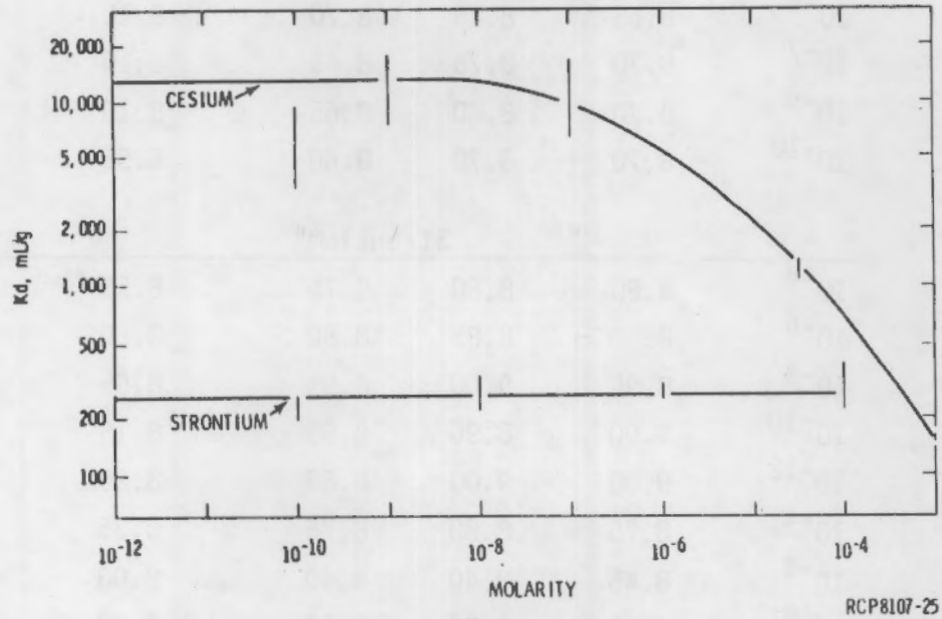
FIGURE 25. Graph of the Effects of Strontium and Cesium Concentration on the Kd Values for Secondary Mineralization at 60°C with GR-2 Groundwater.

The pH values of the GR-2 final solution are listed in Table 25. For the most part, the pH was lower in the higher concentrations, which is perhaps due to increased salt concentrations. It should be noted that the large increase in the cesium $60^{\circ}C$ secondary mineralization pH at the $10^{-10}\underline{M}$ concentration yielded a decreased cesium Kd value for the same sample parameters. This decrease in Kd could possibly be due to a very small amount of calcite or some other impurity present in the secondary mineralization used.

TABLE 25. Cesium and Strontium Isotherm pH Values for GR-2 Groundwater Experiments.

Temperature	Molarity	Umtanum	Flow E	Pomona	Secondary Mineralization	Blank
				Cesium		
$25^{\circ}C$	10^{-3}	8.60	8.70	8.55	8.20	9.00
	10^{-5}	8.70	8.85	8.70	8.15	9.00
	10^{-7}	8.75	8.55	8.55	8.25	8.95
	10^{-9}	8.70	8.70	8.70	8.10	9.00
	10^{-10}	8.65	8.70	8.70	8.10	9.00
$60^{\circ}C$	10^{-3}	8.60	8.60	8.50	7.95	
	10^{-5}	8.65	8.75	8.70	8.10	
	10^{-7}	8.70	8.75	8.65	8.10	
	10^{-9}	8.70	8.80	8.65	8.10	
	10^{-10}	8.70	8.70	8.60	8.55	
				Strontium		
$25^{\circ}C$	10^{-4}	8.80	8.80	8.75	8.50	9.15
	10^{-6}	8.90	8.85	8.80	8.50	9.20
	10^{-8}	8.95	9.00	8.95	8.55	9.20
	10^{-10}	9.00	8.90	8.85	8.15	9.20
	10^{-12}	9.00	9.00	8.80	8.20	9.15
$60^{\circ}C$	10^{-4}	8.75	8.80	8.75	8.35	
	10^{-6}	8.45	8.40	8.40	8.00	
	10^{-8}	8.35	8.35	8.25	7.80	
	10^{-10}	8.35	8.35	8.25	7.80	
	10^{-12}	8.40	8.35	8.30	7.80	

Specific sorption data are presented for cesium and strontium (Tables 26 and 27, respectively). Further use may be made of the isothermal sorption data for strontium and cesium given in Tables 26 and 27 by attempting a fit to various sorption equations.

Fitting to three basic types of sorption curves was attempted. The three types include exponential, power, and logarithmic curves. Exponential curves are of the general type $y = ae^{bx}$ ($a > 0$), power curves of the type $y = ax^b$ ($a > 0$), and logarithmic curves of the type $y = a + b \ln x$. The sorption data fit to a logarithmic curve was unsatisfactory and will be dropped from consideration here. The power curve is exemplified by the Freundlich equation: $x/m = kC^{1/n}$, where x is the amount of material (cesium and strontium) sorbed on mass, m, of the solid, C is the equilibrium solution concentration, and k and n are constants. One method of deriving k and n is to linearize $y = ax^b$ to $\ln y = \ln a + b \ln x$, or $\ln x/m = \ln k + 1/n \ln C$. Hence, $\ln x/m$ plotted versus $\ln C$ should yield a straight line with 1/n the line slope and k the antilogarithm of the intercept. Implicit in the Freundlich or power isotherm is that the amount of material sorbed increases indefinitely with increasing material (cesium or strontium) concentration in the solution. Hence, this isotherm may be unsatisfactory for high sorption values.

The exponential curve is represented by the DR isotherm, where $x/m = Xm \exp(B\epsilon^2)$ (Dubinin and Radushkevich, 1947). Linearizing, $\ln x/m = \ln Xm + B\epsilon^2$, where x/m was defined above, Xm is the maximum amount that the solid will sorb in that system, B is a constant related to sorption energy, and $\epsilon = RT \ln(1 + 1/C)$. R is a gas constant ($8.3147 \times 10^{-3}$ kJ deg^{-1} mol^{-1}), and T is absolute temperature. The mean energy of sorption degree ^{O}, $E = (-B)^{-1/2}/\sqrt{2}$, is the free energy of transfer of 1 mol of material (cesium or strontium) from the bulk solution to solid surface. A knowledge of the values for E allows interpretation of the type of removal reaction involved (ion exchange, precipitation, etc.). The Langmuir isotherm was not considered for interpretation of the sorption results due to its shortcomings. The Langmuir equation, for example, implicitly assumes a homogeneous sorption surface.

49

TABLE 26. Initial (C_i) and Final (C) Cesium Solution Concentrations and Moles of Cesium per Gram of Solid (x/m) for the Cesium Isotherms with Basalts and Secondary Mineralization.

		GR-1 Synthetic Groundwater							
		Umtanum Basalt		Flow E Basalt		Pomona Basalt		Secondary Mineralization	
Temperature	C_i, M	C, M	x/m, mol/g	C, M	x/m, mol/g	C, M	x/m, mol/g	C, M	x/m, mol/g
23°C	1.00×10^{-3}	2.72×10^{-4}	7.28×10^{-6}	3.61×10^{-4}	6.39×10^{-6}	1.71×10^{-4}	8.29×10^{-6}	4.51×10^{-5}	9.55×10^{-6}
	1.00×10^{-5}	2.95×10^{-7}	9.71×10^{-8}	5.02×10^{-7}	9.50×10^{-8}	2.13×10^{-7}	9.79×10^{-8}	9.17×10^{-8}	9.91×10^{-8}
	1.00×10^{-7}	1.03×10^{-9}	9.89×10^{-10}	2.34×10^{-9}	9.77×10^{-10}	8.30×10^{-10}	9.22×10^{-10}	7.66×10^{-11}	9.99×10^{-10}
	1.00×10^{-9}	9.11×10^{-12}	9.91×10^{-12}	2.17×10^{-11}	9.78×10^{-12}	6.37×10^{-12}	9.34×10^{-12}	1.02×10^{-12}	9.99×10^{-12}
	1.00×10^{-10}	1.87×10^{-12}	1.96×10^{-12}	3.98×10^{-12}	1.94×10^{-12}	1.39×10^{-12}	1.78×10^{-12}	7.23×10^{-14}	1.78×10^{-12}
60°C	1.00×10^{-3}	3.55×10^{-4}	6.46×10^{-6}	4.56×10^{-4}	5.44×10^{-6}	2.06×10^{-4}	7.95×10^{-6}	5.66×10^{-5}	9.43×10^{-6}
	1.00×10^{-5}	4.88×10^{-7}	9.51×10^{-8}	6.79×10^{-7}	9.32×10^{-8}	2.96×10^{-7}	9.70×10^{-8}	1.05×10^{-7}	9.89×10^{-8}
	1.00×10^{-7}	2.18×10^{-9}	9.78×10^{-10}	3.97×10^{-9}	9.60×10^{-10}	1.39×10^{-9}	9.86×10^{-10}	8.57×10^{-11}	9.99×10^{-10}
	1.00×10^{-9}	2.08×10^{-10}	9.79×10^{-11}	3.59×10^{-11}	9.64×10^{-12}	1.31×10^{-11}	9.87×10^{-12}	8.90×10^{-13}	9.99×10^{-12}
	1.00×10^{-10}	4.09×10^{-12}	1.94×10^{-12}	6.73×10^{-12}	1.91×10^{-12}	1.96×10^{-12}	1.77×10^{-12}	1.20×10^{-13}	1.79×10^{-12}
		GR-2 Synthetic Groundwater							
23°C	1×10^{-3}	2.63×10^{-4}	7.41×10^{-6}	3.39×10^{-4}	6.61×10^{-6}	1.51×10^{-4}	8.51×10^{-6}	4.27×10^{-5}	9.55×10^{-6}
	1×10^{-5}	3.31×10^{-7}	9.55×10^{-8}	4.47×10^{-7}	9.55×10^{-8}	2.57×10^{-7}	9.99×10^{-8}	4.68×10^{-8}	1.00×10^{-7}
	1×10^{-7}	1.05×10^{-9}	9.99×10^{-10}	2.00×10^{-9}	9.77×10^{-10}	1.17×10^{-9}	9.99×10^{-10}	1.70×10^{-10}	1.00×10^{-9}
	1×10^{-9}	9.77×10^{-12}	9.99×10^{-12}	1.78×10^{-11}	9.77×10^{-12}	1.05×10^{-11}	1.00×10^{-11}	1.17×10^{-12}	1.00×10^{-11}
	1×10^{-10}	1.95×10^{-12}	2.00×10^{-12}	3.24×10^{-12}	2.00×10^{-12}	1.74×10^{-12}	1.58×10^{-12}	2.40×10^{-13}	2.00×10^{-12}
60°C	1×10^{-3}	3.39×10^{-4}	6.61×10^{-6}	3.98×10^{-4}	6.03×10^{-6}	1.86×10^{-4}	8.13×10^{-6}	6.17×10^{-5}	9.33×10^{-6}
	1×10^{-5}	6.31×10^{-7}	9.33×10^{-8}	8.51×10^{-7}	9.12×10^{-8}	2.57×10^{-7}	9.77×10^{-8}	8.51×10^{-8}	1.00×10^{-7}
	1×10^{-7}	2.63×10^{-9}	9.77×10^{-10}	2.63×10^{-9}	9.77×10^{-10}	1.17×10^{-9}	1.00×10^{-9}	1.07×10^{-10}	1.00×10^{-9}
	1×10^{-9}	2.34×10^{-11}	9.77×10^{-12}	4.17×10^{-11}	9.55×10^{-12}	1.05×10^{-11}	1.00×10^{-11}	8.91×10^{-13}	1.00×10^{-11}
	1×10^{-10}	3.63×10^{-12}	1.58×10^{-12}	6.17×10^{-12}	1.58×10^{-12}	1.74×10^{-12}	1.58×10^{-12}	3.98×10^{-13}	1.62×10^{-12}

TABLE 27. Initial (C_i) and Final (C) Strontium Solution Concentrations and Moles of Strontium per Gram of Solid (x/m) for the Strontium Isotherms with Basalts and Secondary Mineralization.

GR-1 Synthetic Groundwater

Temperature	C_i, M	Umtanum Basalt C, M	Umtanum Basalt x/m, mol/g	Flow E Basalt C, M	Flow E Basalt x/m, mol/g	Pomona Basalt C, M	Pomona Basalt x/m, mol/g	Secondary Mineralization C, M	Secondary Mineralization x/m, mol/g
23°C	1.00×10^{-4}	8.24×10^{-6}	9.12×10^{-7}	8.07×10^{-6}	9.19×10^{-7}	8.98×10^{-6}	9.10×10^{-7}	3.75×10^{-6}	9.63×10^{-7}
	1.00×10^{-6}	6.17×10^{-8}	9.38×10^{-9}	5.90×10^{-8}	9.41×10^{-9}	6.79×10^{-8}	9.32×10^{-9}	2.85×10^{-8}	9.72×10^{-9}
	1.00×10^{-8}	7.36×10^{-10}	9.36×10^{-11}	6.52×10^{-10}	9.35×10^{-11}	6.66×10^{-10}	9.33×10^{-11}	3.20×10^{-10}	9.68×10^{-11}
	1.00×10^{-10}	6.01×10^{-12}	9.40×10^{-13}	4.69×10^{-12}	9.53×10^{-13}	6.21×10^{-12}	9.38×10^{-13}	2.25×10^{-12}	9.77×10^{-13}
	1.00×10^{-12}	6.06×10^{-14}	9.39×10^{-15}	5.39×10^{-14}	9.46×10^{-15}	5.81×10^{-14}	9.35×10^{-15}	2.77×10^{-14}	9.72×10^{-15}
60°C	1.00×10^{-4}	8.24×10^{-6}	9.12×10^{-7}	1.15×10^{-5}	8.84×10^{-7}	8.97×10^{-6}	9.77×10^{-7}	2.28×10^{-6}	9.77×10^{-7}
	1.00×10^{-6}	7.11×10^{-8}	9.29×10^{-9}	7.00×10^{-8}	9.30×10^{-9}	6.05×10^{-8}	9.83×10^{-9}	1.68×10^{-8}	9.83×10^{-9}
	1.00×10^{-8}	6.42×10^{-10}	9.36×10^{-11}	6.44×10^{-10}	9.36×10^{-11}	5.17×10^{-10}	9.89×10^{-11}	1.05×10^{-10}	9.89×10^{-11}
	1.00×10^{-10}	5.54×10^{-12}	9.45×10^{-13}	6.60×10^{-12}	9.34×10^{-13}	5.44×10^{-12}	9.74×10^{-13}	2.62×10^{-12}	9.74×10^{-13}
	1.00×10^{-12}	6.26×10^{-14}	9.37×10^{-15}	6.64×10^{-14}	9.34×10^{-15}	6.48×10^{-14}	9.65×10^{-15}	3.54×10^{-14}	9.65×10^{-15}

GR-2 Synthetic Groundwater

Temperature	C_i, M	Umtanum Basalt C, M	Umtanum Basalt x/m, mol/g	Flow E Basalt C, M	Flow E Basalt x/m, mol/g	Pomona Basalt C, M	Pomona Basalt x/m, mol/g	Secondary Mineralization C, M	Secondary Mineralization x/m, mol/g
23°C	1.00×10^{-4}	1.10×10^{-5}	8.91×10^{-7}	1.02×10^{-5}	8.91×10^{-7}	7.41×10^{-6}	9.33×10^{-7}	4.37×10^{-6}	9.55×10^{-7}
	1.00×10^{-6}	6.17×10^{-8}	9.33×10^{-9}	6.76×10^{-8}	9.33×10^{-9}	5.75×10^{-8}	9.33×10^{-9}	4.68×10^{-8}	9.55×10^{-9}
	1.00×10^{-8}	6.61×10^{-10}	9.33×10^{-11}	6.17×10^{-10}	9.33×10^{-11}	5.75×10^{-10}	9.33×10^{-11}	4.57×10^{-10}	9.55×10^{-11}
	1.00×10^{-10}	6.76×10^{-12}	9.33×10^{-13}	6.61×10^{-12}	9.33×10^{-13}	5.25×10^{-12}	9.55×10^{-13}	3.98×10^{-12}	9.55×10^{-13}
	1.00×10^{-12}	7.08×10^{-14}	9.33×10^{-15}	5.50×10^{-14}	9.55×10^{-15}	5.25×10^{-14}	9.55×10^{-15}	2.95×10^{-14}	9.77×10^{-15}
60°C	1.00×10^{-4}	6.31×10^{-6}	9.33×10^{-7}	6.03×10^{-6}	9.33×10^{-7}	4.90×10^{-6}	9.55×10^{-7}	2.00×10^{-6}	9.77×10^{-7}
	1.00×10^{-6}	4.27×10^{-8}	9.55×10^{-9}	5.25×10^{-8}	9.55×10^{-9}	3.89×10^{-8}	9.55×10^{-9}	4.07×10^{-8}	9.55×10^{-9}
	1.00×10^{-8}	4.57×10^{-10}	9.55×10^{-11}	5.25×10^{-10}	9.55×10^{-11}	5.75×10^{-10}	9.33×10^{-11}	3.89×10^{-10}	9.55×10^{-11}
	1.00×10^{-10}	5.13×10^{-12}	9.55×10^{-13}	5.13×10^{-12}	9.55×10^{-13}	3.89×10^{-12}	9.55×10^{-13}	3.55×10^{-12}	9.55×10^{-13}
	1.00×10^{-12}	5.50×10^{-14}	9.55×10^{-15}	5.37×10^{-14}	9.55×10^{-15}	5.37×10^{-14}	9.55×10^{-15}	4.79×10^{-14}	9.55×10^{-15}

Most surfaces, especially those involved in ion exchange, are considered to be heterogeneous. The Langmuir may not satisfactorily represent sorption data if more than a small percentage of the sorption sites have been exchanged. However, the Langmuir equation and DR equation both linearize the cesium sorption data.

A series of graphs for Umtanum basalt will be used to illustrate which of the curve types fit the cesium and strontium sorption data for Tables 26 and 27, and how well.

A DR plot of the strontium sorption data on Umtanum basalt is shown in Figure 26. Two curves result, one at 23^oC and another at 60^oC. Each temperature includes experimental points for strontium sorption on Umtanum basalt from GR-1 and GR-2 synthetic groundwaters. These data are obviously not linearized by the DR equation.

A simple linearized power curve or Freundlich plot of the same data is shown in Figure 27. A single, straight line results for both synthetic groundwaters and temperatures. In addition to the usual Freundlich plot of ln x/m versus ln C, ln x /m versus ln C_i is shown in Figures 28 and 29, respectively. Both are straight lines. Hence, if the cesium or strontium source terms (initial cesium or strontium solution concentration) are known, the basalt loading and amount of cesium or strontium remaining in solution, C, can be obtained easily.

Cesium sorption on Umtanum basalt, on the other hand, was plotted on a linearized power curve with the results shown for ln x/m versus ln C and ln C_i versus ln C in Figures 30 and 31, respectively. Both resulted in separate curves for GR-1 and GR-2 synthetic groundwaters. On the other hand, a similar plot for ln x/m versus ln C_i did result in a straight-line relationship. However, the relationship between the cesium loading of Umtanum basalt (plus the other basalts and secondary mineralization) and the cesium solution concentration at equilibrium best fit a DR plot as shown in Figures 32 and 33. Two lines resulted: one for GR-1 and -2 at 23^oC and one for GR-1 and -2 at 60^oC.
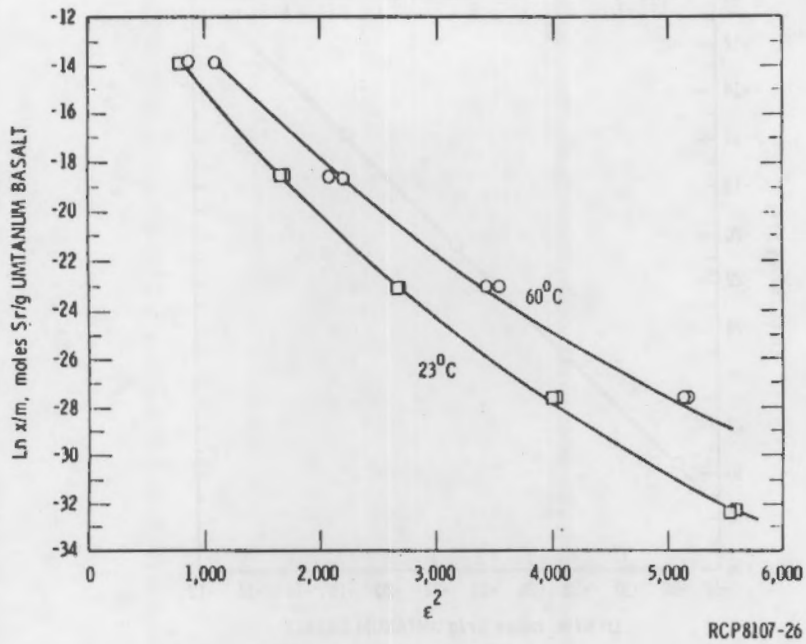
FIGURE 26. Two Curves Resulting from a Dubinin-Radushkevich Plot of the Strontium Sorption Data on Umtanum Basalt. The two curves represent sorption at 23° and 60°C from GR-1 and GR-2 synthetic groundwaters.
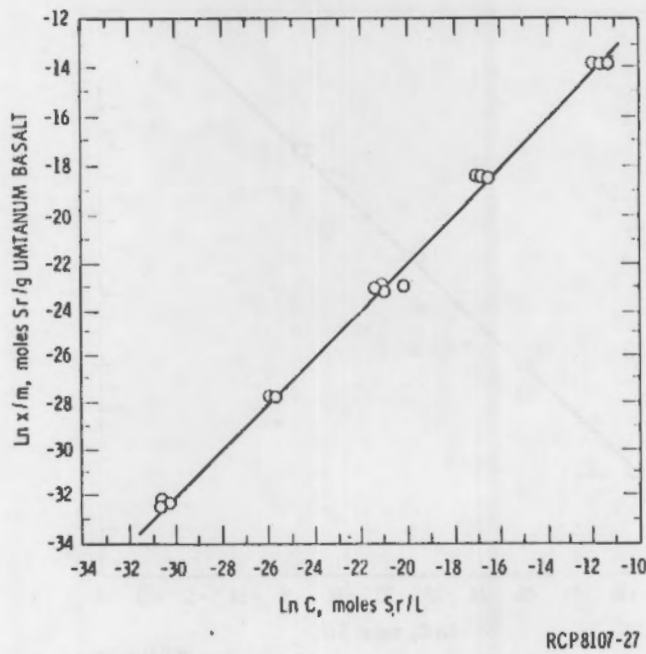

FIGURE 27. A Graph of Equilibrium Solution Strontium Concentration (C) Versus Strontium Loading (x/m) (Freundlich Isotherm) on Umtanum Basalt at 23° and 60°C from GR-1 and GR-2 Synthetic Groundwaters.

53

RCP8107-28
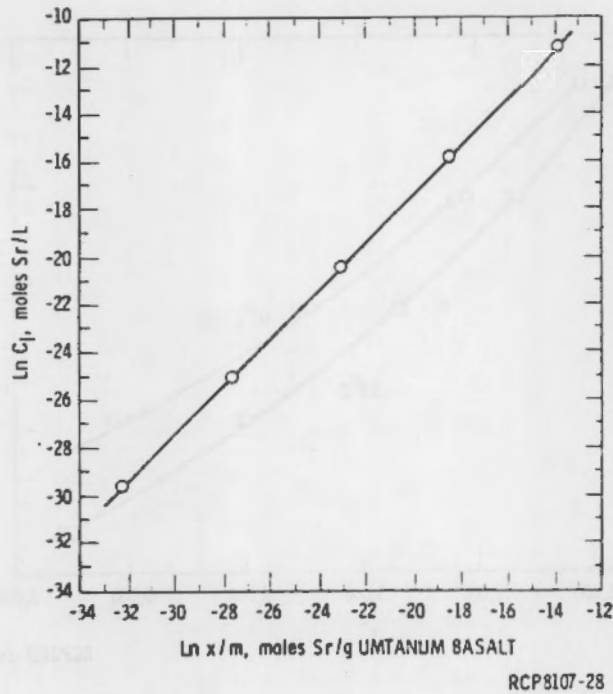
FIGURE 28. A Graph of Initial Strontium Solution Concentration (C_i)
Versus Strontium Loading (x/m) on Umtanum Basalt at 23° and
60°C from GR-1 and GR-2 Synthetic Groundwaters.

RCP8107-29

FIGURE 29. A Graph of Initial Strontium Solution Concentration (C_i)
Versus Equilibrium Solution Strontium Concentration (C) for
Umtanum Basalt and GR-1 and GR-2 Synthetic Groundwaters at
23° and 60°C.
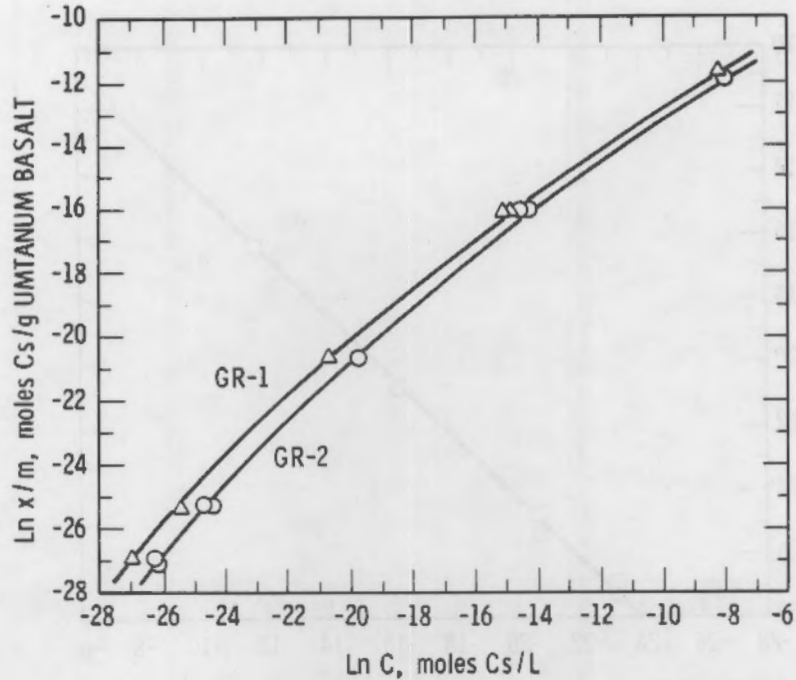
RCP8107-30

FIGURE 30. Two Curves Resulting from a Plot of Equilibrium Solution
Cesium Concentration (C) Versus Cesium Loading (x/m)
(Freundlich Isotherm) on Umtanum Basalt at 23° and 60°C.
The two curves are for GR-1 and GR-2 synthetic groundwaters.
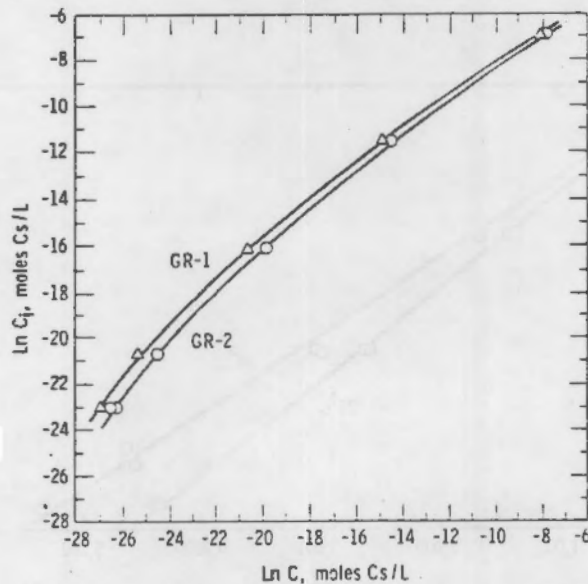
RCP8107-31

FIGURE 31. Two Curves Resulting from a Plot of Equilibrium Solution Cesium
Concentration (C) Versus Initial Solution Cesium Concentration
(C_i) for Umtanum Basalt at 23° and 60°C. The two curves
are for GR-1 and GR-2 synthetic groundwaters.

55
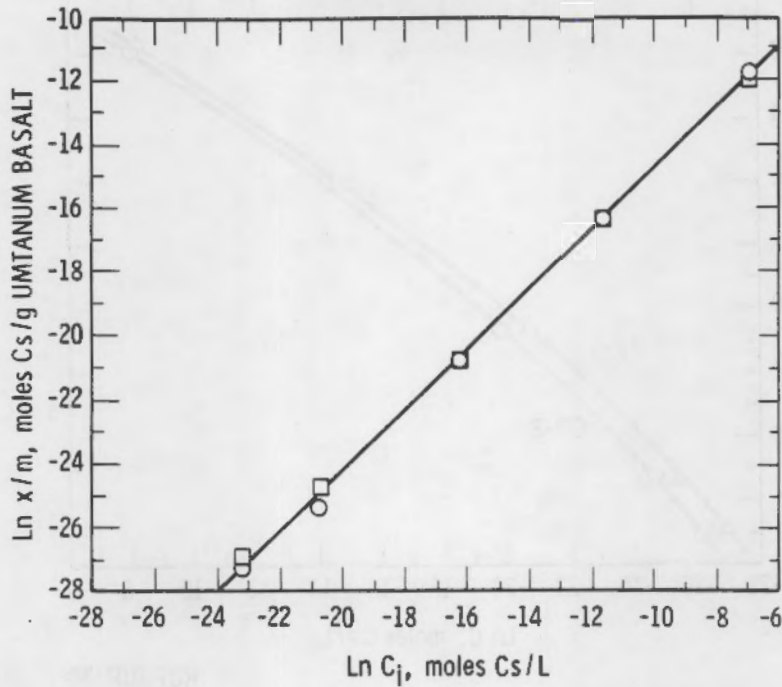
RCP8107-32

FIGURE 32. A Graph of Umtanum Basalt Cesium Loading (x/m) Versus Initial
Solution Cesium Concentration (C_i) at 23° and 60^oC from
GR-1 and GR-2 Synthetic Groundwaters.
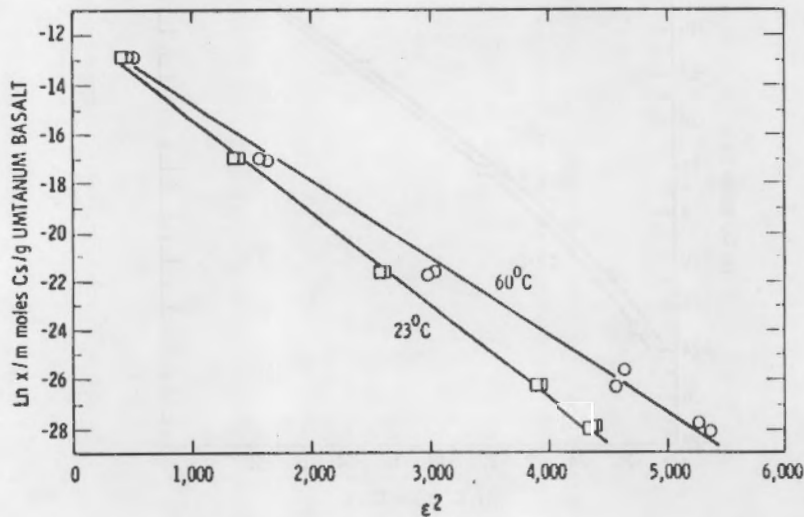
RCP8107-33

FIGURE 33. A Dubinin-Radushkevich Plot of the Cesium Sorption Data on Umtanum
Basalt from GR-1 and GR-2 Synthetic Groundwaters. Two lines
result: one for GR-1 and GR-2 cesium sorption at 23^oC and
another for GR-1 and GR-2 cesium sorption at 60^oC.

To aid in computing strontium distributions between basalt and solution, the constants or coefficients derived from linearized forms of the power curve equation (Freundlich equation) are given in Table 28. The linearized exponential (DR) curve constants for the cesium sorption data are given in Table 29. The $r^2$ values are a coefficient of determination and indicate the quality of fit achieved by the regression. An r^2 value of 1.00 is a perfect fit of the computed regression to the experimental data.

E values given in Table 29 ranged from 11 to 14 kJ/mol (2.6 to 3.3 kcal/mol), within in the energy range expected of ion exchange reactions (Helfferich, 1962).

The maximum cesium sorption values for these systems (Xm) varied from 1.60×10^{-5} mol Cs/g Flow E basalt to 4.82×10^{-5} mol Cs/g secondary mineralization. With cesium as the sorbing cation, these Xm values ranged from 4.82 meq/100 g secondary mineralization to 1.60 meq/100 g Flow E basalt. The cesium cation exchange capacity of the secondary mineralization was measured and found to be 71.66 ± 4.87 meq/100 g. Hence, only ∿7% of the ultimate cesium capacity at most was utilized in these systems.

TECHNETIUM

Technetium isotherm experiments using GR-1 and GR-2 synthetic groundwaters were also performed at the 1 g solid:10 mL groundwater ratio at both the 23° and 60°C temperatures for a solution-solid contact time of 62 d. The original concentration of technetium in the synthetic groundwater was $6.55 \times 10^{-8}\underline{M}$. This concentration was increased two, three, and four times, giving four separate concentrations of technetium in synthetic groundwater.

TABLE 28. Power Curve Constants Describing Strontium Sorption by Three Basalts and Secondary Mineralization.

Solid	Synthetic Ground-water	Temp. °C	$\ln x/m = \ln k + 1/n \ln C$			$\ln x/m = \ln k + 1/n \ln C_i$			$\ln C = \ln k + 1/n \ln C_i$		
			k	1/n	r^2	k	1/n	r^2	k	1/n	r^2
Umtanum Basalt	GR-1	23	0.1008	0.9848	0.9998	0.00911	0.9987	0.9999	0.0867	0.0139	0.9998
	GR-1	60	0.0943	0.9813	0.9999	0.00906	0.9985	0.9999	0.0916	1.0174	0.9998
	GR-2	23	0.0834	0.9804	0.9992	0.00891	0.9980	0.9999	0.1008	1.0172	0.9993
	GR-2	60	0.1254	0.9725	0.9995	0.00933	0.9990	0.9999	0.0530	1.0020	0.9995
Flow E Basalt	GR-1	23	0.0942	0.9762	0.9997	0.00913	0.9985	0.9999	0.0910	1.0225	0.9997
	GR-1	60	0.0697	0.9725	0.9994	0.00882	0.9975	0.9999	0.1181	1.0251	0.9995
	GR-2	23	0.0719	0.9702	0.9997	0.00879	0.9970	0.9999	0.1139	1.0273	0.9997
	GR-2	60	0.1531	0.9934	0.9999	0.00933	0.9990	0.9999	0.0598	1.0055	0.9999
Pomona Basalt	GR-1	23	0.0861	0.9782	0.9999	0.00907	0.9987	0.9999	0.0999	1.0208	0.9999
	GR-1	60	0.1106	0.9840	0.9994	0.00991	1.0007	0.9999	0.0852	1.0164	0.9994
	GR-2	23	0.1095	0.9817	0.9999	0.00916	0.9985	0.9999	0.0797	1.0169	0.9999
	GR-2	60	0.2172	1.0033	0.9993	0.00951	1.0000	0.9999	0.0437	0.9960	0.9994
Secondary Mineral-ization	GR-1	23	0.2200	0.9812	0.9996	0.00961	0.9995	0.9999	0.0409	1.0183	0.9997
	GR-1	60	0.8612	1.0268	0.9965	0.00991	1.0007	0.9999	0.0121	0.9712	0.9966
	GR-2	23	0.1488	0.9786	0.9997	0.00942	0.9990	0.9999	0.0593	1.0206	0.9998
	GR-2	60	0.5995	1.0362	0.9990	0.00977	1.0010	0.9999	0.0185	0.9650	0.9991

TABLE 29. Dubinin-Radushkevich Equation Constants and Derivatives Describing
Cesium Sorption by Three Basalts and Secondary Mineralization.

Solid	Synthetic Groundwater	Temp. $^{\circ}$C	Xm, meq Cs 100 g^{-1} solid	B	E, kJ mol^{-1}	r^2
Umtanum Basalt	GR-1	23	2.25	-0.003742	11.56	0.997
	GR-1	60	1.84	-0.003055	12.79	0.973
	GR-2	23	2.22	-0.003751	11.55	0.997
	GR-2	60	1.80	-0.003124	12.65	0.995
Flow E Basalt	GR-1	23	1.88	-0.003944	11.26	0.996
	GR-1	60	1.60	-0.003210	12.48	0.996
	GR-2	23	1.92	-0.003885	11.34	0.998
	GR-2	60	1.83	-0.003248	12.41	0.997
Pomona Basalt	GR-1	23	2.86	-0.003735	11.57	0.996
	GR-1	60	2.60	-0.003040	12.83	0.995
	GR-2	23	3.15	-0.003865	11.37	0.996
	GR-2	60	2.86	-0.003028	12.85	0.996
Secondary Mineralization	GR-1	23	3.00	-0.003116	12.67	0.989
	GR-1	60	3.06	-0.002499	14.14	0.993
	GR-2	23	4.82	-0.003380	12.16	0.996
	GR-2	60	4.29	-0.002584	13.91	0.994

The Kd values for the technetium isotherms in GR-1 and GR-2 groundwaters
are listed in Table 30. Technetium was sorbed onto the Umtanum basalt only.
The GR-2 groundwater shows a slightly higher ability to inhibit sorption than
the GR-1 groundwater, although the difference between the two groundwater Kd
values was rather small. The results also indicated that the 23°C samples
sorbed slightly more than the 60°C samples, and that the technetium-concen-
trations had little effect on the sorption capacity of the solid. These data
fit none of the usual isotherms. These experiments will be repeated when a new
technetium isotope (^{95m}Tc) is obtained to allow a wider technetium-concen-
tration range and a better understanding of technetium-removal mechanisms.

TABLE 30. Corrected ^{99}Tc Kd Values in GR-1 and GR-2 Groundwaters
for 62 Days.

GR-1

| Temperature | Concentration | Kd, mL/g | | | |
		Umtanum	Flow E	Pomona	Secondary Mineralization
23°C	X (6.55 x 10⁻⁸M)	5.6 + 3.5	0	0	0
	2X	2.5 + 1.7	0	0	0
	3X	2.2 + 1.2	0	0	0
	4X	3.9 + 2.6	0	0	0
60°C	X	5.0 + 2.3	0	0	0
	2X	1.3 + 1.0	0	0	0
	3X	1.6 + 0.9	0	0	0
	4X	4.2 + 2.4	0	0	0

GR-2

| Temperature | Concentration | Kd, mL/g | | | |
		Umtanum	Flow E	Pomona	Secondary Mineralization
23°C	X (6.55 x 10⁻⁸M)	1.3 + 0.4	0	0	0
	2X	1.6 + 0.7	0	0	0
	3X	1.7 + 0.4	0	0	0
	4X	1.7 + 0.3	0	0	0
60°C	X	0.5 + 0.7	0	0	0
	2X	0.7 + 0.7	0	0	0
	3X	0.9 + 0.5	0	0	0
	4X	0.9 + 0.7	0	0	0

Eh-pH CONTROL

A system is said to be poised when it contains two minerals with an element in common with different oxidation states. A systematic search was made of possible basalt poising systems of this type in order to determine the Eh range of interest for the sorption work. A pH range of 7.0 to 10.0 seems reasonable as pertinent to most repository conditions. Several possible Eh poising systems were investigated, including, for example, magnetite-hematite. It was found in all cases that either there was only one of the two required minerals present in the basalt (the basalt contains no hematite) or the system was not reflected by the basalt groundwater analyses. The only poising system that seems to fit the mineralogy and groundwater chemistry as they exist is one involving magnetite (10 to 15 wt% in the basalt) and pyrite (1 wt% or less in the basalt), and the equilibrium reactions, Fe_3O_4 (magnetite) + $8H^+ + 2e^- \rightleftharpoons 3Fe^{2+} + 4H_2O$, $\log K^O = 35.69$; $SO_4^{2-} + 7e^- + 8H^+ \rightleftharpoons 1/2S_2^{2-} + 4H_2O$, $\log K^O = 28.54$; FeS_2 (pyrite) $\rightleftharpoons Fe^{2+} + S_2^{2-}$, $\log K^O = -26.93$.

Assuming that pyrite, FeS_2, and magnetite, Fe_3O_4, are the minerals involved in the Eh poising system, we can determine the Eh limits of interest between the pH limits of 7.0 and 10.0 as follows:

$$Fe_3O_4 + 8H^+ + 2e^- \rightleftharpoons 3Fe^{2+} + 4H_2O, \ \log K^O = 35.69$$

$$6SO_4^{2-} + 42e^- + 48H^+ \rightleftharpoons 3S_2^{2-} + 24H_2O, \ \log K^O = 6(28.54)$$

$$3Fe^{2+} + 3S_2^{2-} \rightleftharpoons 3FeS_2, \ \log K^O = 3(26.93)$$

$Fe_3O_4 + 6SO_4^{2-} + 56H^+ + 44e^- \rightleftharpoons 3FeS_2 + 28H_2O, \ \log K^O = 287.72.$

Dividing through by 44,
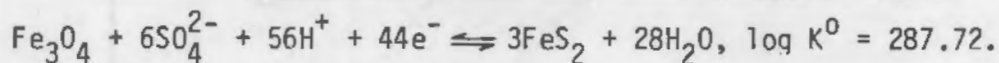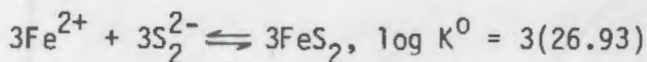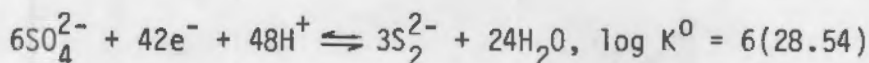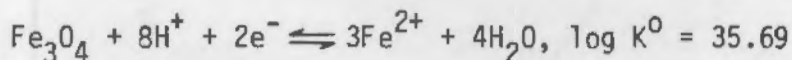
$Fe_3O_4/44 + 0.14SO_4^{2-} + 1.27H^+ + e^- \rightleftharpoons 3/44FeS_2 + 28/44H_2O, \ \log K^O = 6.54.$
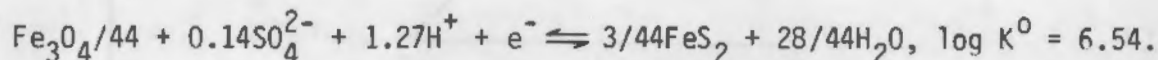
Using pe instead of Eh, $K^O = \dfrac{1}{(SO_4^{2-})^{0.14}(H^+)^{1.27}(e^-)}$

or log K^O = -0.14 log (SO_4^{2-}) + 1.27 pH + pe. Taking the groundwater
sulfate ion content from groundwater analyses as 0.108 g/L, 6.54 +
0.14(-2.95) - 1.27 pH = pe, or 6.13 - 1.27 pH = pe.

Figure 34 is a plot of pe versus pH, with an Eh scale as well. The
pH 7.0 to 10.0 range shows an Eh of -160 mV to -400 mV for the probable
repository Eh-pH range. It should be emphasized that unless the system is
electrochemically reversible, the system is not poised. The above system,
upon reaching equilibrium, for example, is poised at a given pH until one of
the solids (pyrite, magnetite) is consumed.

RCP8107-34
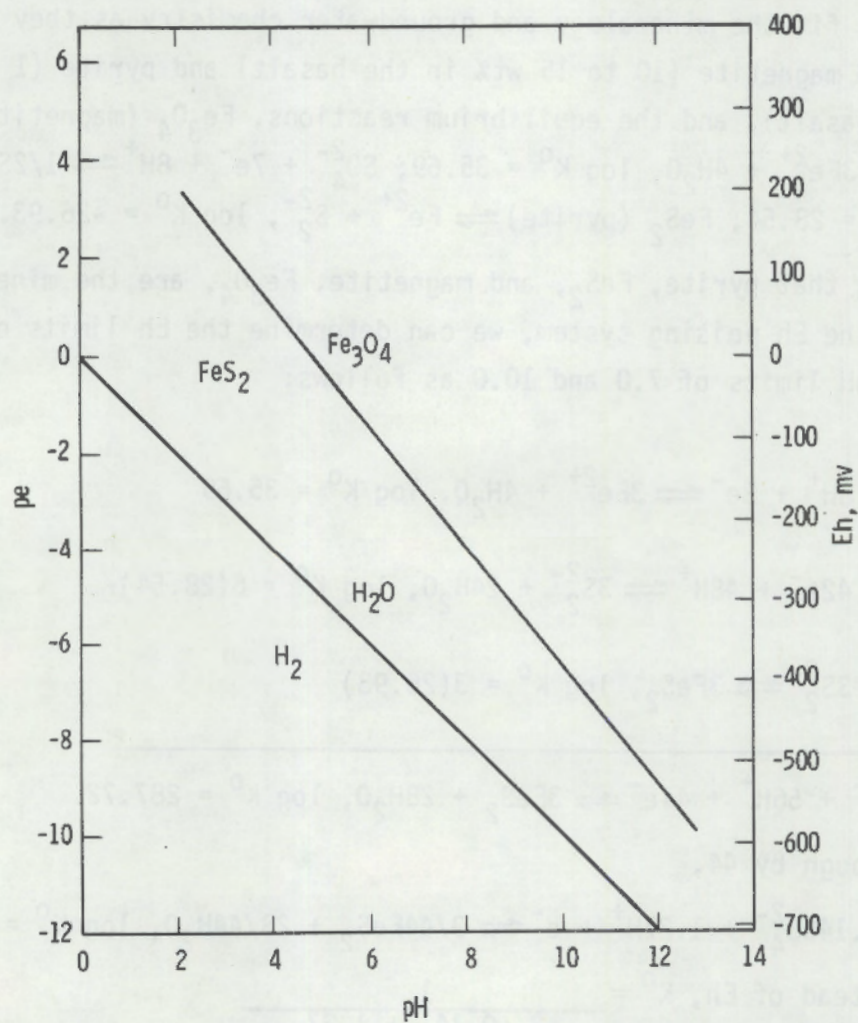
FIGURE 34. Position of the Magnetite-Pyrite Eh-Poising System on a pe-pH
Diagram. The H_2(gas)-H_2O refers to the lower Eh limit of
water stability.

The need for radionuclide distribution measurements under controlled Eh and pH conditions without adding pyrite or magnetite to the system prompted the investigation of several control systems. In addition to the usual requirements for pH buffering and Eh stabilization, such systems also must allow for noninterference with the radionuclide sorption processes usually active without the pH buffering and Eh stabilizing agents present in the system.

System pH buffers of definite ionic strength, such as monobasic weak acid or monoacidic weak base systems (Bates, 1973), can be used to ascertain the effects of ionic strength, as well as pH, on the resulting Kd values. The pH buffer effects are, thus, a relatively simple problem. The Eh agents, on the other hand, have to be thoroughly tested in radionuclide-solid-solution systems to determine whether or not problems such as radionuclide-Eh agent complexing arise with their use.

One of the best known and thoroughly tested Eh stabilization agents is quinhydrone, an equimolecular compound of benzoquinone (OC_6H_4O) and hydroquinone (HOC_6H_4OH). About 4 g of quinhydrone are soluble in distilled water at 25^OC.

Several electro-motive force (EMF) measurements were made at 25° and 60^OC in quinhydrone systems buffered at specific pH values. Quinhydrone may be represented in solution as $C_6H_4O_2 + 2H^+ + 2e \rightleftharpoons C_6H_4(OH)_2$, a mixture of quinone and hydroquinone. It functions as a dibasic acid, ionizing in two stages: $H_2Q \rightleftharpoons H^+ + HQ^-$ and $HQ \rightleftharpoons H^+ + Q^{2-}$, with $K_1 = 10^{-7.9}$ and $K_2 = 10^{-10.6}$ (Glasstone, 1942). Hence, the use of quinhydrone in Eh poising is confined to buffered pH values of ~ 7.5 or less, with lower buffered limits of about pH 1.0. Within the above pH range, response is very rapid. Beckman combination electrodes were used to measure EMF. These electrodes consist of an indicating platinum disc electrode in combination with a silver/silver chloride reference electrode. The pH was measured simultaneously and both readings were continuously recorded by a dual-pen recorder until equilibrium was attained. The combination electrode was sealed into the container of solution to avoid evaporation losses and oxidation. Readings were taken over several hours. The results of these EMF measurements with the combination electrode are shown in Table 31. The EMF curves are shown in Figure 35. The 60^OC slope is not quite parallel to the 25^OC slope as expected (Bates, 1973).

TABLE 31.   Electro-Motive Force Measurements on a pH-Buffered
Quinhydrone System at 23° and 60°C. Eh-minus-measured EMF
should equal a constant millivolt characteristic of the
silver/silver chlorine reference electrode.

23°C			
Buffered pH	EMF, mV	Eh, mV	(Eh)-(EMF), mV
2.0	380	581	201
3.0	323	521	198
4.0	266	462	202
6.0	139	344	205
7.0	98	285	187

| 60°C			
Buffered pH	EMF, mV	Eh, mV	(Eh)-(EMF), mV
1.4	374	541	217
2.7	308	514	206
3.9	225	443	218
6.0	88	319	231
6.9	50	266	216
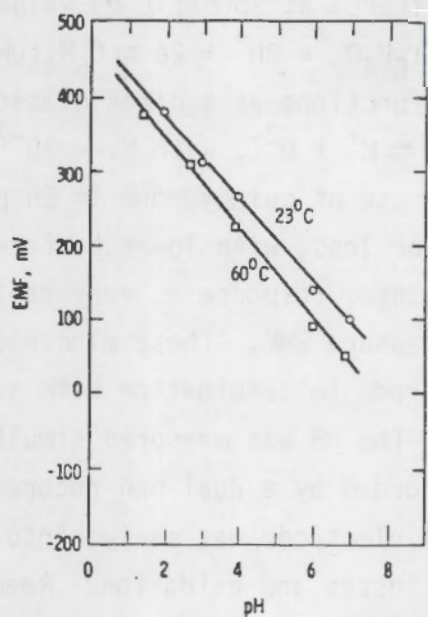
FIGURE 35.   Graph of the 23° and 60°C EMF Measurements of the
pH-Buffered Quinhydrone System Given in Table 31.

Eh values can be determined from quinhydrone reaction standard potentials at $25^\circ C$ (0.699 V) and $60^\circ C$ (0.674 V) and pH = 0. The Eh equals E - pH (59.2) at the proper temperature. An equation formulated by Ives and Janz (1961) was used to determine the standard potential at $60^\circ C$. These authors state that quinhydrone could be used in the presence of many metallic salts (zinc, cadmium, mercury, nickel, cobalt, iron, and copper) without ill effects.

If the reaction $2H_2O \rightleftharpoons O_2(g) + 4H^+ + 4e^-$ or Eh = E + 0.0592/4 log PO_2 - 0.0592 pH is used to determine PO_2, it is approximately equal to 10^{-36} atm at $25^\circ C$ for the quinhydrone system. While this is not down to the range of the iron (II)/(III) couple, it would be useful to have Kd data at this intermediate PO_2 level. Figure 36 shows where the quinhydrone pH-buffered solutions would fall on the Eh-pH diagram for selenium at the concentration


RCP8107-36
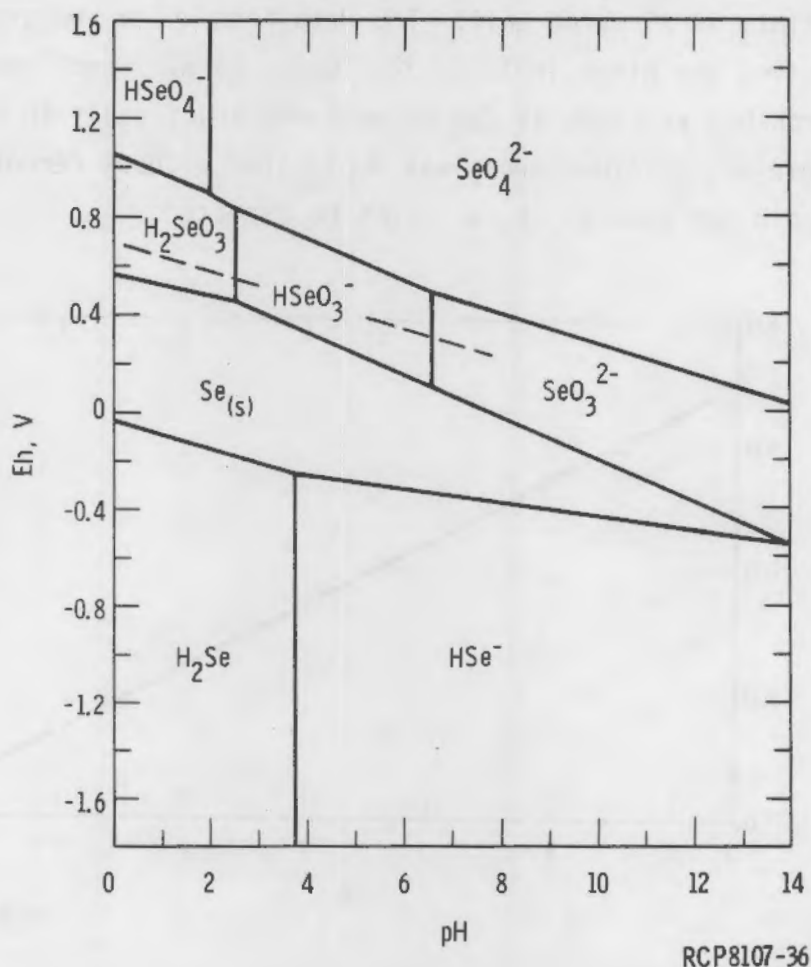
FIGURE 36. Eh-pH Diagram for Selenium-Water at $25^\circ C$ and Selenium = 3 x $10^{-12}M$. The dashed line represents quinhydrone pH-buffered solutions at $25^\circ C$.

normally used in this tracer work. The data used in constructing Figure 36
were from Pourbaix (1966). While the Eh would not be low enough to obtain
selenium$_{(s)}$ at pH 4 to 7.5 (the lower proposed working pH range for
distribution coefficient determinations with quinhydrone and basalts), a
different selenium species will be formed: (HSeO$_3^-$ or SeO$_3^{2-}$ rather
than SeO$_4^{2-}$). However, the Kd effects may be minor, since all species are
anionic. The transformation from technetium(VII) to (IV) and from uranium(VI)
to (IV) also occurs at lower Eh values.

Ferroin (1, 10-phenanthroline-ferrous sulfate complex) also was tested as
an agent to stabilize or buffer the system Eh. The two molarities used were
4.17×10^{-4} and 2.08×10^{-3} ferroin in pH-buffered solutions containing
Umtanum basalt. The EMF measured is given in Figure 37. Both levels of
ferroin yielded the same EMF results. The slope of the line connecting the
experimental points is 55 mV/pH unit. The data from which the experimental
points were derived are given in Table 32. While 55 mV is not the theoretical
59 mV, it is probably as close as can be measured practically in such a
system. The same set of experiments was duplicated without ferroin. The pH
buffer systems did not control Eh, as might be expected.

RCP8107-37
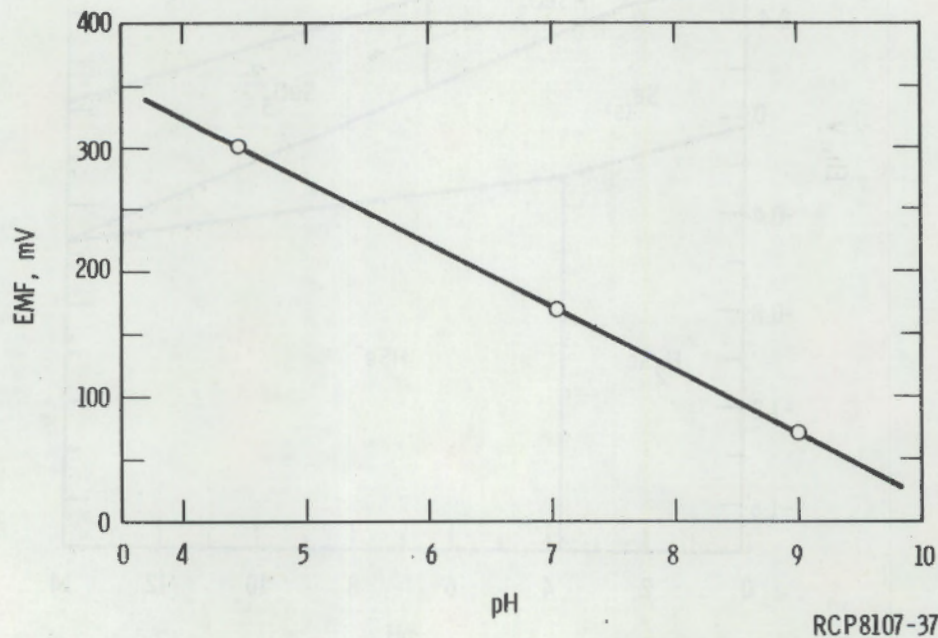
FIGURE 37. Solution pH versus EMF Measured with a Point-Indicating Electrode
and a Silver/Silver Chlorine Reference Electrode at $23^0 \pm 2^oC$
for Ferroin Solution.

TABLE 32. Electro-Motive Force Measurements on pH-Buffered
Ferroin Systems at 23°C.

Ferroin Molarity	Umtanum Basalt Present	Measured pH	Measured EMF, mV	Average EMF, mV
2.08×10^{-3}	no	8.95	68	
2.08×10^{-3}	yes	9.00	70	70
4.17×10^{-4}	no	8.95	70	
4.17×10^{-4}	yes	8.95	70	
2.08×10^{-3}	no	7.05	175	
2.08×10^{-3}	yes	7.05	170	171
4.17×10^{-4}	no	7.00	170	
4.17×10^{-4}	yes	7.00	170	
2.08×10^{-3}	no	4.40	320	
2.08×10^{-3}	yes	4.50	288	303
4.17×10^{-4}	no	4.35	315	
4.17×10^{-4}	yes	4.55	288	

The basalt itself attempted to control system Eh, but poising reactions such as magnetite/hematite or magnetite/pyrite were too slow. The data showed relatively poor Eh control by the basalt alone. Using the EMF values, the Eh verses pH curve of Figure 38 was generated and compared to that of quinhydrone. The ferroin curve is above the quinhydrone curve.

The use of ferroin in natural systems also presents some problems. For example, Bussetti et al. (1980) and Burheiser and Mortland (1977) reported that 1, 10-phenanthroline and ferroin were readily irreversibly adsorbed by montmorillonite, kaolinite, silica gel, aluminum hydroxide, and hematite as a function of pH.
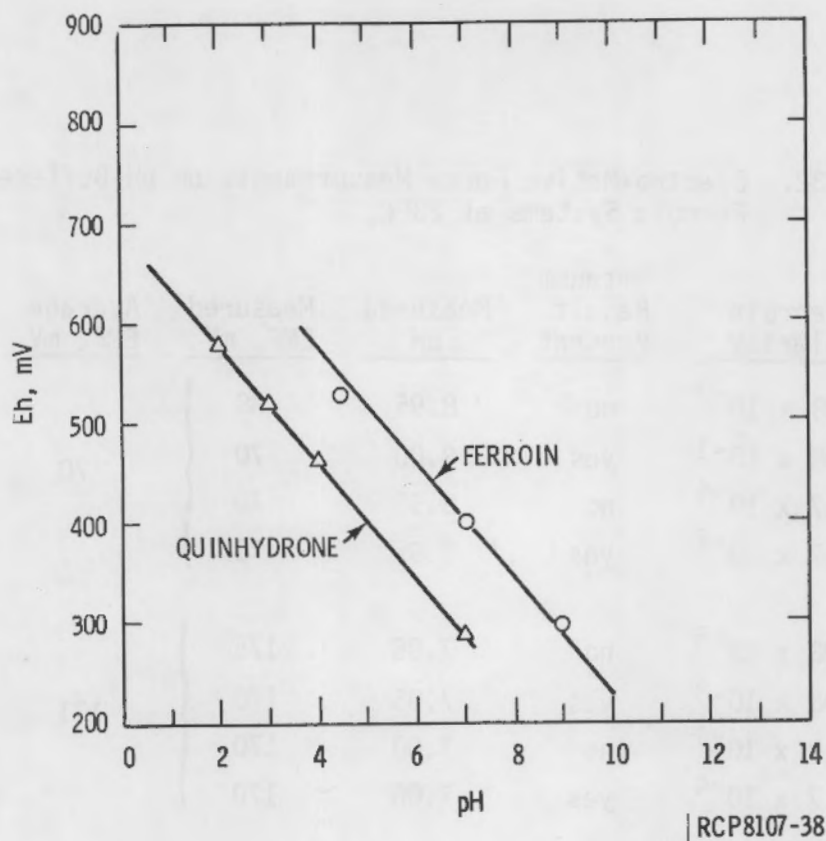
FIGURE 38. Curves of Eh Versus pH at 23°C for Ferroin and Quinhydrone.

Some initial Kd results in ferroin-stabilized systems are given in Table 33. These data were compared to Kd data from systems containing the pH buffer to certify that ferroin does not complex the radionuclide. There were substantial Kd changes when ferroin was present in the system, as shown in Table 31 data. Ferroin cannot be used for Eh poising in systems containing geologic materials, because it has adverse effects on Kd.

TABLE 33.   Cesium-137 Kd Values for Buffer Experiments with Umtanum
            Basalt at 23° and 60°C Containing Various Eh-Poising Agents,
            30-Day Contact. The specific pH values for each Kd value
            are shown below.

		Kd, mL/g		
23°C	$2.08 \times 10^{-3}\underline{M}$ ferroin + pH buffer	902 ± 169	33 ± 1	14 ± 0
	$4.17 \times 10^{-4}\underline{M}$ ferroin + pH buffer	831 ± 231	34 ± 1	14 ± 1
	Saturated quinhydrone + pH buffer	-	24 ± 1	14 ± 0
	pH buffer only	796 ± 30	27 ± 1	14 ± 1
60°C	$2.08 \times 10^{-3}\underline{M}$ ferroin + pH buffer	411 ± 11	18 ± 1	8 ± 1
	$4.17 \times 10^{-4}\underline{M}$ ferroin + pH buffer	401 ± 33	19 ± 1	8 ± 1
	Saturated quinhydrone + pH buffer	-	12 ± 1	7 ± 1
	pH buffer only	476 ± 22	14 ± 1	7 ± 0

|		pH		
23°C	$2.08 \times 10^{-3}\underline{M}$ ferroin + pH buffer, blank	8.95	7.05	4.40
	Umtanum	9.0	7.05	4.50
	$4.17 \times 10^{-4}\underline{M}$ ferroin + pH buffer, blank	8.95	7.00	4.35
	Umtanum	8.95	7.00	4.45
	Saturated quinhydrone + pH buffer, blank	-	6.60	4.00
	Umtanum	-	6.62	4.10
	pH buffers only, blank	9.05	6.90	4.00
	Umtanum	9.00	6.90	4.15

APPENDIX

## UMTANUM BASALT AND MINERAL CHARACTERIZATION

In order to derive a maximum amount of useful data from the equilibration experiments, the basalt and its secondary minerals have to be adequately characterized. This is especially true of the basalt, which consists of five or more mineral phases that are cemented with a glass containing micro-crystallites. Characterization also allows the documentation of any physical or chemical changes that may have taken place in the basalt or minerals as a result of equilibration with the groundwater.

UMTANUM BASALT

As a first step in the characterization, a 2-cm chip of Umtanum basalt obtained from the surface outcrop was mounted in epoxy resin, sawed, ground, and polished. The finished mount was used to take optical photographs by reflected, polarized light as (Figure A1). Several magnifications of the basalt surface are shown from 12 to 200 times that seen by the eye. The Umtanum basalt is partially crystalline, but the crystal dimensions are relatively small (0.1 to 0.01 mm). Many of the black areas on the photographs are vugs that are partially filled with noncrystalline to crystalline, clay-like material consisting of iron oxides, silica, and alumina. The filling was probably formed during late-stage cooling of the basalt flow. The vesicles or vugs were formed much earlier by gases that separate from the cooling lava.

X-ray emission photographs of area A in Figure A1 are shown in Figures A2 and A3. The X-ray characteristic of each given element is produced by electron bombardment of the mount. The emission data for each wavelength X-ray characteristic of an element were stored and later projected onto a phosphored screen where an optical photograph was taken. In the emission photographs, the various mineral phases can usually be identified. For example, the plagioclase feldspars are outlined in the photographs for silicon, aluminum, and calcium, while the pyroxenes are outlined in the calcium, iron, magnesium, and silicon photographs. By comparing photographs, the several phases present in the basalt can be identified. Going back to Figure A1, area A, the lightest-colored crystals are metallics, such as magnetite or ilmenite, the light-gray crystals are pyroxenes, and the darker

12X

A   200X

B
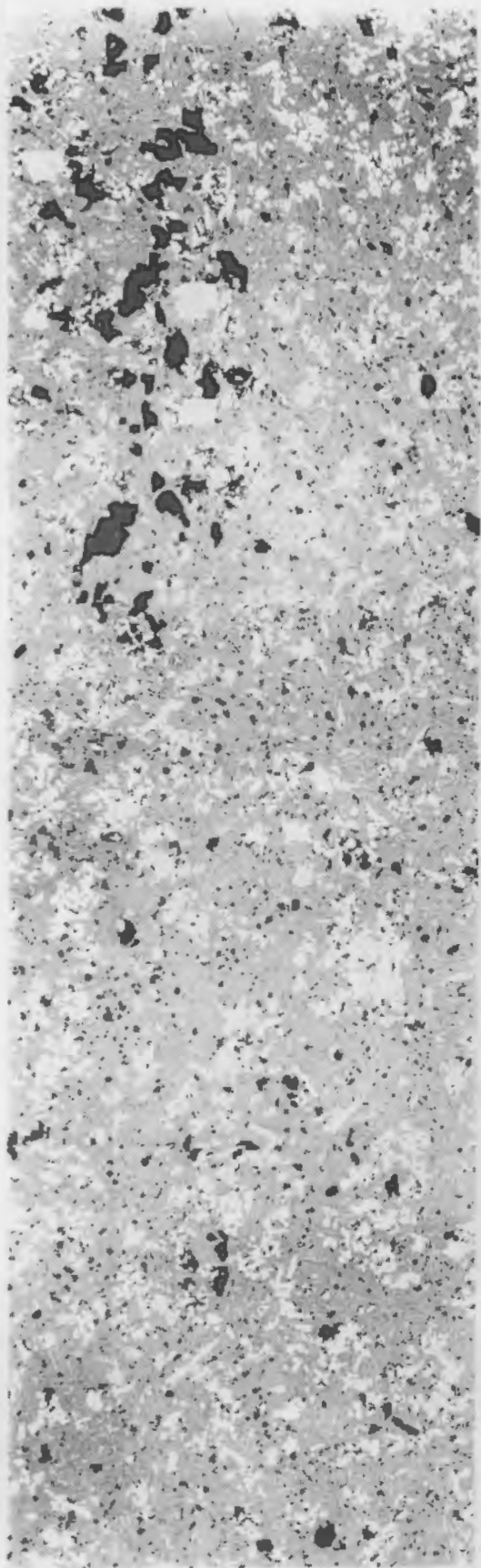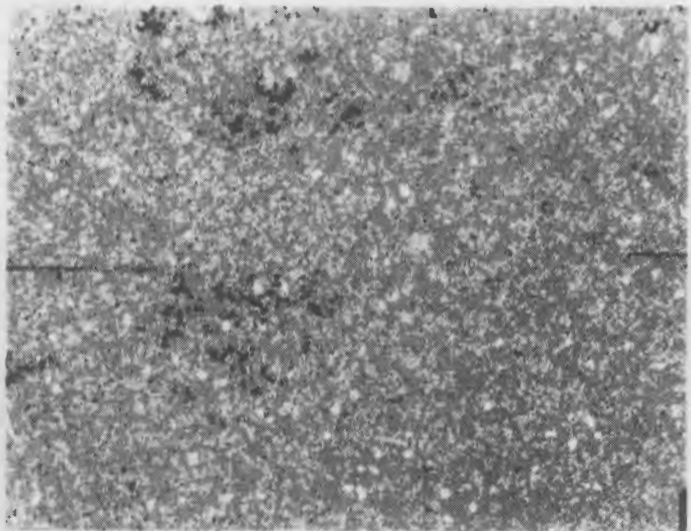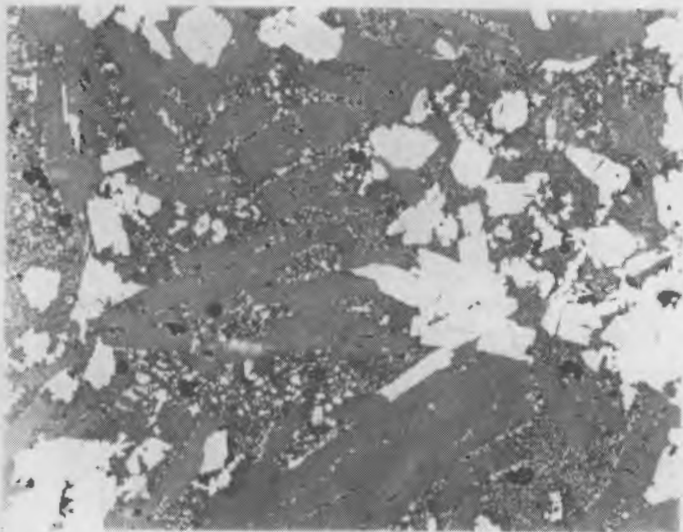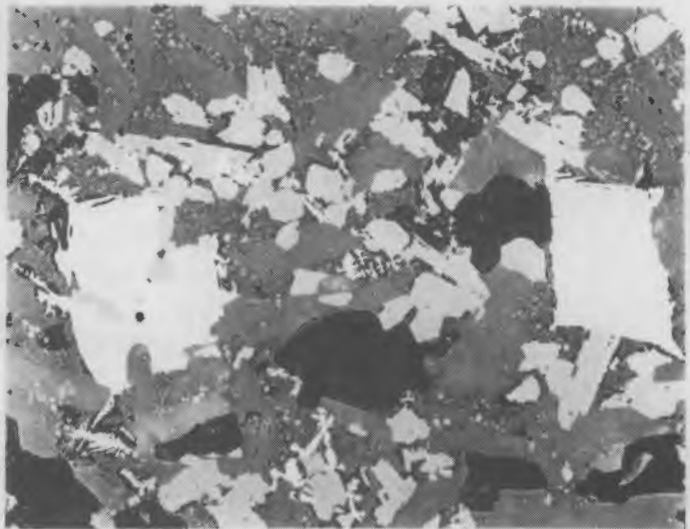
50X   B   200X

RCP8107-146

FIGURE A1. Umtanum Basalt Optical Microphotographs.

71

Electron Scattering   200X
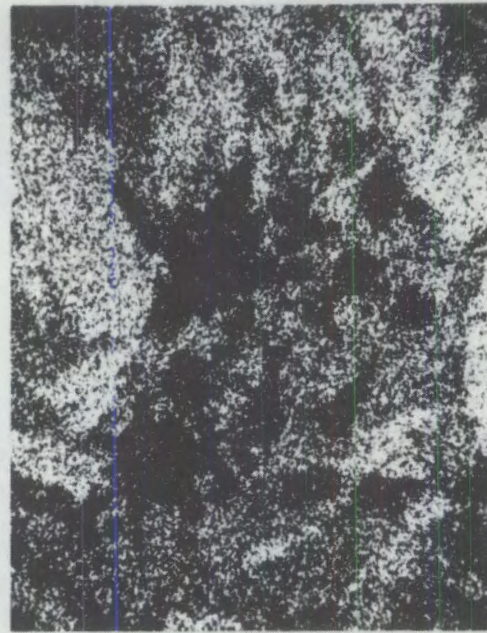
Al
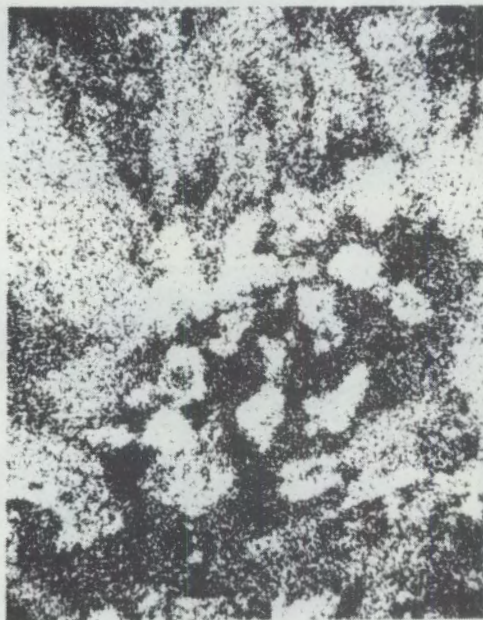
Co

Fe

RCP8107-147

FIGURE A2. Umtanum Basalt Optical Microphotographs, Area A.
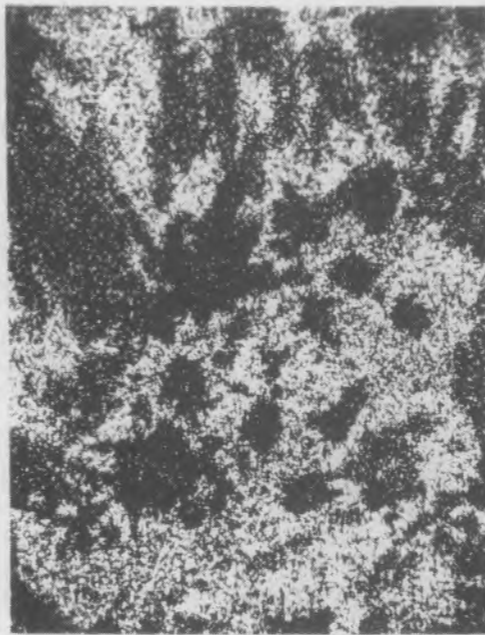
K
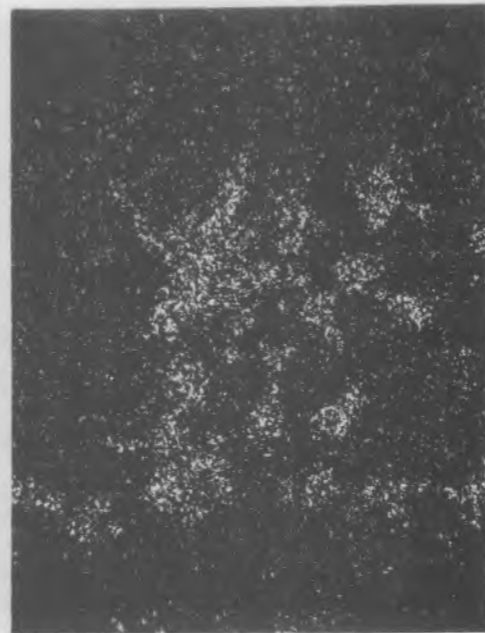
Mg
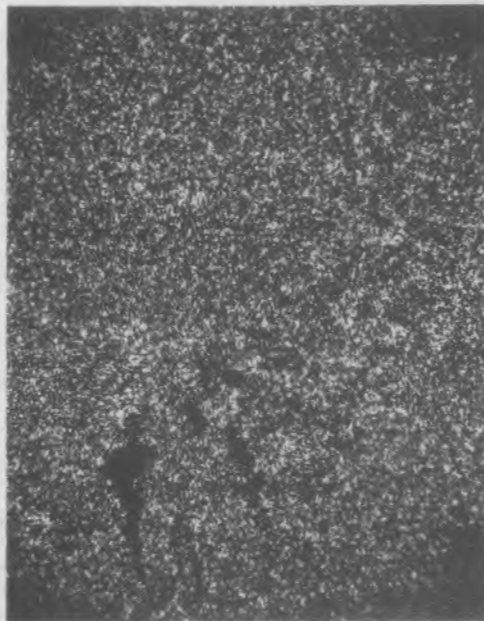
Si

Ti

RCP8107-148

FIGURE A3.   Umtanum Basalt Optical Microphotographs, Area A.

gray laths are plagioclase feldspars. The very small crystals between the
feldspar laths are groundmass, the residual silicate liquid left after
crystallization of the main-stage minerals. Some crystallites can be seen in
the groundmass embedded in rapidly cooled, noncrystalline, silicate glass. At
least two generations of titaniferous metallics are indicated by the presence
of small dendritic crystals and larger equidimensional ones.

Area B of Figure A1 is shown in X-ray emission photographs in Figures A4
and A5: note that both the large and small metallic crystals are titaniferous.
The high magnesium concentration seen in the magnesium emission photograph is
part of the material deposited in a vug. A more detailed examination of the
vug-filling material in area B is shown in Figure A6. It is a clay-like
material that may not be crystalline, but contains essentially the same
constituents as a clay or a zeolite.

The collected Umtanum basalt was crushed and screened to obtain a 20- to
50-mesh (850 to 300 µm) size fraction (Hodge and Grutzeck, 1978). Weathered
surfaces were hand-picked and removed from the material to avoid contamination
of the fresher basalt. A photomicrograph of the selected size fraction is
shown in Figures A7 and A8: note that the size of the mineral crystals in the
basalt fragments is still much less than the diameters of the fragments--an
exception is the large metallic fragment shown in area B of Figure A8.
Chemical analysis of this fragment strongly suggested that it was a piece of
the crusher or grinder worn off of the machinery during the sizing and
grinding operations. However, as can be seen in the bright field photograph
in Figure A7, such fragments of machinery were very scarce and constitute a
minor contaminant in the crushed sample. The iron fragments could be removed
magnetically, but not without also removing at least a portion of the
metallics in the sample, which would result in a biased sample with part of
the ferrous iron removed. The ferrous iron is part of the system that tends
to maintain a low redox potential in the system, and, thus, it would be more
detrimental to remove the iron fragments than leave them in. Therefore, no
attempts were made to remove the few iron fragments from the sized basalt.
Two samples were split from the 27.3 kg of sized basalt and sent to Washington
State University for X-ray fluorescence analysis by their Basalt Research
Group.
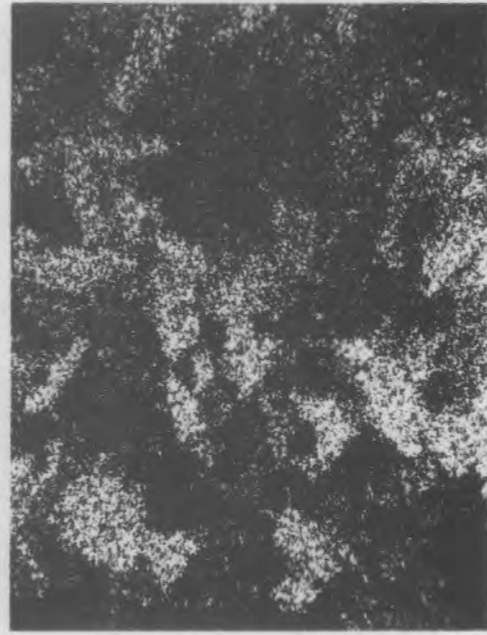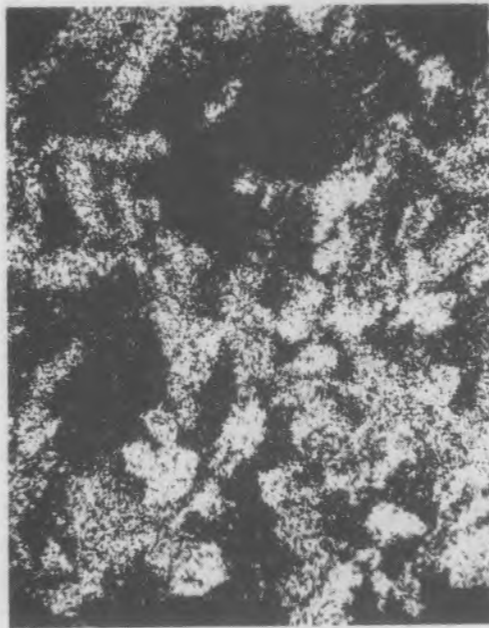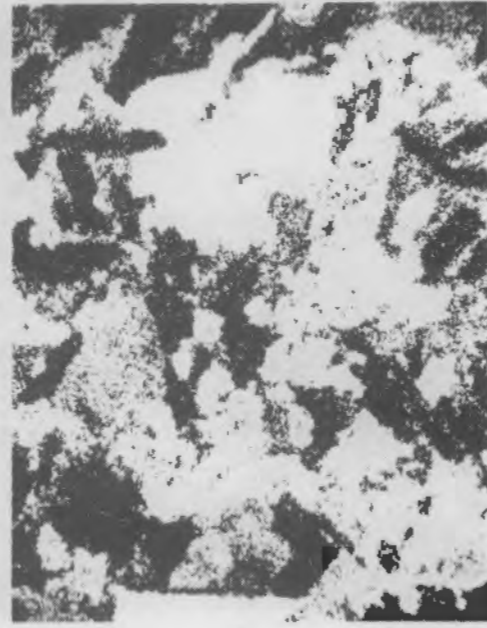
FIGURE A4. Umtanum Basalt Optical Microphotographs, Area B.
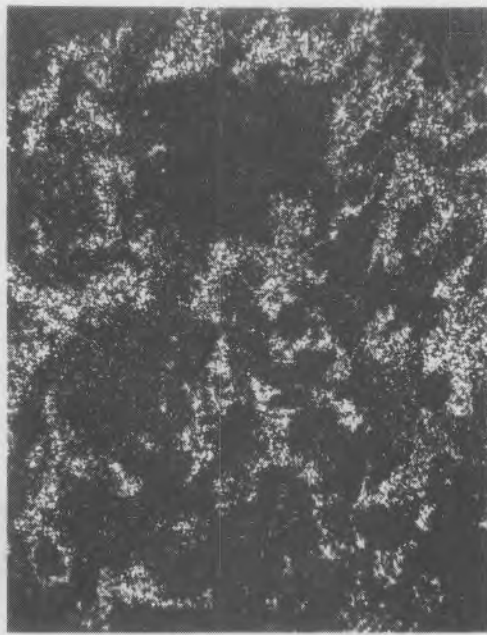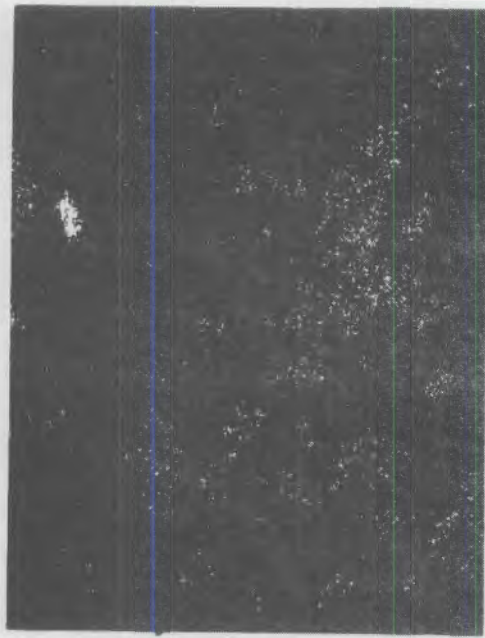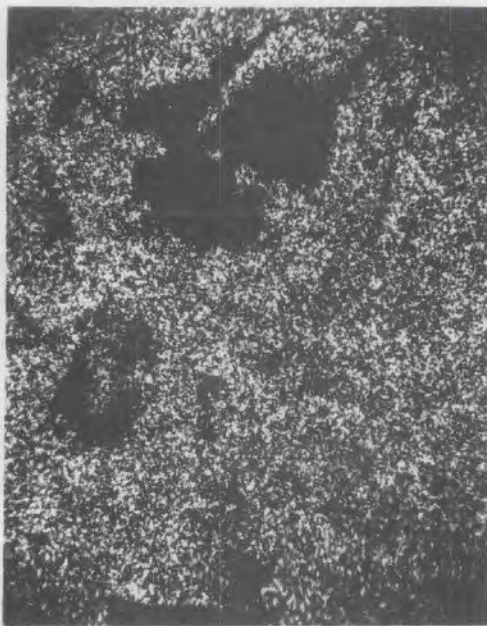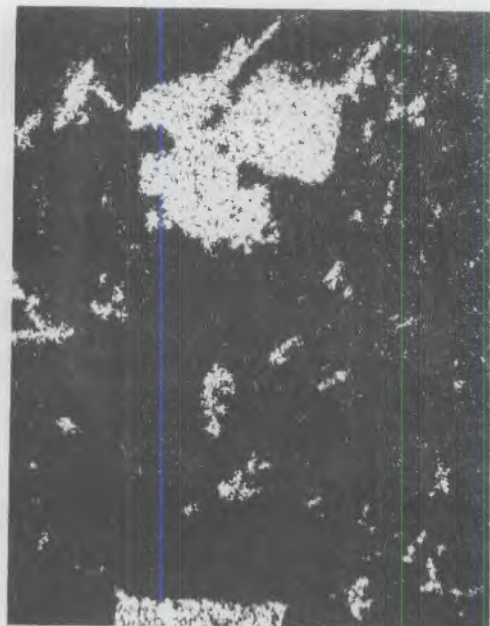
FIGURE A5. Umtanum Basalt Optical Microphotographs, Area B.

RCP8107-150

SEM   200X

SEM   600X   SEM   3000X

RCP8107-151

FIGURE A6.   Umtanum Basalt Optical Microphotographs, Vug Filling.
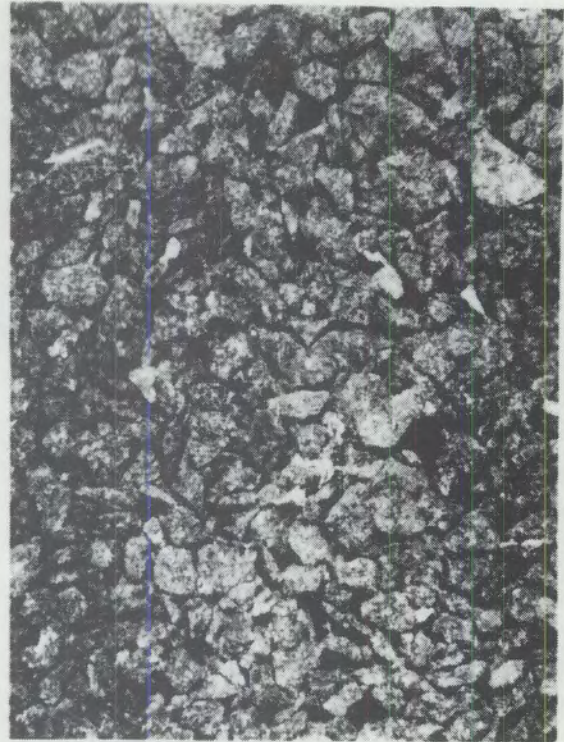
D.F.   12X

B.F.   12X

RCP8107-152

FIGURE A7. Umtanum Basalt Optical
            Microphotographs, 20-
   to 50-Mesh Size.

50X

78

FIGURE A8. Umtanum Basalt Optical Microphotographs, 20- to 50-Mesh Size.

RCP8107-153

79

In preparation for X-ray fluorescence work, the basalt samples were broken into small pieces with a hammer and then crushed in an aluminum-plated jaw crusher. Approximately 20 g of chips were hand-picked to avoid weathered surfaces and possible small slivers of steel or aluminum, and placed in a swingmill (shatter box) where they were ground for 6 min. This provided a fine, even-grained powder, which is a prerequisite to the production of homogeneous samples. A normal ballmill was found inadequate for this purpose.

Seven grams of lithium tetraborate ($Li_2B_4O_7$) and 3.5 g of the rock powder were thoroughly mixed in a plastic jar on a spex ballmill and then fused in graphite crucibles for 5 min at $1,000^\circ C$. When cooled, the lithium tetraborate beads had one edge ground with fine-silicon carbide powder.

The flat surface of the bead was irradiated in a Philips P. W. 1410 manual spectrometer with a chromium target tube. The recorded count rate for each element was related to the calibration curve derived from the count rate of eight analyzed basalts supplied by the U.S. Geological Survey. The raw oxide values were corrected for absorption and normalized on a volatile-free basis with Fe_2O_3 assumed to be 2.00%.

Chemical Analyses and Results

The resulting analyses of the aforementioned Umtanum basalt samples from Priest Rapids are given in Table A1, where they are compared to an analysis of the Umtanum flow at Sentinel Gap: note that there are minor differences in several constituents between the two locations. These differences suggest that at least part of the proposed radionuclide-basalt distribution work should be repeated when enough repository basalt becomes available to be certain that no major distribution coefficient changes occur due to sample differences.

TABLE A1. Umtanum Basalt Chemical Analyses and Analytical Precision
Determined with 13 Sets of Triplicate Samples.

	wt%			
Constituent	Priest Rapids Umtanum		Sentinel Gap Umtanum	Analytical Precision, 95% Level (2σ),
SiO_2	55.64	55.23	54.47	± 0.550
Al_2O_3	13.62	13.70	14.37	± 0.310
Fe_2O_3	2.00	2.00	2.00	-
FeO	10.68	10.86	11.16	± 0.350
MnO	0.20	0.20	0.22	± 0.010
CaO	7.17	7.23	7.36	± 0.220
MgO	3.33	3.30	3.56	± 0.150
Na_2O	3.30	3.36	2.79	± 0.160
K_2O	1.62	1.64	1.58	± 0.030
TiO_2	2.05	2.07	2.11	± 0.050
P_2O_5	0.39	0.40	0.36	± 0.014
Total	100.00	99.99	99.98	

The distribution of some of the above elements in the Umtanum basalt
sample used in the Kd work is shown in the X-ray emission photographs of
Figures A9 and A10. The potassium photograph (Figure A10) outlines the
groundmass of each fragment because the potassium does not fit readily into
any of the major mineral phases, and, hence, is finally found in the residual
silicate liquid. Here it can rise to 5 or 6 wt% compared to ~1.5 wt% in the
whole melt.

The crystalline components of a basalt consist of plagioclase feldspars,
pyroxenes, and metallic oxide minerals such as magnetite. These components
can vary compositionally over a rather wide range, which was estimated for the
feldspar and pyroxenes by analyzing several with the microprobe.

Feldspars. Plagioclase feldspars are one of the main crystalline mineral
phases constituting the basalt. The compositional names of the plagioclases
were assigned before the structural complexity of the various solid solution

81

Electron Scattering
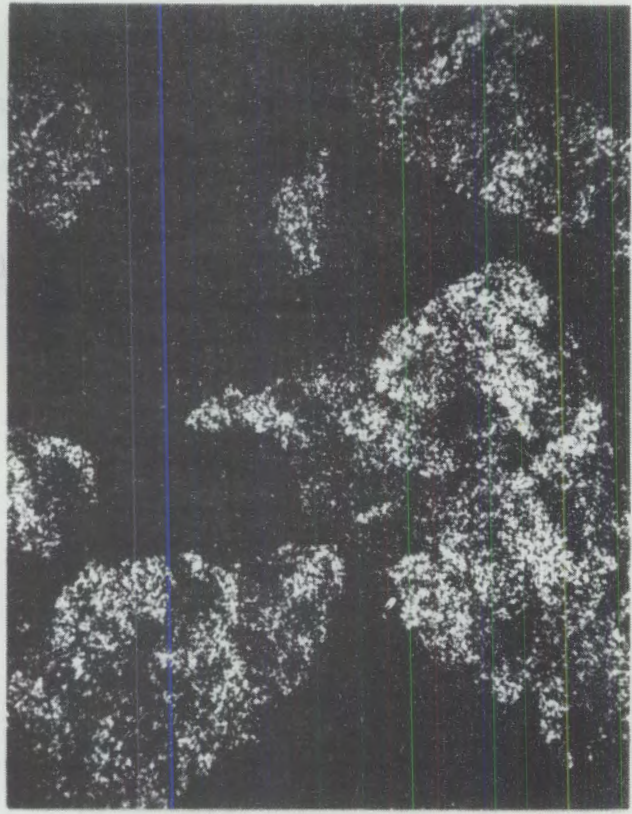
Al

Ca
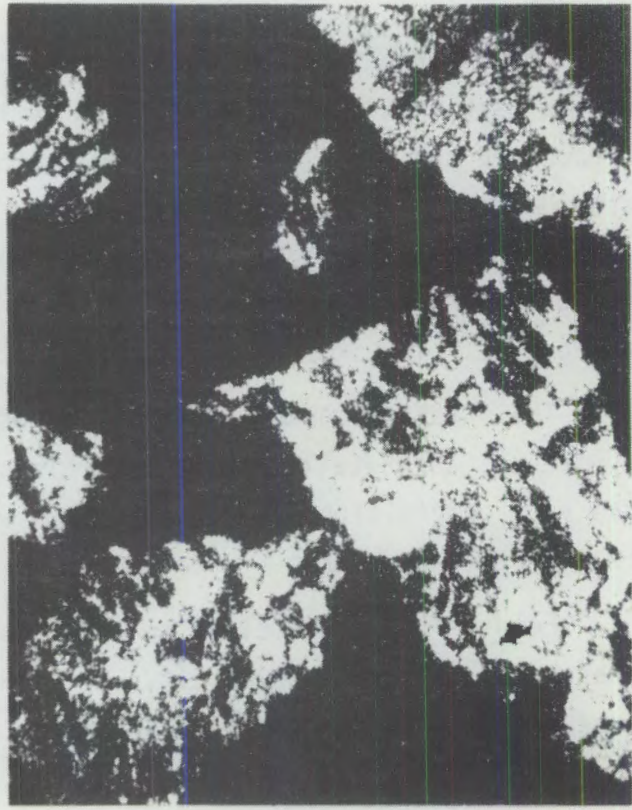
Fe

FIGURE A9. Umtanum Basalt X-Ray Emission Photographs.

RCP8107-154

K

Mg

Si

Ti

FIGURE A10. Umtanum Basalt X-Ray Emission Photographs (Potassium). RCP8107-155

series were realized. Usually the composition of a feldspar in the series can be given in terms of albite-anorthite molecular percentages. But there is also a third molecule that must be taken into account, that of orthoclase, or $KAlSi_3O_8$. Most feldspars can compositionally be considered as falling on the $NaAlSi_3O_8$-$KAlSi_3O_8$-$CaAl_2Si_2O_8$ diagram. The composition of a feldspar is expressed as the "molecular" percentage of albite, anorthite, and orthoclase. This procedure of expressing the feldspar in molecular percentage allows a rapid comparison of two feldspars of differing composition that is not readily available from chemical analyses alone. In the molecular percentage determinations, 32 oxygen atoms per molecule are required for the structural formula $(Na, K, Ca)_4 (Si, Al)_{16}O_{32}$.

The microprobe chemical analyses of the plagioclase, main-stage crystals are given in Table A2. From these analytical data, the cation contents of a feldspar molecule containing 32 oxygen atoms can be computed. Analysis F1 of Table A3 gives an example of how the cation contents were computed. The microprobe gave the weight percent values shown in Table A2 for F1. These values were divided by their respective molecular equivalent weights and recomputed to 100% to yield: silicon, 55.07; albite, 24.39; calcium, 9.60; sodium, 9.82; and potassium, 1.12 mol%. Each of the above cations has a characteristic number of oxygen atoms associated with it (for example, aluminum has 1.5; silicon 2.0; and sodium and potassium have 0.5). These oxygens were summed to give a total of 161.8. Since the desired number of oxygens per molecule is 32, the 161.8 was divided by 32 to yield 5.0563 which, in turn, was used for a divisor of each mole percent of cation present in the analysis.

The resulting cation values (Table A3) represent that number of atoms of cations that would occur in molecules containing 32 oxygen atoms. Furthermore, the percent of albite, anorthite, and orthoclase molecules in the combined 32 oxygen molecule were computed from the contents of sodium, calcium, and potassium. The numbers of cations in the 32 oxygen molecule are given in Table A3; from Table A3 data, the plagioclase feldspars were identified in Table A4. The compositional data from Table A4 were plotted on triangular coordinates to locate the variety of plagioclase feldspars in Figure A11: note that five of the six feldspars are labradorites, while the sixth is just into the andesite field. The typical plagioclase variety found in basalts is labradorite, so that the Umtanum basalt flow is a typical basalt with respect to feldspar content.

TABLE A2. Electron Microprobe Chemical Analyses of Several Main-Stage
Crystals (F1-F6) in the Umtanum Basalt.

	wt%					
Constituent	F1	F2	F3	F4	F5	F6
SiO_2	62.0	57.6	57.5	57.1	58.1	56.9
Al_2O_3	23.3	25.4	26.4	24.8	25.0	25.5
CaO	10.1	12.3	13.4	12.5	11.5	12.9
Na_2O	5.7	4.1	4.0	4.4	4.3	4.2
K_2O	1.0	0.5	0.4	0.5	0.6	0.5
Total	102.1	99.9	101.7	99.3	99.5	100.0

TABLE A3. The Numbers of Cations Per Feldspar Molecule Containing
32 Oxygen Atoms as Determined Directly from the
Chemical Analyses of Table A2.

Number	Si	Al	Si + Al	Na	Ca	K	Na, Ca, K
F1	10.89	4.82	15.71	1.94	1.90	0.22	4.06
F2	10.33	5.47	15.80	1.42	2.36	0.12	3.90
F3	10.21	5.53	15.74	1.38	2.55	0.10	4.03
F4	10.38	5.31	15.69	1.55	2.43	0.12	4.10
F5	10.49	5.32	15.81	1.51	2.22	0.14	3.87
F6	10.28	5.43	15.71	1.47	2.50	0.12	4.09

TABLE A4. Feldspar Compositions as Determined from the Chemical
Data of Table A3. Ab = albite = $NaAlSi_3O_8$;
An = anorthite = $CaAl_2Si_2O_8$;
Or = orthoclase = $KAlSi_3O_8$.

	mol%			
Number	Ab	An	Or	Feldspar
F1	47.8	46.8	5.4	Andesine
F2	36.4	60.5	3.1	Labradorite
F3	34.2	63.3	2.5	Labradorite
F4	37.89	59.3	2.9	Labradorite
F5	38.9	57.4	3.7	Labradorite
F6	35.9	61.2	2.9	Labradorite
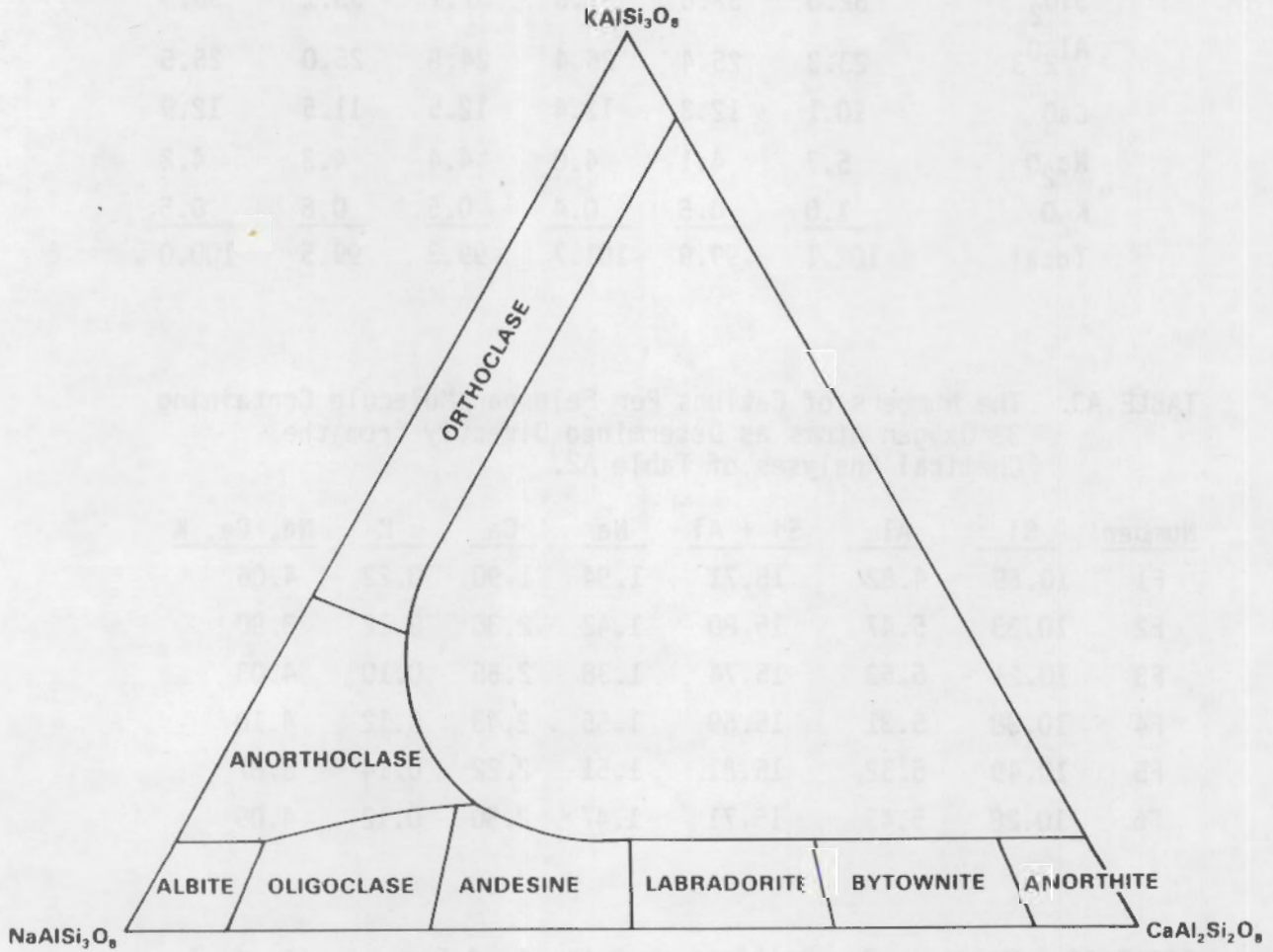
FIGURE A11. Graph of Feldspar Compositions.

RCP8107-39

Pyroxenes. The next most prevalent crystalline mineral phase in the basalt is clinopyroxene. Pyroxenes are essentially a family of calcium-iron-magnesium silicates of varying composition and crystal structure, as shown in Table A5. The microprobe chemical analyses of several pyroxene crystals in the Umtanum basalt flow are given in Table A6. The calcium contents are rather wide ranging and should be reflected in the pyroxene varieties represented. The chemical analyses of Table A6 are referenced to a 6-oxygen molecule to compare molecule cation contents, or ideally, $(K, Na, Ca, Mg, Fe^{+2}, Ti, Al)_2 (Al, Si)_2 O_6$, in Table A7. When the sum of silicon plus the aluminum in tetrahedral coordination exceeds 2.00, part or all of the aluminum was transferred to an octahedral coordination. The molecular percentages of magnesium, iron, and calcium silicates are given in Table A8. These are based on the pyroxene compositions of Tables A6 and A7. Most are augites, the most common pyroxene in basalts, but they do show a considerable variation in composition. The compositions shown in Table A8 can also be plotted in triangular coordinates, with $CaSiO_3$, $MgSiO_3$, and $FeSiO_3$ constituting the apexs as shown in Figure A12. This figure gives a visual concept of the variation of the Umtanum pyroxenes in a calcium-magnesium-iron system.

Other Phases. The groundmass can constitute up to 40% of the basalt and consists of microcrystallites of plagioclase in a rhyolitic composition glass, as seen in the analyses of the groundmass in Table A9.

The metallic oxides or opaque constituents were also examined, as seen in Table A10. Most of the metallics studied were titaniferous magnetites, but a sulfide phase also was identified. These sulfide phases represent original magma constituents that were insoluble in the predominantly silicate melt of the basalt. These are not simple chemical compounds as such, but vary considerably in chemical composition (Carmichael et al., 1974). Sulfides, of course, tend to keep the redox potential low in their vicinity.

TABLE A5. Solid Solution Series and End Members
of the Pyroxenes.

Orthorhombic Pyroxenes

Enstatite-Ferrosilite	$(Mg,Fe^{+2})2Si_2O_6$

Monoclinic Pyroxenes

Diopside-Hedenbergite	$Ca(Mg,Fe^{+2})Si_2O_6$
Johannsenite	$CaMnSi_2O_6$
Aegirine	$NaFe^{+3}Si_2O_6$
Spodumene	$LiAlSi_2O_6$
Jadeite	$NaAlSi_2O_6$
Augite	$(Ca,Mg,Fe^{+2},Al)_2(Si,Al)_2O_6$
Pigeonite	$(Mg,Fe^{+2},Ca)(Mg,Fe^{+2})Si_2O_6$
Omphacite	$(Ca,Na)(Mg,Fe^{+2},Fe^{+3},Al)Si_2O_6$
Fassaite	$Ca(Mg,Fe^{+2},Fe^{+3},Al)(Si,Al)_2O_6$

TABLE A6. Microprobe Chemical Analyses of Seven
Pyroxene Crystals (P1-P7).

wt%

Number	SiO_2	Al_2O_3	TiO_2	MgO	CaO	FeO	MnO	Total
P1	55.1	0.2	0.3	17.1	6.6	20.4	0.3	100.0
P2	51.5	0.6	0.9	10.3	17.4	19.4	0.4	100.6
P3	54.5	0.5	0.3	17.7	6.8	18.9	0.4	99.1
P4	53.0	1.2	0.7	13.8	19.6	14.2	0.1	102.6
P5	53.7	1.6	0.6	13.7	21.4	12.5	0.2	103.7
P6	54.5	0.9	0.3	16.5	6.7	19.5	0.3	98.7
P7	52.3	0.7	1.2	13.3	7.0	23.5	0.4	98.4

TABLE A7. The Number of Cations Referred to a Six-Oxygen Molecule for Pyroxene Compositions Based on the Microprobe Chemical Analyses of Table A4.

Number	Si	Al	Si + Al	Mg	Fe	Ca	Ti	Mn	Al	ε
P1	2.054	-	2.054	0.950	0.636	0.264	0.018	0.009	0.009	1.886
P2	1.981	0.028	2.009	0.591	0.626	0.716	0.025	0.014	-	1.972
P3	2.039	-	2.039	0.987	0.598	0.272	0.009	0.014	0.023	1.880
P4	1.953	0.053	2.006	0.765	0.442	0.774	0.020	0.002	-	1.994
P5	1.951	0.049	2.000	0.742	0.380	0.833	0.018	0.006	0.019	1.998
P6	2.051	-	2.051	0.925	0.613	0.271	0.009	0.009	0.041	1.868
P7	2.025	-	2.025	0.767	0.760	0.291	0.035	0.013	0.033	1.899

TABLE A8. Molecular Percentages of Magnesium Iron and Calcium Silicates Comprising the Pyroxenes of Tables A6 and A7.

Number	$MgSiO_3$	$FeSiO_3$	$CaSiO_3$	Pyroxene
	mol%			
P1	51.4	14.2	34.4	Augite
P2	30.6	37.0	32.4	Ferroaugite
P3	53.2	32.2	14.6	Augite
P4	38.3	22.4	39.3	Augite
P5	38.0	19.4	42.6	Augite
P6	51.1	33.9	15.0	Subcalcic augite
P7	42.2	41.8	16.0	Subcalcic augite
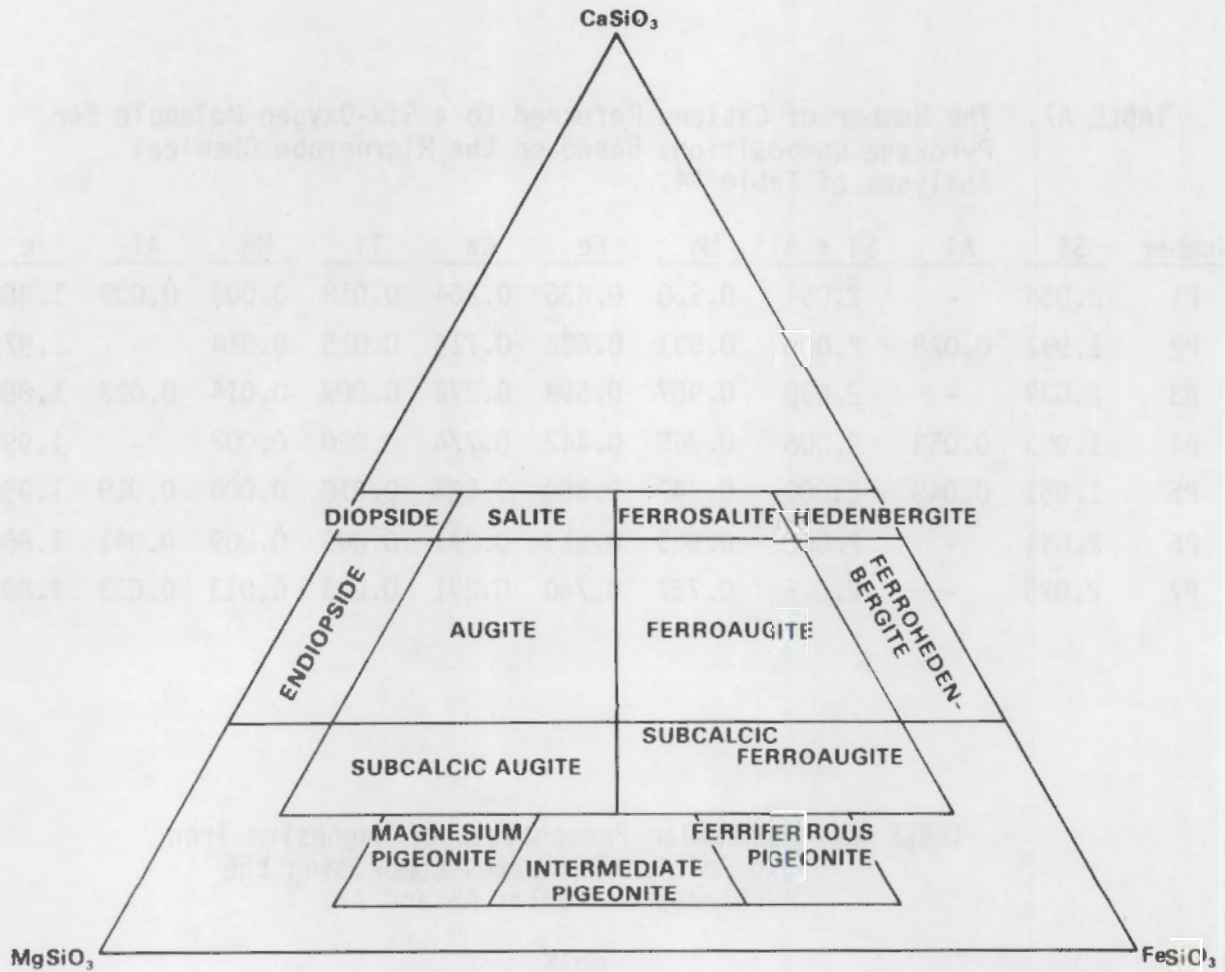
RCP8107-40

FIGURE A12. Graph of Pyroxene Compositions.

TABLE A9. Chemical Analyses of Groundmass Areas Between Main-Stage Crystals in the Umtanum Basalt Flow Compared with Whole Rock Analyses.

	wt%			
	Groundmass		Whole Rock	
SiO_2	63.1	71.8	55.64	55.23
Al_2O_3	10.6	10.9	13.62	13.70
Fe_2O_3	-	-	2.00	2.00
FeO	12.3	5.3	10.68	10.86
MnO	-	-	0.20	0.20
BaO	0.2	0.1	-	-
CaO	4.3	2.1	7.17	7.23
MgO	0.2	-	3.33	3.30
Na_2O	0.6	-	3.30	3.36
K_2O	4.1	5.2	1.62	1.64
TiO_2	2.5	0.9	2.05	2.07
P_2O_5	1.2	-	0.39	0.40
Total	99.1	96.3	100.00	99.99

TABLE A10. Opaque Metallic Crystals Found in the Umtanum Basalt and Analyzed by Microprobe.

		wt%			
Immiscible Sulfide		Titaniferous Magnetite			
SiO_2	1.3	SiO_2	0.6	0.5	0.8
Al_2O_3	2.6	Al_2O_3	2.6	2.8	2.7
TiO	-	TiO	23.5	23.2	24.0
MgO	1.3	MgO	2.2	2.9	2.0
CaO	0.7	CrO_3	-	0.2	0.1
Cr	0.2	MnO	0.4	0.4	0.4
Mn	40.5	FeO	69.7	71.0	68.7
Fe	26.5	Total	99.0	101.0	98.7
S	25.9				
Total	99.0				

91

Surface Area

The technique of Brunauer et al. (1938), a nitrogen or argon gas adsorption method referred to as B.E.T., was used to measure specific surface areas of the 20- to 50-mesh rock samples. Another method used was that of ethylene glycol adsorption first proposed by Hendricks and Dyal (1950) and further refined by Rai and Franklin (1978). Supposedly, the B.E.T. method measures only external surface areas, while glycol adsorption measures both external and internal surfaces with the swelling surfaces of smectite an example of the latter. In any case, the two methods do not measure the same quantities (Haynes 1961).

The B.E.T. surface area reported for the Umtanum basalt in the 20- to 50-mesh size range was $2.8 \text{ m}^2/\text{g}$. Ethylene glycol surface area was $17.7 \pm 3.75 \text{ m}^2/\text{g}$. The latter method is considered to be more readily correlated with cation exchange capacity.

Cation Exchange Capacity

The cation exchange capacities of the various 20- to 50-mesh basalt samples were measured with ^{85}Sr tracer in a strontium chloride solution of known concentration (Routson et al., 1973). A small, 2-g quantity of 20- to 50-mesh representative rock sample was placed in a 1-cm diameter tube with a fine-glass frit base and saturated with an excess of the 1N (normal) strontium solution. An equal volume of 0.05N strontium solution traced with ^{85}Sr was then equilibrated with the geologic material. The excess strontium solution remaining in the 2-g rock sample was displaced with two alcohol washes before counting.

The comparison of counts on the rock sample to counts in a similar volume of solution of known concentration allowed computation of the amount of strontium retained by exchange on the 2-g rock sample. The cation exchange capacity is not an absolute value, but varies to a greater or lesser extent as a function of the cation, pH, and procedure used in the capacity determination. The cation exchange capacity of the 20- to 5D-mesh Umtanum basalt was 1.65 ± 0.1 meq/100 g.

Quantitative Estimation of Mineral Phases

A Quantimet was used to electronically scan five photographs of areas of the Umtanum basalt flow at 500X magnification. The Quantimet responds to the various shades (which represent different minerals) on the film, such as metallics (white) through clays (black). The groundmass was mottled in appearance and was obtained by the areal difference between the sum of the scanned phases and the total area scanned. The results for the average of the five scanned areas are given in Table A11. Density corrections should be applied if the weight percent of each phase is desired.

TABLE A11. Quantitative Estimation of Umtanum Basalt
Phases by Quantimet.

Phases	Total Area, %
Metallics	6.8
Pyroxene	21.0
Clays	8.7
Plagioclase	26.0
Groundmass	37.5

REFERENCES

Ames, L. L., and J. E. McGarrah. 1980. Basalt-Radionuclide Distribution Coefficients - Fiscal Year 1979 Annual Report. PNL-3146. Pacific Northwest Laboratory, Richland, Washington.

Ames, L. L. and D. Rai. 1978. Radionuclide Interactions with Soil and Rock Media. 520/6-78-007, Vol. 1. U.S. Environmental Protection Agency, Washington, D.C.

Andelman, J. B. and T. C. Rozzell. 1970. "Plutonium in the Water Environment. I. Characteristics of Aqueous Plutonium." Radionuclides in the Environment. Adv. Chem. Ser. 93:118-137.

Bates, R. G. 1973. Determination of pH. 2nd Edition. J. Wiley and Sons, New York.

Berner, R. A. 1971. Principles of Chemical Sedimentology. McGraw-Hill Book Co., New York. p. 222.

Brunauer, S., P. H. Emmett, and E. Teller. 1938. "Adsorption of Gases in Multimolecular Layers." Jour. Am. Chem. Soc. 60:309-319.

Burheiser, V. E. and M. M. Mortland. 1977. "Hectorite Complexes with Cu(II) and Fe(II)-1,10-phenanthroline Chelates." Clays and Clay Minerals. 25:105-112.

Bussetti, S. G., E. A. Ferreiro, and A. K. Helmy. 1980. "Adsorption of 1, 10-phenanthroline by Some Clays and Oxides." Clays and Clay Minerals. 28:149-154.

Carmichael, I. S. E., F. J. Turner, and J. Verhoogen. 1974. Igneous Petrology. McGraw-Hill, New York.

Clark, S. P. 1966. Handbook of Physical Constants. Geol. Soc. Am. Memoir 97. The Geol. Soc. Am., New York.

Cleveland, J. M. 1979. "Critical Review of Plutonium Equilibria of Environmental Concern." Chemical Modeling in Aqueous Systems. ACS Symposium Series 93. Amer. Chem. Soc., Washington, D.C. pp. 332-333.

Deju, R. A., R. K. Ledgerwood, and P. E. Long. 1978. Reference Waste Form, Basalts, and Groundwater Systems for Waste Interaction Studies. RHO-BWI-LD-11. Rockwell Hanford Operations, Richland, Washington.

Dubinin, M. M. and L. V. Radushkevich. 1947. "Equation of the Characteristic Curve of Activated Charcoal." Proc. Acad. Sci. USSR 55:331-333.

Fournier, R. O. and J. J. Rowe. 1977. "The Solubility of Amorphous Silica in Water at High Temperatures and High Pressures." Amer. Mineral. 62:1052-1056.

Garrels, R. M. and C. L. Christ. 1965. Solutions, Minerals and Equilibria. Harper and Rowe, New York. p. 177.

Glasstone, S. 1942. Introduction to Electrochemistry. D. Van Nostrand. pp. 291-295.

Haynes, J. M. 1961. "The Specific Surface of Clays." Trans. Brit. Ceram. Soc. 60:691-707.

Helfferich, F. 1962. Ion Exchange. Mc-Graw-Hill, New York. p. 166.

Hendricks, S. B. and R. S. Dyal. 1950. "Surface Measurement by Ethylene Glycol Retention of Clays and Its Application to Potassium Fixation." Trans. 4th Intern. Congress Soil Sci. 2:71-72.

Hodge, C. E. and M. W. Grutzeck. 1978. Preparation of Standard Umtanum Sample by Battelle-Northwest. RHO-BWI-LD-3. Rockwell Hanford Operations, Richland, Washington.

Ives, D.J.G. and G.J. Janz (Eds.). 1961. Reference Electrodes. Academic Press. pp. 270-321.

Izrael, Y. A. and F. Y. Rovinskii. 1970. Hydrological Uses of Isotopes Produced in Underground Nuclear Explosions for Peaceful Purposes. UCRL-trans-10458.

Krauskopf, K. B. 1979. Introduction to Geochemistry. McGraw-Hill Book Co., New York. pp. 456-457.

Lloyd, M. H. and R. G. Haire. 1973. "Studies on the Chemical and Colloidal Nature of Pu(IV) Polymer." Proceedings of the XXIVth IUPAC Congress. CONF 730927.2. Hamburg Germany.

Mackay, D. 1979. "Finding Fugacity Feasible." Environ. Sci. Tech. 13(10):1218-1223.

Potter, R. W. II, W. L. Marshall, R. O. Fournier, and O. I. Martynova. 1978. Bibliography of the Available Data on the Solubility of Silica in Water Substance. Open File Report 78-731. U.S. Geological Survey.

Pourbaix, M. 1966. Atlas of Electrochemical Data. Pergamon Press. pp. 555-558.

Rai, D. and W. T. Franklin. 1978. "Effect of Moisture Content on Ethylene Glycol Retention by Clay Minerals." Geoderma. 21:75-79.

Relyea, J. F., R. J. Serne and D. Rai. 1980. Methods for Determining Radionuclide Retardation Factors: Status Report. PNL-3349. Pacific Northwest Laboratory, Richland, Washington.

Routson, R. C., R. E. Wildung, and R. J. Serne. 1973. "A Column Cation-Exchange-Capacity Procedure for Low-Exchange-Capacity Sands." Soil Sci. 115:107-112.

DISTRIBUTION

Number of
Copies

2   ARGONNE NATIONAL LABORATORY

       A. M. Friedman
       M.   Seitz

1   ARIZONA STATE UNIVERSITY

       J. R. Holloway

5   BATTELLE-OFFICE OF NUCLEAR WASTE ISOLATION

       S. J. Basham
       P. L. Hofmann
       Library (3)

1   BROOKHAVEN NATIONAL LABORATORY

       P. W. Levy

1   D'APPOLONIA CONSULTING ENGINEERS, INC.

       W. E. Coons

1   HAHN MEITNER INSTITUTE

       W.   Lutze

1   HARWELL LABORATORY - U.K.

       N. A. Chapman

1   KAISERS ENGINEERS, INC.

       J. S. Ritchie

1   LAWRENCE BERKELEY LABORATORY

       P. A. Witherspoon

1   LAWRENCE LIVERMORE LABORATORY

       A.   Rothman

1   NATIONAL ACADEMY OF SCIENCES
      COMMITTEE ON RADIOACTIVE WASTE MANAGEMENT

       T.   Pigford

Number of
Copies

1   NATIONAL BUREAU OF STANDARDS

              T.   Yolken

1   OAK RIDGE NATIONAL LABORATORY

              Ecological Sciences Information Center

2   OREGON STATE UNIVERSITY

              Department of Chemistry
            - Department of Geology

10   PACIFIC NORTHWEST LABORATORY

              L. L. Ames   J. E. Mendel
              D. J. Bradley   A. M. Platt
              M. O. Cloninger   D.   Rai
              F. H. Dove   R. J. Serne
              J. E. McGarrah   Library

4   SANDIA LABORATORIES

              R. G. Dosch
              J. K. Johnstone
              M. A. Molecke
              E. J. Nowak

1   SAVANNAH RIVER LABORATORIES

              P. H. Permar

2   TEMPLE UNIVERSITY

              D. E. Grandstaff
              G. C. Ulmer

2   UNIVERSITY OF ARIZONA

              J. J. Daemen
              M. E. Wacks

1   UNIVERSITY OF COLORADO

              D. D. Runnels

1   UNIVERSITY OF ILLINOIS

              A. F. Koster van Groos

Number of
Copies

1	UNIVERSITY OF MISSOURI

        S. E. Manaham

1	UNIVERSITY OF NEW MEXICO

        D. G. Brookins

1	UNIVERSITY OF PITTSBURGH

        B. L. Cohen

1	UNIVERSITY OF WASHINGTON

        Library

1	U.S. DEPARTMENT OF ENERGY-ALBUQUERQUE OPERATIONS OFFICE

        D. T. Schueler

2	U.S. DEPARTMENT OF ENERGY-COLUMBUS PROGRAM OFFICE

        J. O. Neff
        W. R. Wunderlich

5	U.S. DEPARTMENT OF ENERGY-HEADQUARTERS

        C. R. Cooley   C.   Klingsberg
        W. K. Eister   G.   Oertel
        C. H. George

1	U.S. DEPARTMENT OF ENERGY-NEVADA OPERATIONS OFFICE

        R. M. Nelson

2	U.S. DEPARTMENT OF ENERGY-PUBLIC READING ROOMS

        Richland, Washington
        Seattle, Washington

1	U.S. DEPARTMENT OF ENERGY-RICHLANO OPERATIONS OFFICE

        R. B. Goranson

1	U.S. ENVIRONMENTAL PROTECTION AGENCY

        W. A. Williams

Number of
Copies

1   U.S. GEOLOGICAL SURVEY

P. R. Steven

1   U.S. NUCLEAR REGULATORY COMMISSION

D.   Alexander

1   WASHINGTON STATE DEPARTMENT OF ECOLOGY

Library

2   WASHINGTON STATE UNIVERSITY

J.   Kittrick
Library

2   WESTINGHOUSE ELECTRIC CORPORATION

C. R. Bomgren
D.   Newby

1   WHITESHELL NUCLEAR RESEARCH ESTABLISHMENT

D. J. Cameron

32   ROCKWELL HANFORD OPERATIONS

H. Babad	P. F. Salter
G. S. Barney	W. W. Schultz
R. A. Deju	M. J. Smith (5)
A. F. Noonan	J. R. Wetch
W. H. Price	

Basalt Waste Isolation Project Library (10)
Document Control (4)
Records Retention Center (2)
R ə E Technical Information Center
Report Coordination and Production Department (2)

	Number of Copies
U.S. GEOLOGICAL SURVEY	1
R. K. Steven	
U.S. NUCLEAR REGULATORY COMMISSION	1
D. Alexander	
WASHINGTON STATE DEPARTMENT OF ECOLOGY	1
Library	
WASHINGTON STATE UNIVERSITY	2
J. Killsig	
Library	
WESTINGHOUSE ELECTRIC CORPORATION	2
Dr R. Remgren	
D. Handy	
UNITED KINGDOM NUCLEAR RESEARCH ESTABLISHMENT	1
D. J. Farmin	
ROCKWELL HANFORD OPERATIONS	72

H. Babad	R. F. Salter
C. S. Harvey	W. W. Schultz
K. A. Deji	M. J. Smith (5)
A. F. Noonan	J. P. Welch
W. H. Price	

Basalt Waste Isolation Project Library (10)
Document Control (4)
Records Retention Center (2)
H + C Technical Information Center
Report Coordination and Production Department (2)